MASTERARBEIT

Analysis of Topotecan induced senescence, apoptosis and vascularization in a neuroblastoma xenotransplant mouse model

verfasst von

Magdalena Schwarz, BSc

angestrebter akademischer Grad

Master of Science (MSc)

This master thesis was performed at the

St. Anna Kinderkrebsforschung

(CCRI)

Tumor biology group: Prof. Dr. Peter F. Ambros

Zimmermannplatz 10a
1090 Wien, Austria

and was supervised by

Dr.^{in} Sabine Taschner-Mandl

ACKNOWLEDGEMENTS

EIDESSTATTLICHE ERKLÄRUNG

Ich erkläre an Eides statt, dass ich die vorliegende Arbeit selbstständig verfasst, andere als die angegebenen Quellen/Hilfsmittel nicht benutzt, und die den benutzten Quellen wörtlich und inhaltlich entnommenen Stellen als solche kenntlich gemacht habe.

Wien, am   _____

STATUTORY DECLARATION

I declare that I have authored this thesis independently, that I have not used other than the declared sources / resources, and that I have explicitly marked all material which has been quoted either literally or by content from the used sources.

Vienna   _____

Table of Contents

1. Introduction

1.1 Neuroblastoma

Neuroblastoma (NB) is the most common solid childhood tumor and most frequent cancer diagnosed during infancy (Brodeur, 2003). Tumors originate from neuronal progenitor cells in the vegatitve nervous system, and arise mostly in the abdomal region. NB is extracranial which means that it is not attached to the brain, and can either be restricted to the site of origin, or spread to nearby lymph nodes and organs such as liver, kidney, bone, bone marrow and spleen (see Fig. 1).

1.1.1   Staging Systems and Subtypes

There are different staging systems and classifications of NB into subtypes, also due to the fact that it is a very heteregenous disease concerning clinical presentation and outcome. The International Neuroblastoma Staging System (INSS) is an official system which classifies the disease depending on the anatomical site of tumors at diagnosis (shown in Fig.1) and distinguishes if tumors have spread and other organs are affected and it includes whether tumors can be completely or partially removed during surgery (Monclair et al., 2009).
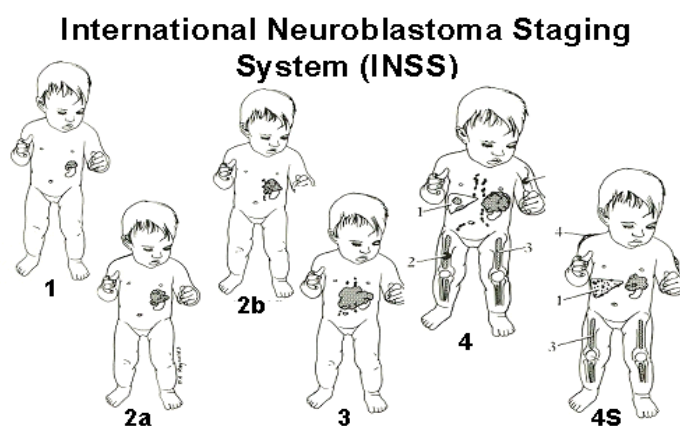
Fig. 1 I Staging System in Neuroblastoma based on affected sites of the body. Taken from http://www.nant.org/pix/inss.jpg

There are several genetic aberrations that characterize high-risk patients, mostly sharing MYCN amplification and alterations of chromosomal arms such as 1p loss, 11q loss or 17q gain.

Another system of staging NB is to seperate localized from metastatic forms. This clinical classification which was elaborated in the INRG (International Neuroblastoma Risk Group) comprises of four groups: L1 and L2 which are localized forms and M and MS which show metastatic behaviour (Cohn et al., 2009). Concerning biologial behaviour, tumors can either develop further and therefore progress or they can decline, hence enter regression. One kind of regression would be maturation during which immature neuroblastic cells differentiate into mature neuronal-like cells (Ambros et al., 1996). Although not considered conventionally as another option, apoptosis and tumor cell senescence could be another fate of NB cells and halt the progression or even lead tumors to regress or disappear.

1.1.2   Genetic alterations in Neuroblastoma

Several genetic aberrations contribute to the development, progression and severity of NB. Among these, somatic mutations, segmental chromosomal aberrations (SCAs) (Schleiermacher et al., 2011), such as gains and losses of chromosomal p or q arms, chromothrypsis as well as numerical chromosomal aberrations (NCAs) can be found (Diskin et al., 2009; Molenaar et al., 2012). Different somatic mutations can be related with poor or good prognosis. One of the most influencing factors of outcome is the age at diagnosis (Deyell & Attiyeh, 2011; Smith et al., 2010). The most important aberration for this study is the amplification of the *MYCN* gene which is shared by approximately 20% of NB patients (Maris, 2010). This *MYCN* amplification (MNA) correlates with clinical outcome since patients with this feature are considered high-risk patients and face a poor prognosis (Brodeur, Seeger, Schwab, Varmus, & Bishop, 1984). Not only the age and type of mutation is decisive for outcome but also the status of ploidy in tumor cells (Ladenstein et al., 2001; Look, Hayes, Nitschke, McWilliams, & Green, 1984).

1.1.3   Treatment
Therapies in several types of solid cancers usually include chemotherapy, surgery, radiation and stem cell transplantation (Chabner & Roberts, 2005).

One approach in NB is to stimulate cancer cells and drive them into maturation by administering retinoic acids (RA), another well established therapy is to target the ganglioside GD2 with specific monoclonal antibodies (Cheung et al., 1987; Yu et al., 2010).

1.1.4   Need for additional therapeutic approaches in MRD patients

Since this study deals with the potential application of senescence induction for high-risk patients, this NB subtype form will be discussed in detail regarding current therapies. High-risk patients can share *MYCN* amplification (MNA) and prognosis as well as survival is poor for them. Study protocols for clinical trials have sequential cytotoxic agents, radiotherapy and surgery with further applications such as stem cell transplantation or the application of retinoic acids with or without immunotherapy such as IL-2 or αGD2 antibodies (Matthay et al., 1999). In order to demonstrate the kind of treatment regimen for those high risk patients, a study high risk NB protocol (HR-NBL-1.5 study) is being illustrated (Ladenstein et al., 2010). Patients first undergo induction therapy which is mostly carried out in combination of high-dose chemotherapies with cytotoxic agents such as Etoposide, Cisplatin or Vincristine, and is followed by surgery. If the tumor cannot be removed during surgery, myeloablative therapy is applied and stem cell transplantations carried out. If remission could not be achieved patients experience radiotherapy. Once the tumor mass has been reduced to a minimal residual disease (MRD) setting, an approach of diminishing residing tumor cells is the application of retinoic acid (RA) and its derivatives. This consolidation therapy uses retinoids to drive NB cells into differentiation so that they can differentiate, immunotherapy has been tested in clinical trials in order to remove residing tumor cells, also from metastatic sites. Although this treatment regimen combines several approaches and targets distinct sites and pathways, however, many high-risk patients suffer from relapse. Since those relapse-patients face a very poor outcome it is necessary to find additional therapeutic possibilities.

1.2 Senescence

1.2.1. Markers of Senescence

It is widely agreen upon that a crucial feature in the definition of the cellular program of senescence is the state of proliferative arrest and that this growth arrest can affect single cells but also contributes to aging of a whole organism. Different types of cells can enter

senescence and in rapidly dividing cells, such as premalignant or tumor cells, senescence can halt proliferation and further growth of the whole tumor, importantly. There is no explicit definition about which makes up a senescent cell but there are some base line characteristics which are taken into account when the phenomenon of cellular senescence is being described: cells enter a state of growth arrest, they alter their morphology e.g. by increasing in size and flattening and – along with other markers – show high expression of the senescence-associated β-Galactosidase (SA-β-Gal) (Rodier & Campisi, 2011). In the following chapter, a panel of markers in use is being described although not all markers are equally well accepted or ubiquitously positive on senescent cells or tissue (for an overview, see Fig. 2). Relevant markers for this study are described in more detail.
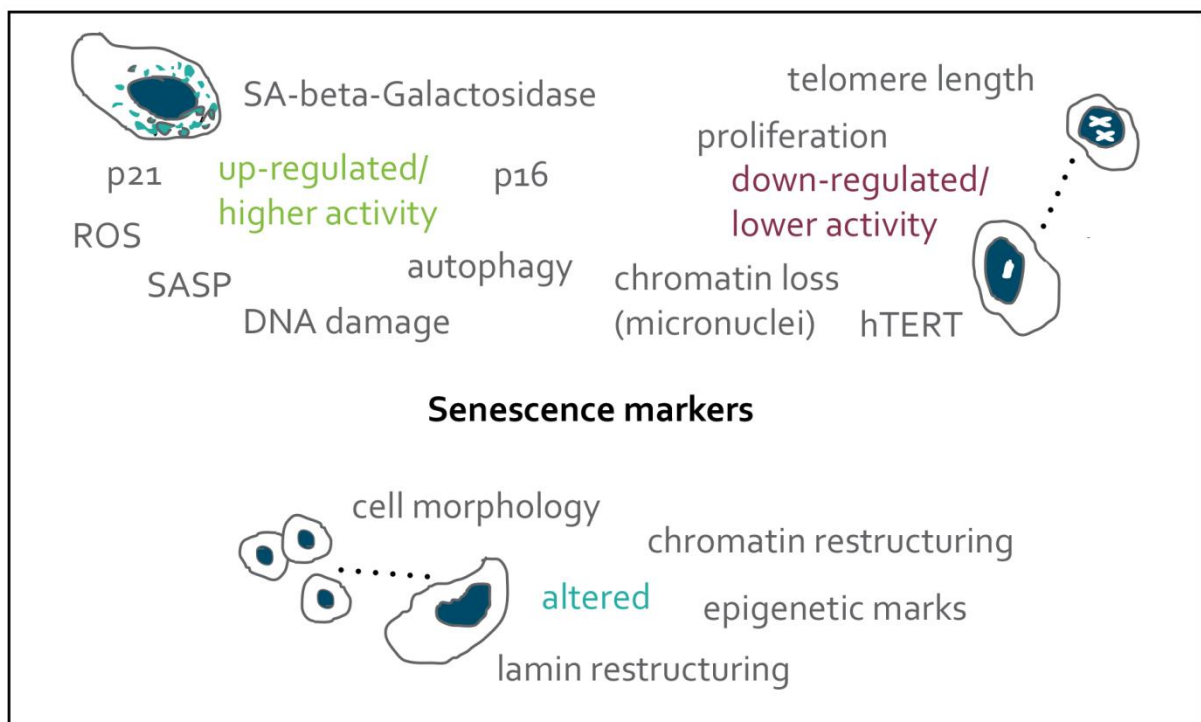
Fig. 2 I Schematic overview of senescence markers. Not all markers have to be expressed or present in senescent cells, this scheme shows a panel of common characteristics, divided into subgroups that show if features are up-/down-regulated or restructured (altered).

Cell cycle arrest

It is widely agreed upon that a defining feature in the definition of senescence is the state of proliferative arrest (Campisi & d'Adda di Fagagna, 2007; Collado, Blasco, & Serrano, 2007; Kuilman, Michaloglou, Mooi, & Peeper, 2010; Roninson, 2003; Shay & Roninson, 2004). Cells are halted in G1/G0 phase of the cell cycle and the proportion of cells that actively

proliferate and the proportion of arrested cells can be measured with flow cytometry analysis or by (IF-) staining of specific proliferation antigens (Sherwood, Rush, Ellsworth, & Schimke, 1988).

It is not reliable to only use negative markers for proofing a certain pathway but in the case of senescence there are several markers that can support the demonstration when combined with other positive markers. Proliferating cells can be detected via immunofluorescence (IF) stainings or immunohistochemistry (IHC) by showing the presence of Ki67 (Verheijen et al., 1989). The Ki67 antibody detects the antigen that is being expressed on proliferating cells while they are actively participating in the cell cycle. Cells show positivity for Ki67, except when they are in Go-phase. The staining patterns differ, depending on the cell cycle phase, and so heavily proliferating tissue can be distinguished from non-proliferating tissue. When cells enter a senescent, non-proliferating state, it is probably dependent on the cell type if they stop or reduce Ki67 expression, or the pattern at least changes from a mitosis-like to a rather weak staining which is confined to nucleoli of cells, respectively.

Senescence-associated β-Galactosidase (SA-β-Gal)

When cells senesce they enlarge their lysosomal compartments in which the enzyme β-Galactosidase is responsible for hydrolysing β-Galactosidases into monosaccarides. If the substituting substrate X-Gal is given to those cells, then there is an increased activity of β-Galactosidase detectable in senescent cells. This increase is demonstrated by staining at a suboptimal pH around 5.0-6.0 with a by-product of the enzymatic reaction which occurs as blue precipitate. Since this signals an increased amount of senescence it is also called senescence-associated β-Galactosidase (SA- β-Gal). It has been first described in in 1995 and since then served as the most widely accepted marker for senescence *in vitro* as well as *in vivo* (Dimri et al., 1995).

DNA damage

Regardless whether an external or intrinsic trigger was responsible for the onset of senescence, DNA damage (DD) is a characteristic feature of most senescent cells which is supported by evidence in the literature (Bartkova et al., 2005; Bartkova et al., 2006; Di Micco et al., 2008; Di Micco et al., 2006; Di Micco et al., 2011; Knizhnik et al., 2013; Seluanov

et al., 2001; Sohn et al., 2012; Sulli, Di Micco, & d'Adda di Fagagna, 2012; te Poele, Okorokov, Jardine, Cummings, & Joel, 2002). DD has been known to trigger apoptosis but it can also evoke a p53 dependent cellular senescence response. The induction of senescence by administering cytotoxic drugs, such as the topoisomerase inhibitor Topotecan, acts via establishing DD and inducing double strand breaks (DSBs) and this type of growth arrest in tumor cells involves p53, p21 as well as p16 (te Poele et al., 2002). DNA lesions and the subsequent DNA damage response can occur due to endogenous or extrinsic signals such as radiation, viruses, replication errors, reactive oxigen species (ROS) or chemicals/drugs. DD also affects the organization and modification of chromatin, hence it can influence not only chromatin changes but also gene expression in the whole genome (Di Micco et al., 2011; Sulli et al., 2012). Nevertheless, it should be noted that not all types of senescence depend on a DD response, but e.g. involve the MAP-Kinase p38 pathway for inducing secretory characteristics of senescent cells *in vitro* (Freund, Patil, & Campisi, 2011). As mentioned before, DNA lesions can initiate several pathways, including senescence, necrosis, apoptosis but also autophagy. Studying the underlying mechanisms of cell fate decision after such a lesion revealed an increase in autophagy which triggers senescence rather than apoptosis (Knizhnik et al., 2013). The best established marker for DSBs is γH2AX which is a variant of the H2A core histone harboring a C-terminal extension which is used for DNA repair.

Morphology

Senescent cells display a different phenotype than non-senescent cells which is largely due to their enlargement of nuclei as well as lysosomal compartments. Senescing cells *in vitro* show a morphologically altered, flattened nuclear shape and can grow several times larger than neighbouring non-senescent cells (Kuilman et al., 2010; Rodier & Campisi, 2011; Shay & Roninson, 2004). In addition to enlargement and flattening, chromosomal reorganisation plays an important role and can be observed by the production of compact, extranuclear heterochromatin. The production of lipofuscin which is commonly defined as a kind of „aging pigment" is also increased and can be observed as a yellow fluorescence around senescent nuclei. *In vivo* the case is somehow different since heavily packed and dense tissue may not allow for cells to flatten and expand to such a high extent as *in vitro*.

Another morphological feature that can be observed in senescent tumor cells is the formation of micronuclei (Ambros et al., 1997; Ivanov et al., 2013; Von Hoff et al., 1992).

Those compact nuclei can bud off from strongly γH2AX positive tumor cells since DD is also involved. Sumernumerous copies of extrachromosomally amplified oncogenes such as *MYCN* can be expulsed and thereby lower tumorigenicity (Ambros et al., 1997; Von Hoff et al., 1992)

p16^{ink4a}/pRB and p53/p21 pathways

It has been unraveled that two pathways are up-regulated in many types of senescence, namely the p16^{ink4a}/pRB and the p53/p21 pathways (Campisi, 2005). Both pathways are key regulators in the suppression of tumor formation and often found mutated in cancers. While p53 is thought to play a role in the onset of senescence, p16 rather stabilizes this cellular program (te Poele et al., 2002). P53 also controls p21, an important cyclin-dependent kinase inhibitor, which can lead to proliferative arrest. P21 has also been shown to be induced in senescence, for example the treatment with cytotoxic drugs reportedly triggered a p53-p21 dependent senescence program in human tumor cells (Chang et al., 1999).

Senescence-associated secretory phenotype (SASP)

Senescent cells alter their shape, size and lysosomal compartments while also rearranging their chromatin and expressing different markers than proliferating cells. While those features are all achieved by the cell itself, it can also influence its environment and neighbouring cells by the factors it secretes (Kuilman & Peeper, 2009). The range of growth factors, cytokines, hormones and inflammatory molecules that is being produced by senescent cells is summed up under the term of senescence-associated secretory phenotype (SASP) . The SASP profile includes benificial as well as harmful factors in terms of cancer therapy: while some factors may attract the innate immune system and thereby evoke a response that is potent to destroy tumor cells, some other factors potentially disturb the equilibrium of growth factors and inhibiting signals in tumor cells and promote tumor growth via cytokine signalling to neighbouring cells (e.g. MMPs, IL-6, IL-8, VEGF). SASP has been the main argument against senescence-induction in cancer therapy for a long time until there were reports that stated the induction of senescence without generating a full-blown SASP expression, secretion, response and communication.

Chromatin and nuclear structure

In addition to those well-established indicators of cellular senescence, several new characteristics have been brought up that include modifications of nuclear structures or DNA itself such as the reorganisation of chromatin, epigenetic marks and restructuring of lamins. It was first observed in normal human fibroblasts that cells that enter a stable growth arrest can form regions of heterochromatin, defined as senescence-associated heterochromatic foci (SAHFs) and that this occurrence coincides with the repression of transcription factor targets and therefore delivers a possible explanation for the stability of senescence (Narita et al., 2003). On an epigenetic level, it has been reported that the senescent state of mesenchymal stem cells *in vitro* is accompanied by a H3K9 trimethylation which is a repressive histone mark (Schellenberg et al., 2011).

1.2.2 Theories of Senescence

Concerning the biological role of senescence, it is still under debate to which pathways or mechanisms this phenomenon contributes but in general it can be considered as a cellular stress response and is often involved in pathological pathways (Collado et al., 2007). There are several summaries and speculations reviewed (Kuilman et al., 2010; Rodier & Campisi, 2011) that state the opinion that senescence can play different roles, depending on the context of its occurence. For example, Rodier and Campisi argue that senescence can contribute to tumor suppression as well as tumor promotion, aging and also tissue repair. They suggest a temporal manner of organisation which decides which fate dominates. Throughout the history of senescence research, its role and importance have significantly changed: first, it was discovered to be a phenomenon of telomere dysfunction and associated with the finite lifespan of cells, later on it was revealed that senescence can be induced in normal and (pre-)malignant cells and exploited for the purpose of cancer therapy, continuously the focus shifted to potential applications of senescence and whether they would be only beneficial or if they also cause side effects or unwanted mechanims. After decades of research that emphasized the role of senescence in pathological conditions, some very recent studies also shed light onto the role in physiological conditions and the involvement in developmental processes such as embryogenesis. In the following chapter it is intended to present different theories of senescence since it can occur as a

natural phenomenon when cells cease to divide but it can be also be induced through several external and applied triggers (Fig. 3).
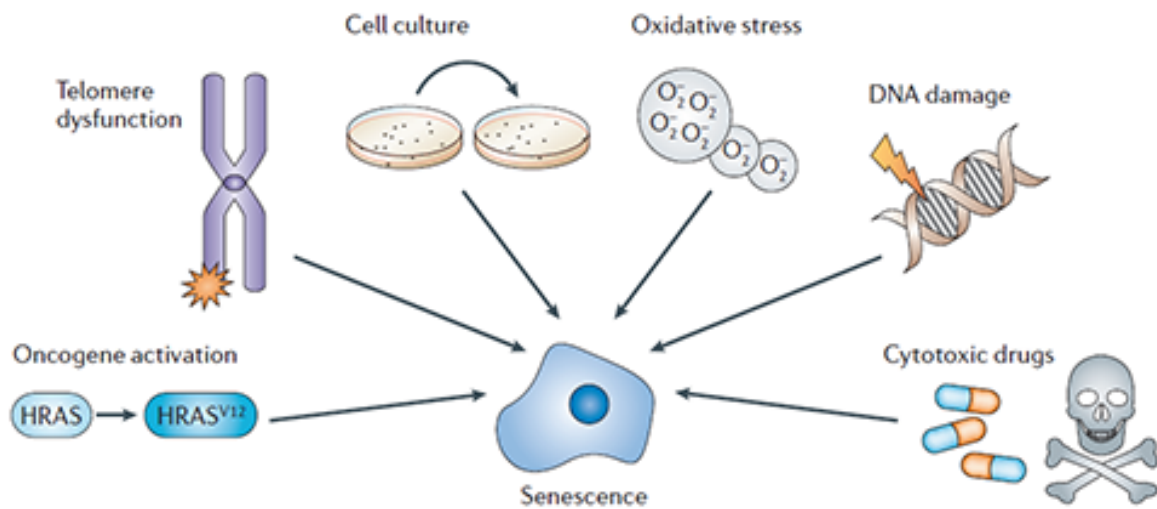
Fig. 3 I Triggers that lead to cellular senescence. Different sorts of stress signals can induce different senescence pathways such as replicative senescence, OIS, DNA damage-induced or drug induced senescence. Taken from (Collado & Serrano, 2006).

Replicative cellular Senescence

Replicative senescence refers to the state of permanent growth arrest which involves the shortening of telomeres and demonstrates the finite life span of cells (Harley, Futcher, & Greider, 1990; Shay & Wright, 2005). It was first observed by Hayflick and Moorhead that cells undergo a certain number of passages or doublings in culture before they stop to divide which has shown the limited life span of cells *in vitro* and ended speculations about immortality of cultured cells (Hayflick, 1965; Hayflick & Moorhead, 1961). Replicative senescence defines the state of a cell in which it cannot continue with replication but neither it undergoes a death pathway, e.g. apoptosis, though the cell can remain metabolically active and influences surrounding cells through secreted factors. Through the continuous shortening of telomeres, life span is limited. To circumvent this problem of telomere attrition, the catalytic subunit of the telomerase holoenzyme (hTERT) is expressed in affected cells and thereby telomere length is maintained resulting in a by-pass of replicative senescence. Earlier studies proofed that the life span of primary human cells could be prolonged by introducing hTERT ectopically *in vitro* (Bodnar et al., 1998).

Stress induced cellular senescence

Besides the type of replicative senescene which involves telomere shortening, there are also other mechanisms that do not depend on telomeric dysfunction, that evoke senescence. Several triggers that produce stress such as DNA damage, radiation, chemicals, oncogene acitvation as well as tumor-suppressor loss can activate a senescence program which differs not so much from replicative senescence in terms of markers but in mechanistic ways. Independently of the exact trigger that forces the process, these forms of senescence have in common their DNA damage signalling, e.g. DNA damage response (DDR) and the induction of DNA double strand breaks (DSBs) (Collado & Serrano, 2006; d'Adda di Fagagna, 2008; Di Micco et al., 2006; Di Micco et al., 2011; Shay & Roninson, 2004).

Oncogene-induced senescence (OIS)

The so-called premature cellular senescence through activation of an oncogene was first observed by Manuel Serrano in 1997 when the *ras* oncogene was shown to induce senescence alongside with accumulating p53 and p16 (Serrano, Lin, McCurrach, Beach, & Lowe, 1997). While it was reported that replicative senescence could be bypassed by expressing hTERT and thereby avoiding the shortening of telomeres, this was not the case for oncogene induced senescence (OIS). This showed its independence from the mechanism of telomere attrition and was confirmed in 1999 (Wei & Sedivy, 1999). According to a 2010 overview by Kuilman *et al* the exact mechanisms and pathways involved in OIS differ among species and the actual genetic predispositions or alterations (Kuilman et al., 2010). Examples of activated genes that are able to evoke the senescence pathway include *Ras, Raf* and *BRAF* oncogenes and they share DDR, so the needed trigger in this type of senescence is derived from some sort of stress that harms DNA (Bartkova et al., 2006; Braig & Schmitt, 2006; Collado & Serrano, 2006; Di Micco et al., 2006; Mason, Jackson, & Lin, 2004; Sarkisian et al., 2007; Zhu, Woods, McMahon, & Bishop, 1998).

Importantly, not only the overexpression and activation of oncogenes can induce senescence but also the loss of tumor suppressor genes such as *PTEN* which is also dependent on p53 (Chen et al., 2005).

Therapy induced senescence (TIS): advantages and downsides

Since most cytotoxic drugs that are applied in chemotherapy induce DD it was a relevant question to ask whether senescence and cancer would be linked to one another. It was speculated earlier that senescence could be a naturally occuring mechanism of tumor suppression because of the limited replication that would protect cells from developing cancer (Sager, 1991). In 2002 it was shown that DNA damage could induce senescence in tumor cells and that this could be achieved *in vitro* as well as *in vivo* (te Poele et al., 2002). In parallel, the group of Clemens Schmitt has been investigating on the topic of therapy induced senescence (TIS) and its potential beneficial as well as negative side effects and outcome for patients. It was shown that senescence could contribute to an improved outcome of cancer patients (Schmitt et al., 2002) and three years later it was demonstrated that OIS could block the development of lymphomas (Braig et al., 2005). The following years have not only revealed that TIS really could serve as an initial barrier to tumor formation but also that tumors regressed when certain oncogenes i.e. *myc* were inactivated and senescence thereby induced (Wu et al., 2007).

However, there is still an ongoing debate about advantages and downsides of senescence induction in cancer therapy and opposing opinions can be found in the literature (Ewald, Desotelle, Wilding, & Jarrard, 2010). Whether senescence in therapy offers potential advantages or disadvantages could strongly depend on the context such as the age of the organism which is supported by the theory of antagonistic pleiotropy (Rodier & Campisi, 2011). The induction of senescence in tumor cells can be achieved either by introducing genetic modifications, e.g. RAF-1 and MKK6 transfection, or applying chemotherapy, radiation or retinoids (Roninson, 2003). It has been believed for a long time that apoptosis was the predominant pathway in cancer therapy upon cytotoxic treatment, but senescence might have been overlooked and not taken into account for the effect of tumor inhibition. Kahlem *et al* argue that the mode of action in cancer treatment with cytotoxic agents could include both apoptosis and senescence but in a temporally ordered manner (Kahlem, Dorken, & Schmitt, 2004). In that sense, senescence would act as a powerful back-up for apoptosis in a delayed way if programmed death is insufficient.

One of the major arguments against the induction of senescence in tumors is the activity of SASP and its aggressive influence on neighbouring cells. Cytokines, such as Interleukin IL-6

and IL-8 can be secreted and may stimulate premalignant cells to invade basement membranes (Coppe et al., 2008), while senescent fibroblasts can also secrete vascular endothelial growth factor (VEGF), a stimulatory molecule that supports cell migration and invasion in the route of angiogenesis (Coppe, Kauser, Campisi, & Beausejour, 2006). In addition the process of cell invasion can be triggered by the secretion of matrix metalloproteinases (MMPs) which were shown to be secreted by senescent keratinocytes and fibroblasts (Millis, McCue, Kumar, & Baglioni, 1992).

Most studies, however, showed negative effects of SASP *in vitro* and are limited to senescent fibroblasts while tumors often display a heterogenous composition and interactions with surrounding tissue or – most importantly – the immune system strongly influence tumor cell fate. A potential benefit of TIS could be the observation that low-dose drug treatment *in vivo* induces senescence while avoiding treatment-related toxic side effects (Schwarze, Fu, Desotelle, Kenowski, & Jarrard, 2005). While DNA damage can occur in both, apoptosis and senescence pathways, high doses often evoke apoptosis and low-dose regimens rather induce senescence and this response was especially true for chronical administration. For example, the application of the cytotoxic drug hydroxyurea at low doses and path of senesce induction in tumor cells was shown to be true for a *MYCN* amplified NB cell line and was published by Peter Ambros' group in 2007 (Narath et al., 2007).

1.3 Introduction on the project and previous findings *in vitro*

Based on studies about spontaneous senescence in *MYCN* amplified NB cells (Ambros et al., 1997) and the induction of senescence in tumor cells via drug treatment and the potential tumor-inhibitory functions of this pathway, *in vitro* studies had been carried out in NB cell lines. Initially, several drug candidates had been tested concerning their ability to evoke senescence in NB cells.

The drugs used in this study were selected based upon their ability to induce DD and application in higher doses in different types of malignancies. They share their potential to induce DD and therefore served as appropriate drug candidates for the induction of senescence. Hydroxyurea (HU), Camptothecin (CPT), Topotecan (TPT) and Bromodeoxyuridine (BrdU) were tested for their ability to induce senescence at low doses. HU has been used in clinics as a cytotoxic agent in cancer therapy for decades and funcitons via the induction of DNA double strand breaks (DSBs) and the development of micronuclei

(Ahmann, Hahn, & Bisel, 1972). CPT is a cytotoxic drug that inhibits the enzyme topoisomerase I and thus and induces DSBs has been described since the 1970s while there were also attempts of synthesizing analogues for cancer treatment (Lock & Ross, 1987). TPT acts in a comparable manner since it is a derivative of CPT and is in use in clinics in high-dose regimens such as induction therapy in combination with other cytotoxic agents (Rowinsky et al., 1992). BrdU is a nucleotide analogon which served as a positive conrol in these experiments and has been shown to induce senescence in NB but is not in use in clinics anymore because of its high toxicity (Acosta et al., 2009).

It was previously shown in Peter Ambros′ group that the treatment of *MYCN*-amplified (MNA) NB cell lines with low-dose hydroxyurea (HU) leads to a reduction of episomal MNA and concomitant senescence induction *in vitro* (Narath, 2007). In parallel NB cells undergo neuronal differentiation or apoptosis, respectively. Also CPT and its derivative TPT were capable of inducing senescence and therefore all three drug candidates had undergone further analysis: SA-β-Gal activity, cell cycle analysis, γH2AX stainings and SASP had been analyzed to show the presence of senescent cells but at the same time the absence of a full blown SASP activity which might be harmful and cause further tumor development *in vivo*. Selected results of those previous *in vitro* studies are summarized in Fig.4. Drug-treated STA-NB-10 cells show altered morphology like flattened and enlarged nuclei and cytoplasms and they are positive for SA-β-Gal (Fig. 4A). Cell cycle analysis showed a higher portion of cells in G1 and less in S phase in HU treated samples compared to control cells (Fig.4 B). Importantly, also the previously published concomitant reduction of *MYCN* copies upon continuous low-dose drug treatment was observed in FISH analyses (Fig.4 D) and MYCN down-regulation was confirmed with Western Blots (Fig.4 C). As discussed earlier, the secretion of unfavorable factors such as certain cytokines and growth factors in the SASP, might lead to further tumor progression when senescent cells thereby would promote proliferation of non-senescent neighbouring cells. Therefore a cytokine antibody array was performed with untreated control NB cells, spontaneous senescent cells and senescent cells which had been treated with BrdU, CPT or HU (Fig.4 E). This array revealed a more "benign" secretion pattern in HU and CPT treated cells by showing no or very low secretion of potentially aggressive SASP-candidates such as VEGF or MMP-9 (Fig.4 E, green box). These findings led to the selection of HU and TPT (as a CPT derivative) for *in vivo* studies in NB-xenotransplanted mice. Pilot experiments had indicated that Topotecan

induces senescence in NB cells *in vitro* in a shorter period of time (i.e. 3 weeks) than HU (8-10 weeks), thus making TPT the more attractive candidate.
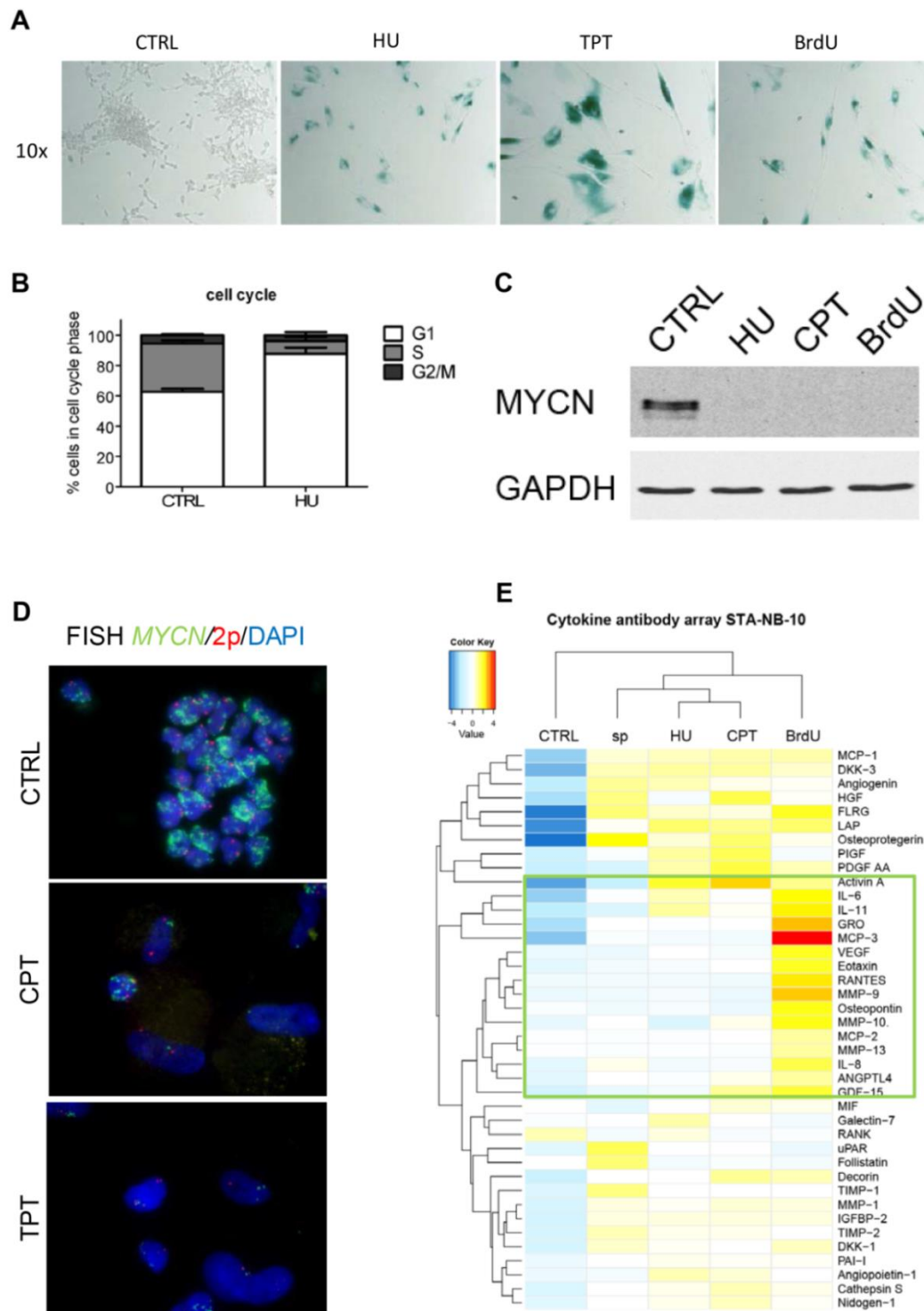
Fig. 4 | *In vitro* findings about drug-induced senescence in STA-NB-10 cells. SA-β -Gal Staining (A) and cell cycle analysis (B) show presence of senescence and proliferative arrest, respectively. Down-regulation of MYCN in drug-treated and control cells is demonstrated with Western Blot (C) and FISH with MYCN probe (green) and 2p reference (red) (D). Cytokine antibody array shows more benign secretion patterns for HU and CPT treated cells (E), green box contains factors considered as unfavorable when highly expressed. All results shown for STA-NB-10 cell line, all data were validated in another NB cell line.

23

1.4 Experimental Setup

In pilot experiments different mouse strains, cell lines, routes of administration and cell numbers had been tested regarding optimal conditions for this NB-xenotransplant mouse model. In this project the experimental setup included 40 mice that were divided into 5 treatment groups. Female, partly immunodeficient, nude mice were used at 6-10 weeks of age and inoculated with a NB cell line (STA-NB 10) which had been established previously from a high-risk patient with a *MYCN* amplification in-house (for detailed information see chapter 3 "Material and Methods"). Starting from the day of inoculation, the neuroblastoma tumors grew for 2.5 weeks until they were palpable in all mice and then treatment started.

After Topotecan (TPT) had been revealed to induce senescence *in vivo* it was administered in three different dosages in this experiment. From the literature it is known that the TPT dose used in other mice studies ranged from 0.2 – 1.0 mg per kg per day. In the previous *in vivo* study tumors completely regressed after 2 weeks of treatment with 1.0 mg/kg/d TPT so that no material was left to analyze from that dosage group. Since our aim was to inhibit neuroblastoma progression and induce senescence at continuous low-dose treatment, we chose doses below 1.0 mg/kg/d in the present study. One group received 0.1 mg/kg/d TPT, the second group received 0.03 mg/kg/d TPT and the very-low-dose group received 0.01 mg/kg/d TPT intraperitoneally. All of these treatment groups consisted of 10 animals (Fig. 5). In addition, we had 5 untreated animals that served as controls and received 0.1% DMSO in PBS which was the vector for the administration of TPT in the treated animals (Fig. 5). In order to study the effect of prolonged TPT treatment and to see whether tumors would recur after they had disappeared when treatment stopped, there was another group that consisted of 5 mice and received 0.1 mg/kg/d TPT over a period of 40 days. After those 6 weeks treatment was stopped and they were observed for another 31 - 46 days.

In the short-term treatment group, after 14-15 days of TPT treatment mice were sacrificed and besides their tumors, also other organs, blood and bone marrow were prepared and stored (detailed information in chapter 3 Material and Methods). Tumors were cut into pieces so that there was material for touching tumors onto slides, cutting 4 µm sections of fresh frozen material for immunofluorescence IF stainings and isolating RNA for expression arrays.
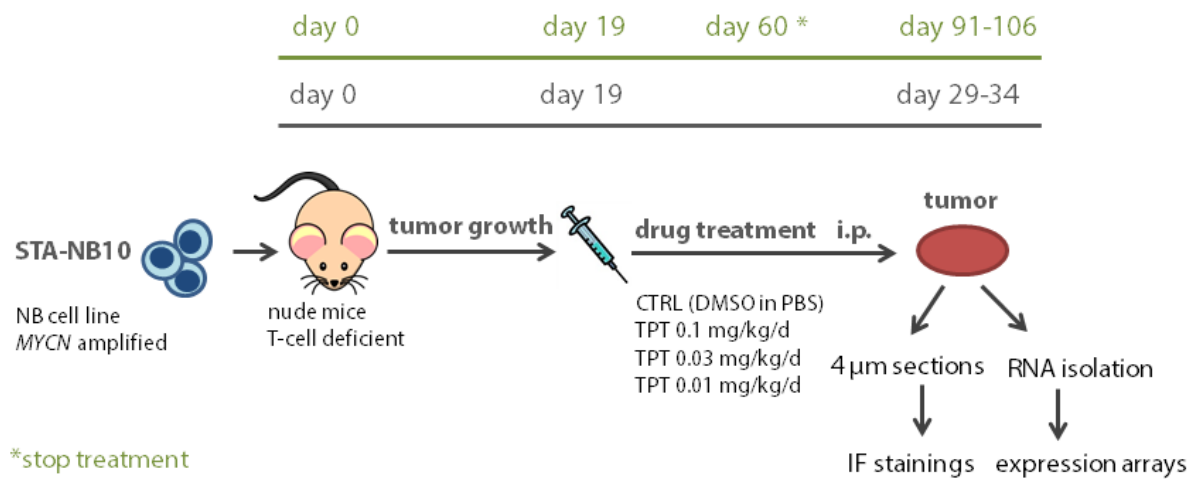
Fig. 5 l Experimental setup for the NB xenotransplant study on drug induced senescence. STA-NB-10 cells are inoculated in partly immune deficient CD1 nude mice (day 0) and after tumors have reached a palpable size in all mice, drug treatment starts (day 19). Three different doses of topotecan are administered peritoneally (i.p.) in a daily manner, or mice are treated with DMSO in PBS as a control (CTRL), respectively. Mice are sacrifized after 29 to 34 days and tumor pieces are used for IF stainings and RNA isolation for expression arrays. The green line indicates the treatment scheme for the 0.1mg/kg/d TPT treated animals in the long-term treatment and observation group.

2. Aim of the Study

Since previous findings *in vitro* had proved the induction of senescence in NB tumor cells via continuous low-dose cytotoxic drug treatment, the main aim for this study was to explore whether this was also true *in vivo*. The most pressing question was if continuous low-dose Topotecan treatment would evoke a senescence pathway in human-derived NB xenotransplanted tumors in mice. It was known that Topotecan (TPT) inhibits Topoisomerase I and induces DSBs, so the activation of a DNA damage response was expected but concerning its ability to induce senescence in tumor cells, it had to be clarified if, at which dose ranges and to which extent this would be possible. To this end, it was planned to apply several TPT dose regimens. Along with the analysis of senescence in tumors, it was important to investigate alternative cell fates, such as apoptosis, proliferation and angiogenesis. It was shown in the literature that high doses of cytotoxic agents predominantly induced apoptosis while lower doses rather promoted the senescence pathway (Spallarossa et al., 2009). Therefore it was relevant to analyze apoptosis markers and relate the proportion of apoptotic cells to senescent cells in tumors. Senescent cells – mostly work done on fibroblasts – had earlier been described to secrete factors that may influence neighboring cells in a harmful manner by promoting further tumor growth, e.g. by supporting vascularization of the tissue, on the other hand, high-dose CPT/TPT was shown to cause a down-regulation of vascularization. Hence, it had to be addressed whether angiogenesis plays a role in this model and also if activity of proliferation markers would decline in TPT treated NB xenotransplant tumors. Further on, expression patterns of TPT treated tumors and untreated control tumors should disclose if there was differential expression and if specific markers for senescent tumor cells would be detectable.

Taken together, the application of senescence induction via continuously administered, low-dose TPT in NB tumor cells and its potential benefits or downsides concerning further tumor development should be elucidated in a preclinical mouse model.

3. Material and Methods

3.1 Xenotransplant mouse model and sample preparation

Preparation of cells and inoculation

The same cell line used in previous *in vitro* studies of senescence induction was used in this *in vivo* study. The STA-NB10 cell line had been generated from a NB patient in 1995 and was established in-house. This cell line has a *MYCN* amplification and was derived from a high-risk patient who was 18 months of age at diagnosis died of disease. The STA-NB10 (passage between p14 and p21) cell line was adjusted to $1x10^8$ per ml PBS and a cell number of $1x10^7$ per mouse was mixed 1:1 with BD Matrigel™ Basement Membrane Matrix containing growth factors (BD Biosciences, USA). Cells were harvested according to standard tissue culture protocols, counted and every mouse received 200 µl of cell suspension in Matrigel™. The suspension was injected subcutaneously into the right hind leg. In some cases it was not assured that the whole volume stayed inside so the left hind leg was also inoculated and those mice later on developed tumors on both sides.

Mice

40 mice of the mouse strain Crl:CD1-*Foxn1^{nu}* (Charles River, USA) were divided into 5 treatment groups. They were all female, hairless and between 6 and 10 weeks of age. That mouse strain was generated to be partly immunodeficient which means that the animals do not develop any T-cells.

Monitoring

Starting from the day of inoculation (day 0) the animals were monitored which included measuring the growing tumors twice a week in x, y and z axis and weighing them once every week. No injuries, acute weight loss or other abnormal or pathological conditions were observed and tumors were allowed to grow for 19 days until they reached a size of 0.53 (±0.2) cm3. From that day on the monitoring was continued in the same manner until mice were sacrificed.

Treatment

Treatment started on day 21 after tumors had grown and were palpable in all mice. Mice were divided into 5 groups. 10 Animals belonged to the group which was treated with 0.1 mg/kg/d TPT. The second group (n=10) received 0.03 mg/kg/d TPT, the third group (n=10) 0.01 mg/kg/d TPT and one group (n=5) served as an observation group which was treated and monitored in a different way over an extended period of time. In all treated animals the drug was dissolved in 0.1% DMSO in PBS and injected intraperitoneally. In addition there was a control group (n=5) where mice received injections of the vector DMSO in PBS. For a mouse weighing 20g, a total volume of 100 µl was injected and when mice later weighed up to 30g, the injected volume was 150 µl. The treatment schedule consisted of daily injections over a period of 14-15 days in all groups except the long term observation group. In this specific group mice were treated for an extended period of 40 days and subsequently monitored for another 31-46 days. Two mice from the control group had to be sacrificed earlier than planned because the tumor measurements exceeded humane endpoints of 1.5 cm in diameter according to ethics regulations of GV-SOLAS.

Tumor and organ preparation

Mice were sacrificed after 14-15 days of treatment, except for two control mice with fast growing tumors (sacrificed at day 10) and the long term observation group (n=5). In order to obtain blood by heart puncture terminally, animals were anesthetized with an overdose of 200 mg/kg Ketamin (Pfizer, USA) and 30 mg/kg Xylazin (Bayer, Germany). First, the skin layer covering the thorax was removed in order to have access to the heart from where 0.5-1.0 ml blood was collected. Blood was clotted for 30 min. at RT and further processed by centrifuging for 15 min at 13,000 g and 4°C, then the serum (top phase) was transferred into a new tube and stored at -80°C. The subsequent steps of tumor and organ preparation were all followed by immediately shock freezing tissue pieces in tubes in liquid nitrogen until they were stored in boxes at -80°C. After partly removing skin that covered the whole abdomen area and limbs, the lymph nodes could be dissected and tumors were prepared without any surrounding fat tissue. Tumors were measured and weighed and then cut into pieces of different size in order to have tissue for protein extraction, DNA and RNA isolation, the preparation of cryopreserved tissue sections and formalin fixed and paraffin embedded (FFPE) sections. In addition, tumor touch slides from freshly prepared tumor pieces were

frozen. Whole organs (spleen, kidney and adrenal gland) or parts of organs (liver, lung and skin) were also shock-frozen. Muscle and fat tissue from hind legs were removed in order to have access to the bone. After cutting the edges of the femur and tibia they were placed into a 6-well plate on ice and rinsed with 3 ml 1x PBS in order to collect bone marrow (BM) cells. After transferring the BM to a 15 ml Falcon tube it was centrifuged at 1200 rpm for 5 min. at 4°C and the pellet was resuspended in 1 ml Erylysisbuffer (4.15 g NH_4Cl, 0.5 g $KHCO_3$, 18.6 g EDTA 0.5 M, add dest. water to 500 ml) and incubated for 8 min. at RT. After spinning again at 1200 rpm for 5 min. at 4°C the pellet was resuspended in RPMI 1640 (1x) + GlutaMAX™-I medium (gibco® by life technologies, USA) and 3 cytospins per mouse were prepared and stored at -20°C. The remaining BM cells were dissolved in FCS (PAA, Germany) / 10% DMSO (SERVA, Germany) and stored at -80°C.

Preparation of tissue sections and touched tumor sections

For IF stainings, tissue sections of frozen tumor material were prepared. On a microtome (Leica, Germany) which was cooled to -20°C, tumors were cut into sections of 4 µm thickness and collected on glass slides (Marienfeld, Germany). Depending on the antibody, tumor sections were stained immediately or stored at -20°C for later applications.

For immunohistochemical stainings such as Hematoxylin and Eosin (HE) staining, tissue was fixed in formalin, dehydrated in an alcohol series and embedded in hot paraffin wax, according to standard procedures at the Institute of Cancer Research MUW (Medical University of Vienna). These formalin fixed and paraffin embedded (FFPE) pieces were cut into sections of 5 µm on a microtome (Leica, Germany) and collected on glass slides (Marienfeld. Germany).

For SA-β-Gal stainings, tumor touch slides were used. When tumors were prepared immediately after sacrificing, one piece of tumor tissue was softly touched onto glass slides (Marienfeld, Germany) and frozen at -80°C.

3.2 Immunohistochemical and Immunofluorescence Stainings

Antibodies	Clone/ subtype	Conc.	Company
Ki67 mouse anti-human antibody	MM1 clone	1:100	Novocastra
CD31 rat anti-mouse antibody	murine PECAM-1	1:100	Dianova
Anti-phospho-Histone H2A.X (Ser139) mouse anti-human antibody	JBW301 clone	1:500	Millipore
Rabbit anti-human ATRX antibody	polyclonal	1:200	Sigma-Aldrich
Goat anti-mouse Cy3 antibody	Rhodamine (TRITC)-conjugated	1:500	Dianova
Chicken-anti-rat AF594 antibody	Alexa Fluor 594 labeled	1:1000	Life Technologies
Swine-anti-rabbit FITC antibody	FITC-conjugated	1:50	DAKO

Table 1. Primary and secondary antibodies for Immunofluorescence stainings

Hematoxylin end Eosin staining

FFPE slides were immersed in 1xPBS for 10 sec. and then put into filtrated Hematoxylin solution (Hämalaun according to Mayer, Merck, USA) for 1 min. at room temperature (RT). Afterwards, slides were put into tap water which continuously rinsed them for 8 minutes. After this process of "bluening", the slides were put into Eosin G solution (10 mg/ml, Merck, USA) for 30 min. at RT. For stripping the color, tissue sections were slewed shortly in a series of differently concentrated ethanol solutions ranging from 70%, 95% to 100% alcohol. Alcohol series were followed by 5 min. incubation in xylene in a fume hood at RT and tissue sections were covered with Entellan® mounting medium (Merck, USA) and cover slips.

SA-β-Gal Staining

This staining was performed with the Senescence Detection Kit (Biovision, USA). Tumor touch slides were fixed with app. 300 µl (depending on the surface area of the touch preparations) 1x fixation solution for 12 min. at RT. Meanwhile the staining supplement was preheated to 37°C to dissolve precipitates. 3 ml of staining incubation mix were freshly prepared consisting of 2820 µl of 1x staining solution, 30 µl of staining supplement and 150

µl of X-Gal (20 mg/ml in DMSO). When everything had been added, the solution was brought to 37°C and was titrated with 0.1 M HCl to a pH of 5.0. After washing twice with 1x PBS for 5 min at RT, ß-Galactosidase staining incubation mix (app. 300 µl) was added and incubated at 37°C over night in a humid chamber. On the following day slides were washed twice with 1x PBS for 5 min at RT before counterstainig the touched tumor samples for 3 min. with app. 300 µl DAPI (2 µg/ml, Sigma-Aldrich, USA) at RT. Slides were washed with 1x PBS for 10 min. at RT and the appropriate amount of vectashield (Vector, USA) was added, sections were covered with coverslips and sealed with fixogum (Marabu, Germany).

γH2AX Staining

Fresh sections (4 µm) from frozen tumor tissue were washed with 1x PBS for 5 min. at RT. Afterwards slides were fixed in methanol-acetone (1:1) at −20°C for 5 min. and washed again with 1x PBS for 5 min. at RT. For an additional fixing step, slides were incubated in 4% PFA (Roti®-Histofix 4%, Roth, Germany) for 15 min. at RT and then washed three times with 1x PBS for 5 min. at RT. For permeabilization of the cells, 100 µl of a solution containing 0.1% TritonX-100, 0.1% SDS and 1x PBS were added for 2-4 min. (depending on the tissue) at RT. In order to reduce unspecific signal the tissue was blocked with 5% goat serum (normal, DAKO, Denmark) in a 1% BSA in 1x PBS solution for 30 min. at 37°C in a humid chamber. The primary antibody was a mouse γH2AX antibody (Millipore, USA) in a 1:500 dilution (Table 1) in a solution of 1% goat serum, 1% BSA and 1x PBS and incubation was performed for 1 hour at RT. After washing three times with 1x PBS for 5 min. at RT the secondary goat-anti-mouse Cy3 antibody (Dianova, Germany) was diluted 1:500 in 2% BSA in 1xPBS and incubated for 30 min. at 37°C in a humid chamber. Slides were washed twice with 1x PBS for 5 min. at RT and fixed another time with 4% PFA for 10 min. at 4°C. After washing twice with 1x PBS for 5 min. at RT cells were counterstained with DAPI working solution (2 µg/ml, Sigma-Aldrich, USA) for 3 min. at RT and finally washed with 1x PBS for 10 min. at RT before adding vectashield (Vector, USA) and covering tissue sections with cover slips and sealing the slips with fixogum (Marabu, Germany). Analysis was performed on an Axioplan fluorescence microscope (Zeiss, Austria) and images were acquired and processed with the ISIS software (MetaSystems, Germany).

Ki67 Staining

The staining protocol for Ki67 is the same as for γH2AX except for the primary antibody which is a mouse Ki67 antibody (Novocastra, Germany) at a 1:100 dilution (Table 1).

CD31 Staining

The staining protocol for CD31 is the same as for the γH2AX Staining except for the following modifications: the blocking solution did not contain serum as well as the dilution for the primary antibody. The primary antibody was a rat CD31 antibody (Dianova, Germany) in a 1:100 dilution in 1% BSA in 1x PBS, the secondary antibody was an Alexa Fluor 594 chicken-anti-rat antibody (Life Technologies, USA) in a 1:1000 dilution in 2% BSA in 1x PBS (Table 1). The permeabilization step was skipped since CD31 is a surface antigen.

TUNEL Staining

This staining was performed with the "DeadEnd™ Fluorometric TUNEL System" Kit (Promega, USA). First, slides were fixed with 4% PFA (Roti®-Histofix 4%, Roth, Germany) for 25 min. at 4°C and washed twice with 1x PBS for 5 min. at RT. For permeabilizing the cells, 100 µl of 0.2% Triton-X100 in 1x PBS were added for 5 min. at RT. Slides were washed again twice with 1x PBS for 5 min. at RT and then equilibrated with 100 µl of the corresponding buffer (supplied by Promega, USA) for 8 min. Meanwhile the nucleotide mix and rTdT enzyme were thawed on ice and the incubation buffer mix was prepared. A mastermix for all slides was prepared containing 45 µl equilibration buffer, 5 µl nucleotide mix and 1 µl rTDT enzyme per reaction. An additional solution containing everything but water instead of the enzyme was prepared as a negative control. After adding the incubation buffer to each sample, slides were covered with plastic slips, protected from light with aluminium foil and incubated for 1 hour at 37°C in a humid chamber. Plastic cover slips were removed and slides were washed in 2x SSC for 15 min. at RT, then three times in 1x PBS for 5 min. at RT and counterstained with DAPI (2 µg/ml, Sigma-Aldrich, USA) for 3 min. at RT. Once again slides were washed with 1x PBS for 10 min. at RT and then vectashield (Vector, USA) and glass coverslips were added and sealed with fixogum (Marabu, Germany). Analysis was performed on an Axioplan fluorescence microscope (Zeiss, Austria) and images were acquired and processed with the ISIS software (MetaSystems, Germany).

ATRX Staining

Frozen tumor tissue sections (4 μm) were thawed for 30 min. at 37°C in an incubator and washed with 1x PBS for 5 min. at RT. Slides were incubated in 4% PFA (Roti®-Histofix 4%, Roth, Germany) for 15 min. at RT and then washed three times with 1x PBS for 5 min. at RT. For permeabilization of the cells, 100 μl of a solution containing 0.1% TritonX-100, 0.1% SDS and 1x PBS was added for 3 min. at RT. In order to reduce unspecific signal the tissue was blocked with 5% swine serum (normal, DAKO, Denmark) in a 2% BSA in 1x PBS solution for 30 min. at 37°C in a humid chamber. The primary antibody was a rabbit ATRX antibody (Sigma-Aldrich, USA) in a 1:200 dilution in a solution of 1% swine serum, 2% BSA and 1x PBS and incubation was performed for 1 hour at RT. After washing three times with 1x PBS for 5 min. at RT the secondary swine-anti-rabbit FITC antibody (DAKO, Denmark) was diluted 1:50 (Table 1) in 2% BSA in 1xPBS and incubated for 30 min. at 37°C in a humid chamber. Slides were washed twice with 1x PBS for 5 min. at RT and fixed another time with 4% PFA (Roti®-Histofix 4%, Roth, Germany) for 10 min. at 4°C. After washing twice with 1x PBS for 5 min. at RT cells were counterstained with DAPI working solution (2 μg/ml, Sigma-Aldrich, USA) for 3 min. at RT and finally washed with 1x PBS for 10 min. at RT before adding vectashield without DAPI (Vector, USA) and covering tissue sections with cover slips and sealing the slips with fixogum (Marabu, Germany). Analysis was performed on an Axioplan fluorescence microscope (Zeiss, Austria) and images were acquired and processed with the ISIS software (MetaSystems, Germany).

3.3 Quantification with automated Software

Automated Image Acquisition

Before acquiring images automatically, staining quality was checked and the optimal integration time determined (fixed in FITC and TRITC, automatic in DAPI). Images were then automatically acquired on an Axioplan fluorescence microscope (Zeiss, Austria) equipped with a motor-driven stage combined with an 8-slide-holder (MetaSystems, Germany) with 63x objective in two or three channels (DAPI, FITC and/or TRITC) by a CCD Camera (Axiocam MRm, Zeiss, Austria). For automating this process, a modified version of the Metafer® Software (V 3.8.6., 1998-2011, Metasystems, Germany) was used.

(Semi-)Automated image processing and analysis

For image processing and analysis, an in-house developed software based on Matlab was used. First, 100 images were randomly chosen in the DAPI channel and images that were of low quality, fuzzy or blurred, with cells only at the margins, were excluded. After quality control, images were loaded into the software and analyzed as described for the example of Ki67 staining analysis.

Ki67 Analysis with (semi-) automated software

100-150 images were selected from each sample and then type of segmentation, channels and cell features were chosen for all samples. In the DAPI nucleus channel, the following features were selected for analysis: pixelcount, roundness, nuclei burst, mean intensity, median intensity, position x, position y. In the TRITC (Ki67) nucleus channel, the following parameters were selected for analysis: mean intensity, background intensity, spotcount Ki67. After valid cells had been annotated in order to determine the optimal segmentation parameters, these settings have been applied to all samples and analysis was started. 300 cells were analyzed from each sample.

Ki67 staining patterns depend on the cell cycle phase (Dierendonck *et al.* 1989). Regarding those differential patterns, analyzed cells were allocated into six classes: class 1 was defined as negative cells without big spots, low mean intensity and low standard deviation, so those cells would be regarded as negative for Ki67. Class 2 contains cells with 1-4 big spots and not more than two small, weakly stained spots, which would refer to S and early G2 phase. Ki67 staining pattern for cells in class 3 is defined as sharing 1-4 big spots and several (>2) small spots, which would describe nuclei in G1 phase. Class 4 consists of cells that display several (>2) small spots but no big spots which is the case for cells in the onset of G1. Finally, cells that undergo mitosis would show strong overall positivity and also a typical DAPI pattern and are allocated in class 5. Class 0 only served as an additional group for potential cells that could not be related to any of the classes with the described patterns. The output is given in numbers (% of cells in each class and sample) as well as with graphs that illustrate the distribution of cells into different classes with every sample being represented by one column.

3.4 Quantification with other methods

SA-β-Gal Analysis

This senescence marker was analyzed via optical inspection on an Axioplan fluorescence microscope (Zeiss, Austria). First, the stained slides were pseudonymized which means that a researcher unrelated to the project labeled the slides with random numbers and therefore treatment groups as well as mouse tag numbers were not visible anymore in order to obtain unbiased results. Three independent researchers inspected all slides and noted remarks and the amount of SA-β-Gal positivity in tables. The tables consisted of the following categories: general remarks (e.g. nuclei size, morphology), staining quality (e.g. normal, needles), mouse cells (e.g. 1-3 positive mouse nuclei per area in 40x magnification), human tumor cells (e.g. 10% strongly/weakly stained tumor cells), comment (e.g. repeat), rating (TPT treated or untreated). Tumor samples were allocated into three classes depending on the level of SA-β-Gal positivity: no / low positivity (0-10%), intermediate positivity (10-30%) and high positivity (30-100%). 2 independent preparations per tumor were classified by 3 independent researchers.

CD31 Analysis

Images were acquired using the automatic fluorescent microscope as described above. 30 images were selected randomly from each sample and the degree of vascularization was determined by measuring specific, red fluorescent signal in Image J (Software available on http://rsbweb.nih.gov/ij/download.html). Lengths of CD31 positive blood vessels were measured in pixels, cumulative lengths were calculated for each sample and mean values per treatment group calculated.

TUNEL Analysis

TUNEL positive cells were clearly visible under the Axioplan fluorescence microscope (Zeiss, Austria) as distinctive, green fluorescent signals. Areas of comparable cell density and morphology were selected in the DAPI channel with 63x magnification. TUNEL positive cells were counted manually in five areas and the average of those five fields was calculated. All samples were analyzed by three independent researchers.

3.5 RNA isolation and comparative expression analysis

RNA extraction from tumors

Fresh frozen tumors were put into a petri dish on dry ice and a piece of about 2 x 2 x 2 mm was cut off with a scalpel blade, while thawing of tumor material was avoided. 1ml of cooled Trizol (Invitrogen by Life Technologies, USA) was directly pipetted into a M-tube (Miltenyi Biotec, Germany) for tissue homogenization and the tumor piece was added. Tissue homogenization was performed using the MACS Dissociator (Miltenyi Biotec, Germany) which was programmed for RNA homogenization from frozen tissue ("RNA_02") and the M-tube was installed in an upside-down manner. After finishing the homogenization step, the solution was centrifuged for 1 min. at 13,000 g at 4°C and transferred to a new tube. At that point samples were either stored at -80°C or the protocol for RNA isolation was continued. After adding Trizol, samples were incubated for 10 min. at RT, 200 µl Chloroform (Roth, Germany) were added and tubes had to be shaken and incubated for 3 min. at RT. After centrifuging for 15 min. at 11.000 rpm and 4°C the soluble, top phase was transferred into a new tube and the bottom phase containing DNA and proteins was stored at -80°C for potential protein extraction. 1 µl Glycogen (20 mg/ml, Roche, Switzerland) was added. After adding 500 µl of Isopropanol, tubes were shortly mixed and incubated for 10 min. at RT, centrifuged at 11.000 rpm for 10 min. at 4°C and supernatant was removed. 1 ml 75% Ethanol was pipetted onto the side of the tube, not directly onto the pellet, and the tube was inverted several times and centrifuged at 9.000 rpm for 5 min. at 4°C. After removing the supernatant, pellets were dried for 5 min. at RT and dissolved in 15 µl RNase free water (QIAGEN, Germany) by mixing in a vortex shaker (Vortex Genie 2, Scientific Industries, USA). The RNA concentration was measured on a Nanodrop Spectrophotometer ND-1000 (peqlab Biotechnologie GmbH, Germany) and RNA was either stored at -80°C or subjected to sample preparation for expression arrays.

Determination of RNA quantity and quality

All RNA concentration measurements were performed with the Nanodrop Spectro-photometer ND-1000 (peqlab Biotechnologie GmbH, Germany). Quality analysis of RNA was carried out with the Experion System (Experion RNA StdSens Analysis Kit, Bio-Rad, USA) according to manufacturer´s protocol.

DNAse digest (RQ1 RNase-free DNase Promega Kit)

The starting amount for expression arrays was at least 1500 ng of total RNA with RQI/RIN values of at least 8.0, dissolved in 1-8 µl RNase free water (QIAGEN, Germany) which was transferred into new 0.5 ml RNase-free tubes (DNA loBind tubes, Eppendorf, Germany). Then the following reagents were added to each sample: 1 µl of RQ1 RNase-free DNase 10x reaction buffer, 1 unit/µg RNA of RQ1 RNase-free DNase and the missing volume of RNase-free water to complete the reaction in a final volume of 10 µl. After incubating the reactions for 30 min. at 37°C, 1 µl of RQ1 DNase Stop Solution was added to each sample to terminate the reaction and for DNase inhibition the tubes were incubated for another 10 min. at 65°C.

RNA cleanup and purification

The following volumes were used per reaction, reagents were included in the RNeasy MinElute Cleanup kit (QIAGEN, Germany) if not indicated elsewise. 90 µl RNase-free water were added to the DNase treated RNA (10 µl) and transferred into a new 1.5 ml tube (DNA loBind tubes, Eppendorf, Germany). 350 µl RLT1 buffer were added, mixed by pipetting and another 250 µl absolute Ethanol were added and mixed by pipetting. The total volume of 700 µl was transferred into a MinElute spin column and placed in a 2 ml collection tube. Samples were centrifuged for 15 min. at 10.000 rpm at RT with closed lids and flow-through fractions were discarded. Spin columns were placed in new 2 ml collection tubes and 500 µl RPE2 buffer were added, the lids closed and centrifuged for 15 min. at 10.000 rpm. After discarding the flow-through, collection tubes were reused and 500 µl 80% Ethanol were added to the spin column, centrifuged for 2 min. at 10.000 rpm at RT with closed lid and the flow-through as well as the collection tube were discarded. Spin columns were placed in new 2 ml collection tubes and centrifuged at full speed (13,000 g) for 5 min at RT with open lids. Flow-through fractions and collection tubes were discarded; spin columns were placed in new 1.5 ml tubes and 10 µl RNase free water added directly onto the center of the spin column to elute RNA. Tubes were centrifuged for 1 min. at full speed at RT with closed lids. For measuring RNA concentration, 1 µl was used from each sample, another 100 ng of purified RNA were diluted to 3 µl RNase-free water for expression array analysis.

Gene Expression Analysis Protocol

Protocols were performed according to the manufacturer's manual from the Primeview Expression Kit ("Gene Chip 3'IVT Express Kit" by Affymetrix, USA).

First, poly-A RNA controls had to be prepared: 38 µl of thawed and cooled Poly-A Control Dilution (Dil.) Buffer were added to a 0.5 ml non-stick RNase-free microfuge tube. Poly-A RNA controls were diluted in a 1:50 manner as follows: 2 µl of Poly-A Control Stock were added to the microfuge tube containing buffer, mixed and spun down. 98 µl of Poly-A Control Dil. Buffer were added to a new 0.5ml non-stick RNase-free microfuge tube. 2 µl of the first 1:50 dilution was added to the second tube, mixed and spun down. This was repeated another time and for the last dilution 18 µl of Poly-A Control Dil. Buffer were pipetted into a new 0.5 ml non-stick RNase-free microfuge tube and 2 µl of the third dilution was mixed with it and spun down. 2 µl of the last dilution were added to the tubes containing 100 ng RNA so the reaction had a total volume of 5 µl.

First and second strand cDNA synthesis were performed as follows: First strand synthesis reagents were thawed on ice and the first strand master mix (FSMM) pipetted together consisting of 4 µl first strand buffer mix and 1 µl first strand enzyme mix, everything was vortexed and centrifuged for 5 sec. at 5.000 rpm and RT. PCR tubes (from the Affymetrix Kit) were placed on ice and 5 µl of FSMM and 5 µl RNA and poly-A control mix added to each tube, vortexed and spun down. Samples were incubated for 2 hours at 42°C, spun down and placed on ice. The second strand master mix (SSMM) consisting of 13 µl RNase-free water, 5 µl second strand buffer mix and 2 µl second strand enzyme mix was pipetted together, vortexed and centrifuged for 5 sec. 20 µl of SSMM were added to each first strand cDNA sample and mixed by flicking the tube 4 times, then centrifuged for 5 sec. and placed on ice. Reactions were incubated for 1 hour at 16°C and for 10 min. at 65°C, centrifuged for 5 sec. and placed on ice.

For the *in vitro* transcription (IVT) the IVT master mix (IVTMM), consisting of 4 µl IVT biotin label, 20 µl IVT labeling buffer and 6 µl enzyme mix, was pipetted together, vortexed and briefly centrifuged for 5 sec. 30 µl of IVTMM were added to each double-strand cDNA sample, vortexed and centrifuged for 5 sec. In a total volume of 60 µl per reaction the tubes were incubated for 16 hours at 40°C and then placed on ice.

The next step was the purification of aRNA and to that aim aRNA Elution Solution aliquots (50 μl per sample) were preheated to 50°C for 10 min. For every sample the aRNA binding Mix was prepared, containing 10 μl RNA binding beads and 50 μl aRNA binding buffer, and 60 μl of the mix were added to each tube. Every sample was transferred to one well of a U-bottom plate and mixed by pipetting up and down several times. After adding 120 μl of 100% Ethanol samples were again mixed by pipetting up and down and the whole plate was fixed on a Thermomixer (Thermomixer compact, Eppendorf, Germany) which was shaking for 2 min. at 400 rpm. After shaking, the plate was put onto a magnetic stand and magnetic beads were captured for 5 min. the supernatant was carefully discarded and the plate removed from the magnetic stand. After adding 100 μl aRNA wash solution, samples were shaking for 1 min. at 800 rpm and the plate again moved to the magnetic stand to capture the RNA binding beads for 5 min., the supernatant was discarded and the plate removed. The steps from adding aRNA washing solution, shaking and capturing the beads was repeated another time. Afterwards the plate was placed onto a shaker and samples were shaking for 1 min. at 11.000 rpm. 50 μl of preheated (50-60°C) aRNA Elution Solution were added, samples were shaking on a plate for at least 3 min. at 11.000 rpm until beads were fully dispersed. The plate was moved to the magnetic stand, RNA binding beads were captured and supernatants were transferred to new nuclease-free PCR tubes, placed on ice and 1 μl was used for concentration measurement on the Nanodrop Spectrophotometer ND-1000 (peqlab Biotechnologie GmbH, Germany). Fragmentation of labeled aRNA was carried out by adding 6.4 μl of 5x Array Fragmentation buffer to 12 μg aRNA and adding the missing volume of water (supplied by Affymetrix, USA) to receive a final reaction volume of 32 μl. Samples were then incubated for 35 min. at 94°C and placed on ice.

The last step which was carried out in-house was the preparation of the hybridization cocktail in order to target hybridization for cartridge arrays. The cocktail for the 100 Midi Format had a total volume of 200 μl consisting of 10 μg (26.7 μl, respectively) aRNA, 3.3 μl Control Oligonucleotide B2 (3nM), 10 μl 20x Hybridization Controls (bioB, bioC, bioD, cre), 100 μl 2x Hybridization Mix, 20 μl DMSO and 40 μl Nuclease-free water. Samples were either stored at -20°C or immediately brought to the Genomics Core Facility (M. Bilban) at the Anna Spiegel Institute, MUW Vienna, where they were hybridized and scanned.

3.6 Bioinformatics and statistical analysis

Bioinformatics were performed by Maximilian Kauer, CCRI, as follows: CEL files from Affymetrix Primeview arrays were further processed in R statistical environment using Bioconductor packages (Gentleman et al., 2004). Summarized log2 probe set signals were calculated by using RMA (Irizarry et al., 2003). Subsequently the most variable (across all samples) probe set was chosen for each gene for further analysis. Differential expression between groups of samples was determined using the limma package (Smyth, 2004).

Statistical analysis of quantitative evaluations included the calculation of mean values and standard deviations, T-tests, One-Way Analysis of Variance and One-way ANOVA tests with subsequent Bonferroni´s Multiple Comparison Test. Significant values were $p < 0.05$ (*), $p < 0.01$ (**) or $p < 0.001$ (***).

4. Results

4.1 Low-dose TPT treatment reduces tumor growth and alters tumor composition

It was intented to inhibit tumor growth by the administration of low-dose TPT and concomitantly observe if this was accompanied by the induction of senescence. Since TPT has been known to reduce tumor growth *in vivo* at high doses, it was affirmative, noting that tumors disappeared after 2 weeks of treatment with a daily dose of 1 mg/kg. This observation had been made in an earlier experiment and therefore lower doses were used in the study at hand.

Tumors were monitored throughout the whole experiment twice a week by measuring tumors from outside in three axes (x,y,z) as well as when tumors had been prepared at the endpoint. All tumors were growing in the same way after tumor cell inoculation over a period of 17 days, after treatment started untreated animals and those belonging to very low-dose TPT treatment (0.01/0.03 mg/kg/d) showed a steep increase in tumor size. Tumor growth of animals treated with 0.1 mg/kg/d TPT, in contrast, declined or stagnated until the endpoint after two weeks treatment (Fig. 6). Mean sizes of 0.1 mg/kg/d TPT treated tumors (0.25 ± 0.17 cm^3) were lower than mean sizes of untreated (1.32 ± 1.59 cm^3) and very-low-dose (0.01 and 0.03 mg/kg/d) TPT treated tumors at the endpoint (1.00 ± 0. 71 cm^3 and 0.64 ± 0.29 cm^3, respectively).

Fig. 6 I Tumor growth curves. Tumors were measured twice a week from outside and directly at the endpoint (x,y,z axis). CTRL refers to untreated tumors, TPT 0.01/0.03/0.1 refers to daily doses in mg Topotecan per kg of body weight. The orange, dotted line indicates the start of treatment; the black, dotted line indicates the endpoint. Mean sizes and standard deviations (arrow bars) are shown for CTRL (n=5), TPT 0.01 (n=12), TPT 0.03 (n=10) and TPT 0.1 (n=10) tumors. Standard deviations are shown as error bars, * $p < 0.05$.

In order to see whether prolonged treatment would lead to a complete tumor regression, mice were treated over a period of additional 25 days (40 days in total) and tumors were subsequently monitored for up to 25 days without TPT administration. In this case, when treatment was stopped there were small tumors palpable in 2 out of 5 animals and no tumors palpable in 3 out of 5 mice. Tumors developed again but the onset of growth was delayed for 20 days (Fig. 7)

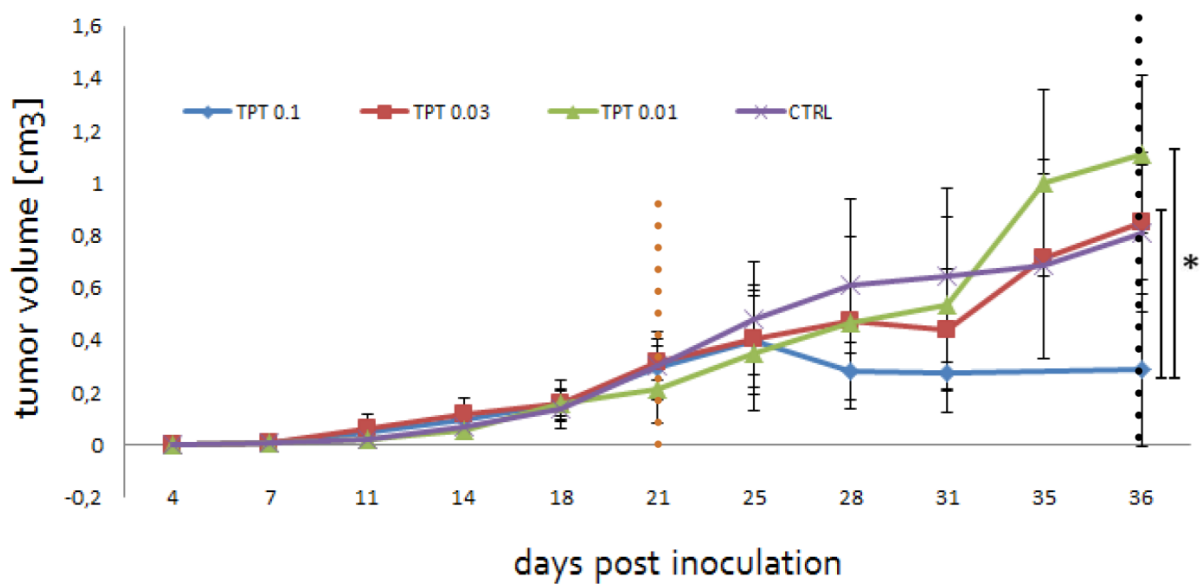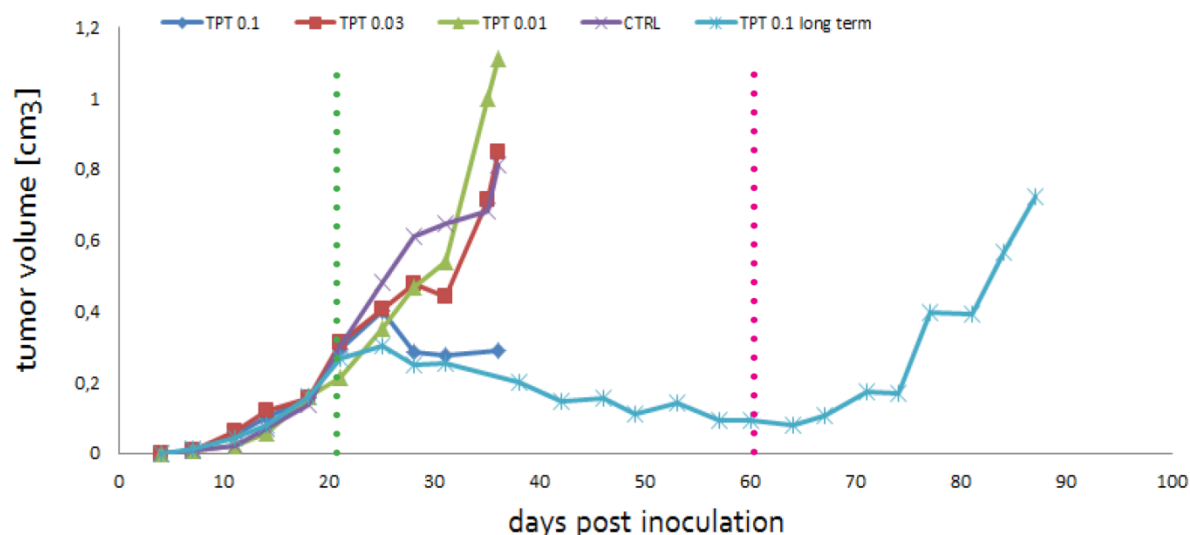**Fig. 7 I Tumor growth including long term treatment group.** Tumors were measured twice a week from outside and directly at the endpoint (x,y,z axis). CTRL refers to untreated tumors, TPT 0.01/0.03/0.1 refers to daily doses in mg Topotecan per kg of body weight. The green, dotted line indicates the start of treatment on day 21 after inoculation, the pink, dotted line indicates the end of treatment on day 60 after inoculation. Mean sizes are shown for CTRL (n=5), TPT 0.01 (n=12), TPT 0.03 (n=10), TPT 0.1 (n=10) and TPT 0.1 long term (n=6) tumors.

Mean sizes of tumors at the endpoint of the experiment revealed an explicit dose-dependent manner of tumor-growth inhibition by TPT treatment. While untreated control tumors showed a wide range of sizes (1.32 ± 1.42 cm^3), all TPT dose-groups shared very similar results within their respective treatment groups. For tumors treated with 0.1 mg/kg/d TPT sizes were 0.25 ± 0.16 cm^3, for tumors treated with 0.03 mg/kg/d TPT sizes were 0.64 ± 0.28 cm^3, for tumors treated with 0.01 mg/kg/d TPT sizes were 1.00 ± 0.68 cm^3 and the long term treatment and observation group showed a measured mean of 0.83 ± 0.39 cm^3. It is important to point out that 2 out of 5 untreated animals had to be sacrificed earlier as tumors had reached the endpoint criteria of 1.5 cm in diameter. In the long term treatment and observation group, animals were sacrificed according to the previously defined endpoint criteria of tumor size, or 46 days after treatment was terminated at the latest, respectively.

Fig. 8 I Tumor sizes at endpoint measured in cm3. Tumors were measured after they had been prepared. CTRL refers to untreated tumors, TPT 0.01/0.03/0.1 refers to daily doses in mg Topotecan per kg of body weight. Statistical significance is indicated, * p value < 0.05, ** p value < 0.01, *** p value < 0.001. Long term treatment group is not shown.

In line with tumor sizes of different treatment groups (Fig. 8) also weights of tumors (Fig. 9) presented a dose-dependent manner of tumor growth inhibition. The fact that tumors that had been treated with 0.1 mg/kg/d TPT had reduced their weight to 0.35 ± 0.26 g, was assuring for the aim to inhibit tumor growth but on the other hand this led to a very small amount of tumor material left for further analysis.
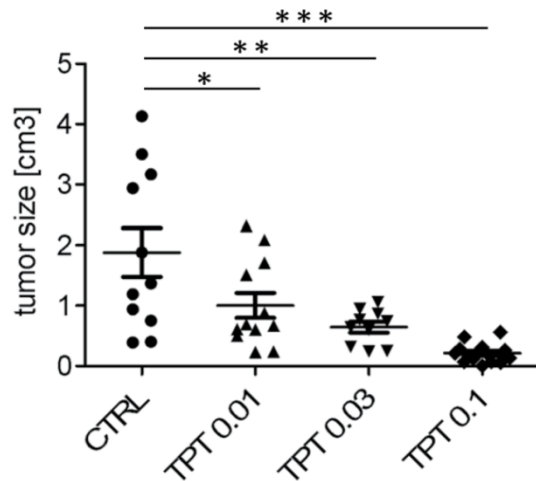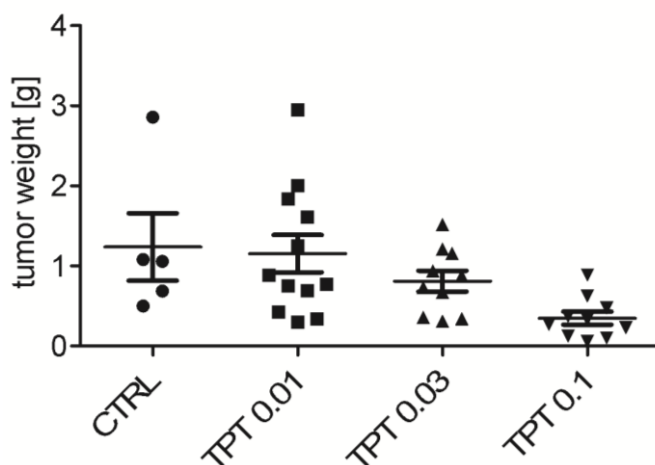

Fig. 9 I Tumor weights at endpoint measured in gramm. Tumors were weighed after they had been prepared. CTRL refers to untreated tumors, TPT 0.01/0.03/0.1 refers to daily doses in mg Topotecan per kg of body weight.

Along with the finding that 0.1 mg/kg/d TPT treated tumors were a lot smaller and lighter than tumors from very-low-dose TPT treated and untreated animals, we could also observe a distinct appearance of those tumors. While in CTRL and 0.01 mg/kg/d TPT treated mice Ecchymosis, bleedings in tumor-surrounding subcutaneous fat tissue, were observed even if tumors were small, 0.1 mg/kg/d TPT and also 0.03 mg/kg/d TPT treated mice showed lower extents of blood coagulates surrounding the tumor site. Another observation in the control group are animals which developed a large tumor and a splenomegaly which could indicate aberrant production of blood cells in the spleen.

For a more thorough look at the composition and morphology of tumors, pieces were fixed in formalin and embedded in paraffin wax. These FFPE pieces were dissected into tissue sections of 5μm thickness and were stained for hematoxylin and eosin (HE, Fig. 10). This staining allows an estimation of the content and morphology of tumor cells, areas of connective tissue and infiltrating blood cells of murine origin. Untreated tissue (Fig. 10, top panel) was quite homogenous compared to TPT treated samples and showed more blood vessels. In 0.1 mg/kg/d TPT treated animals, the heterogeneity was the strongest, also within same samples. The sizes and shapes of nuclei varied a lot and there were lots of mouse cells infiltrating the tumor tissue. The most distinct group was the long term treatment and observation group which had received 0.1 mg/kg/d TPT until tumors had nearly disappeared or completely regressed. All six tumors reappeared. HE staining of these tumors revealed a different pattern from all the other groups. The long term group showed massive areas of necrosis and a low number of viable tumor cells (Fig. 10, bottom panel).
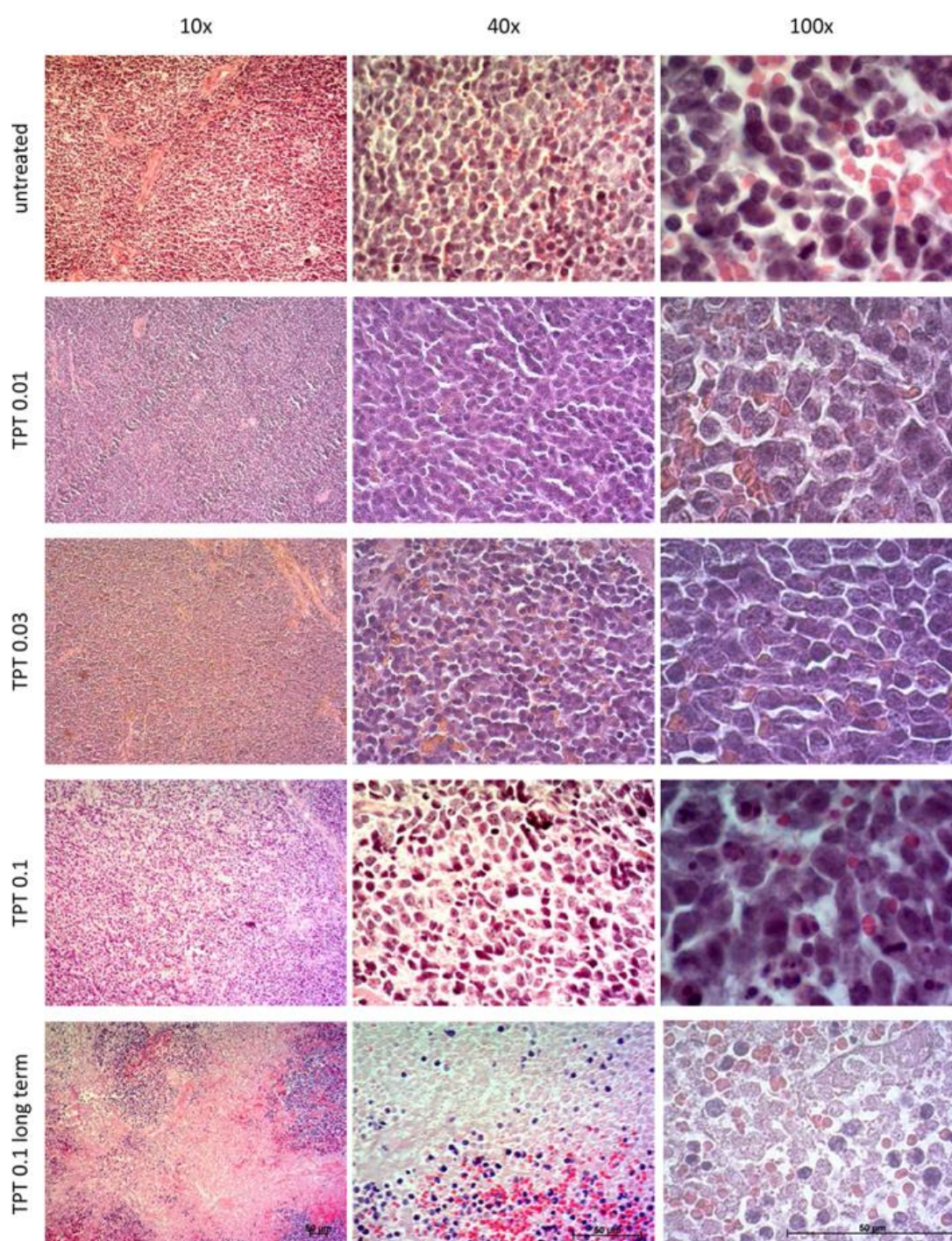
Fig. 10 l HE staining on FFPE tumor sections. FFPE tumor pieces were cut into 5μm sections and stained for HE. Untreated refers to untreated control tumors, TPT 0.01/0.03/0.1 refers to daily doses in mg Topotecan per kg of body weight. Nuclei are shown in dark violet/blue, eosinophilic structures are shown in pink/red/orange. Selected samples are all shown with 10x, 40x and 100x lens, scale bars in the bottom panel are 50 μm of length.

4.2 Low-dose TPT treatment selectively induces tumor cell senescence

The main aim of this study was the induction of senescence in tumors in order to study the beneficial and unfavorable effects of therapy-induced senescence and exploit this as a beneficial feature in this NB xenotransplant setting.

First, it was important to determine if and to which extent senescence could be induced by TPT in xenotransplanted NB tumors. This was analyzed with senescence-associated-β-Galactosidase (SA-β-Gal) staining on tumor touch slides. SA-β-Gal is a widely used marker for cellular senescence (as described in the Introduction chapter in detail) and if cells are stained at pH 5.0, the products of the enzymatic reaction are visible as blue precipitates. Since the tumor samples in this study were xenografts of human cells in mice, it was important to distinguish between SA-β-Gal positive human and SA-β-Gal positive murine cells. To enable this distinction, samples were counterstained with DAPI in order to visualize nuclei and see which SA-β-Gal precipitate belonged to which cell nucleus. Murine nuclei show a distinct appearance and display intensively stained heterochromatic blocks within their dark blue nuclei while human NB tumor cells are typically larger than mouse cells and show a more homogenous, blue DAPI staining and 2-3 prominent nucleoli (Fig 11 B). Senescence was induced in the 0.1 mg/kg/d TPT treatment group in a strong way (Fig. 11 A). In all other groups, there was no or low positivity of SA-β-Gal in tumor cells (for detailed analysis, see Fig. 12). In order to assure staining quality, only those images were selected for evaluation that showed at least one positive cell. In the untreated and the TPT 0.01/0.03/0.1 long term groups only few positive mouse cells were visible but tumor cells were negative or only a small proportion (<10%) was positive.
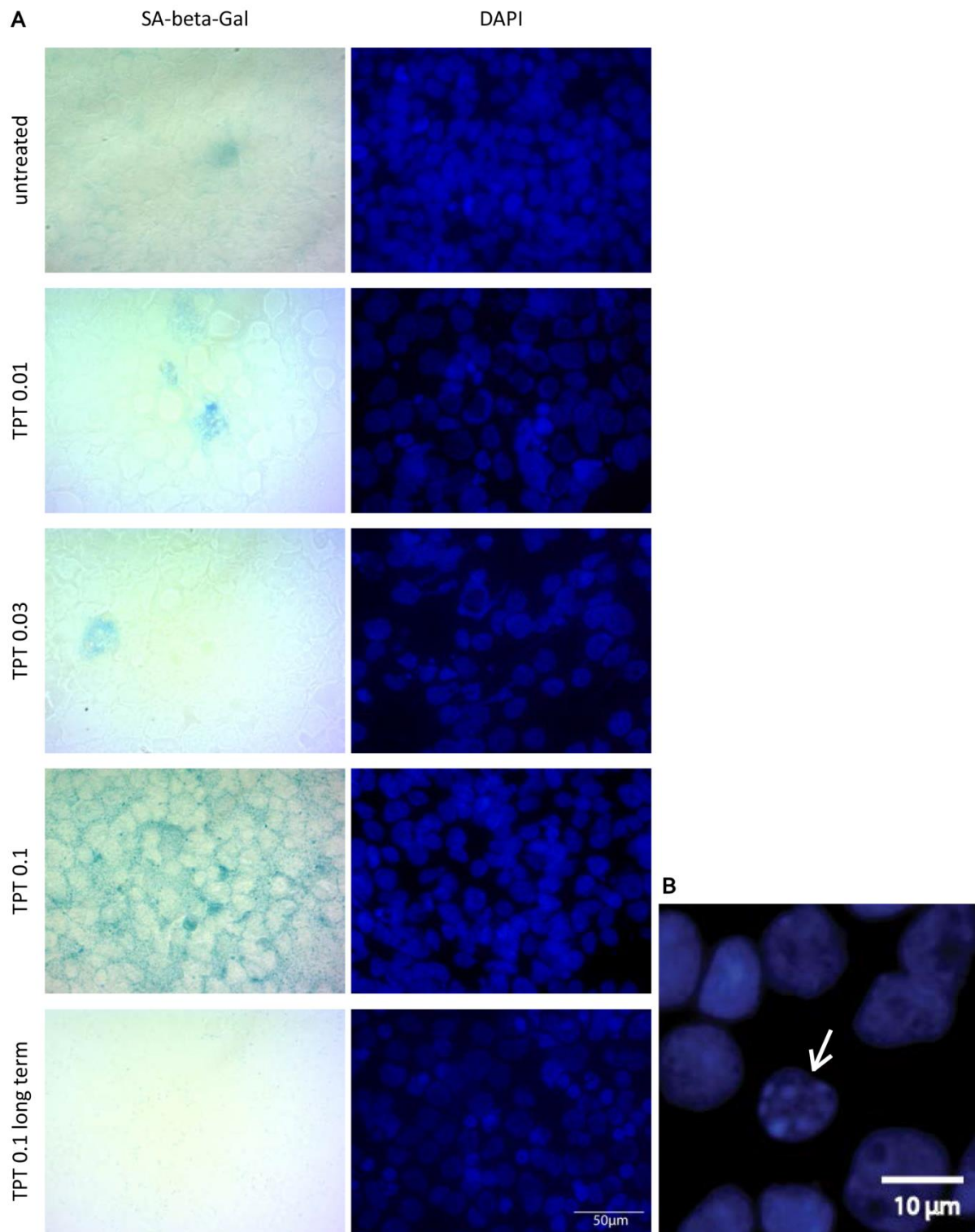
Fig. 11 I Senescence-associated-β-Galactosidase staining on tumor touch slides. A) Touched tumor preparations on glass slides were stained for SA-β-Gal at pH 5.0 to detect senescent cells (shown as blue precipitates) and DAPI as a nuclear counterstain (shown in dark blue). Untreated refers to untreated control tumors, TPT 0.01/0.03/0.1 refers to daily doses in mg Topotecan per kg of body weight. Individual SA-β-Gal positive mouse cells are shown in the top three panels. B) Cells are stained for DAPI. A mouse cell is shown in the center compared to tumor cells surrounding it (white arrow).

48

To quantify SA-β-Gal positivity, samples were analyzed by three different researchers independently and the amount of positive tumor cells was estimated and noted. The staging system consisted of three classes: now or low positivity (0-10%), intermediate positivity (10-30%) and high positivity (30-100%) of tumor cells. In the CTRL group, 7 out of 8 tumors (85.7%) showed no or low SA-β-Gal positivity while one tumor showed intermediate activity. In the 0.01 mg/kg/d TPT and 0.1 mg/kg/d TPT long term groups, 100% of the tumors showed no or very low SA-β-Gal positivity. In the 0.03 mg/kg/d TPT treatment group 6 out of 8 tumors (75%) showed no to low positivity while 2 out of 8 tumors (25%) displayed intermediate visual activity of the enzyme. The most distinct group consisted of the 10 tumors that had been treated with 0.1 mg/kg/d TPT, where 6 showed 10-30% positivity and 4 samples even 30-100% positivity. Taken together, senescence could be evoked via TPT treatment in a dose range that would be considered as low (0.1 mg/kg/d) but not in samples of very low-doses (0.01/0.03 mg/kg/d) (Fig. 12).

As expected the CTRL tumors did not display high amounts of SA-β-Gal positivity, neither there were significant levels of positive tumor cells detected in the TPT long term treatment and in the observation group. The analysis revealed intermediate to high SA-β-Gal positivity in all tumor samples that had been treated with 0.1 mg/kg/d TPT representing the strongest induction of senescence throughout all groups.

Although SA-β-Gal is a common marker for cellular senescence, it was attempted to assure that tumor cells were really senescent via other methods too. More information about the application of other markers and indications can be found in the Discussion chapter.
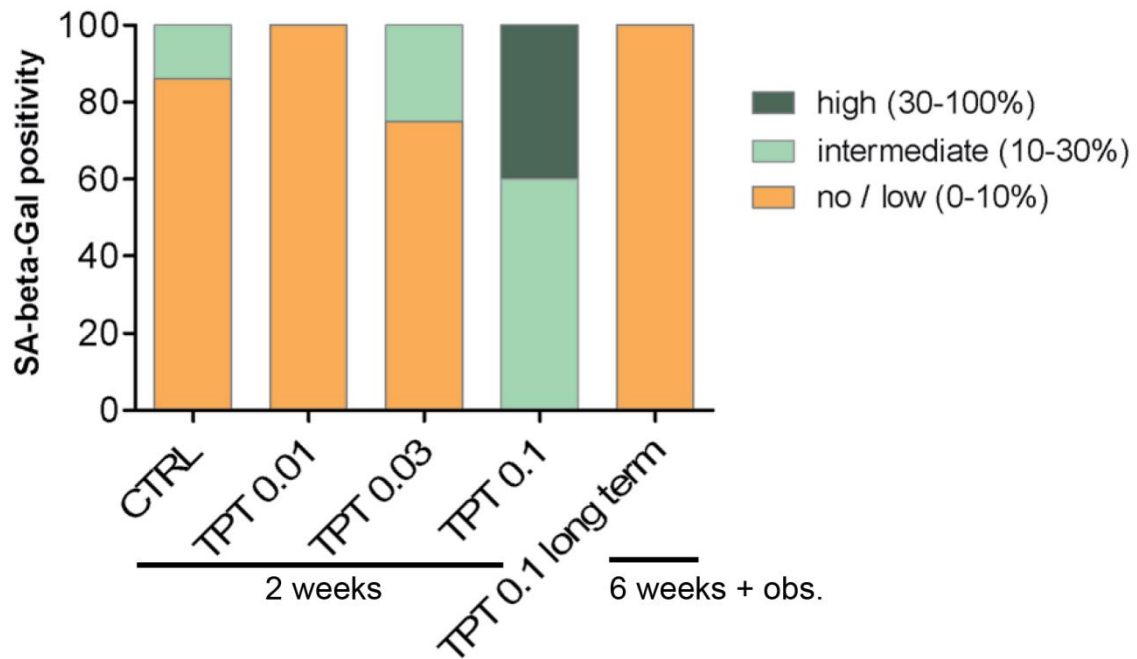
Fig. 12 l Analysis of Senescence-associated-β-Galactosidase stainings. Based on the amount of SA-β-Gal positive tumor cells, samples were allocated into different classes of positivity (no or low=0-10%, intermediate=10-30%, high=30-100%). The composition of different treatment groups is shown concerning their classes of positivity: for CTRL (n=7), TPT 0.01 (n=9), TPT 0.03 (n=8), TPT 0.1 (n=10) and TPT 0.1 long term (n=6) tumors. CTRL refers to untreated tumors, TPT 0.01/0.03/0.1 refers to daily doses in mg Topotecan per kg of body weight.

4.3 TPT treatment increases levels of apoptosis in xenotransplant NB-tumors

To learn more about the mechanisms of TPT treatment at low concentrations, additional cellular pathways were investigated. First, we analyzed whether apoptosis was also induced via TPT treatment. To this end, samples were stained with a TUNEL Kit where DNA 3´ ends of apoptotic cells are labeled with green fluorescent dye. This staining gave a strong, explicit signal for fragmented DNA in apoptotic cells and it was easy to detect TUNEL positive cells within tumor cell tissue (Fig. 13). In untreated tumor samples (19.3 ± 10.6 positive cells/image) and 0.01 mg/kg/d TPT treated tumors (22.1 ± 3.3 positive cells/image), the amount of apoptotic cells was about the same whereas the amount was twice as much in 0.03 mg/kg/d TPT (45.9 ± 22.0 positive cells/image) and 0.1 mg/kg/d TPT treated tumors (41.6 ± 8.1 positive cells/image). The most distinct group was the long term treatment (0.1 mg/kg/d TPT) and the observation group in which some areas displayed nearly 100% positivity (shown in Fig. 13, bottom panel). However, the overall positivity was about the same as in the 0.03 and 0.1 mg/kg/d TPT groups (Fig. 14). Nonetheless, it was still intriguing how strongly apoptotic some areas appeared and in context with the massive necrosis in the same tumors it was an interesting observation to find rather fast growing tumors with such immense areas of dead or degrading cell material at the same time.
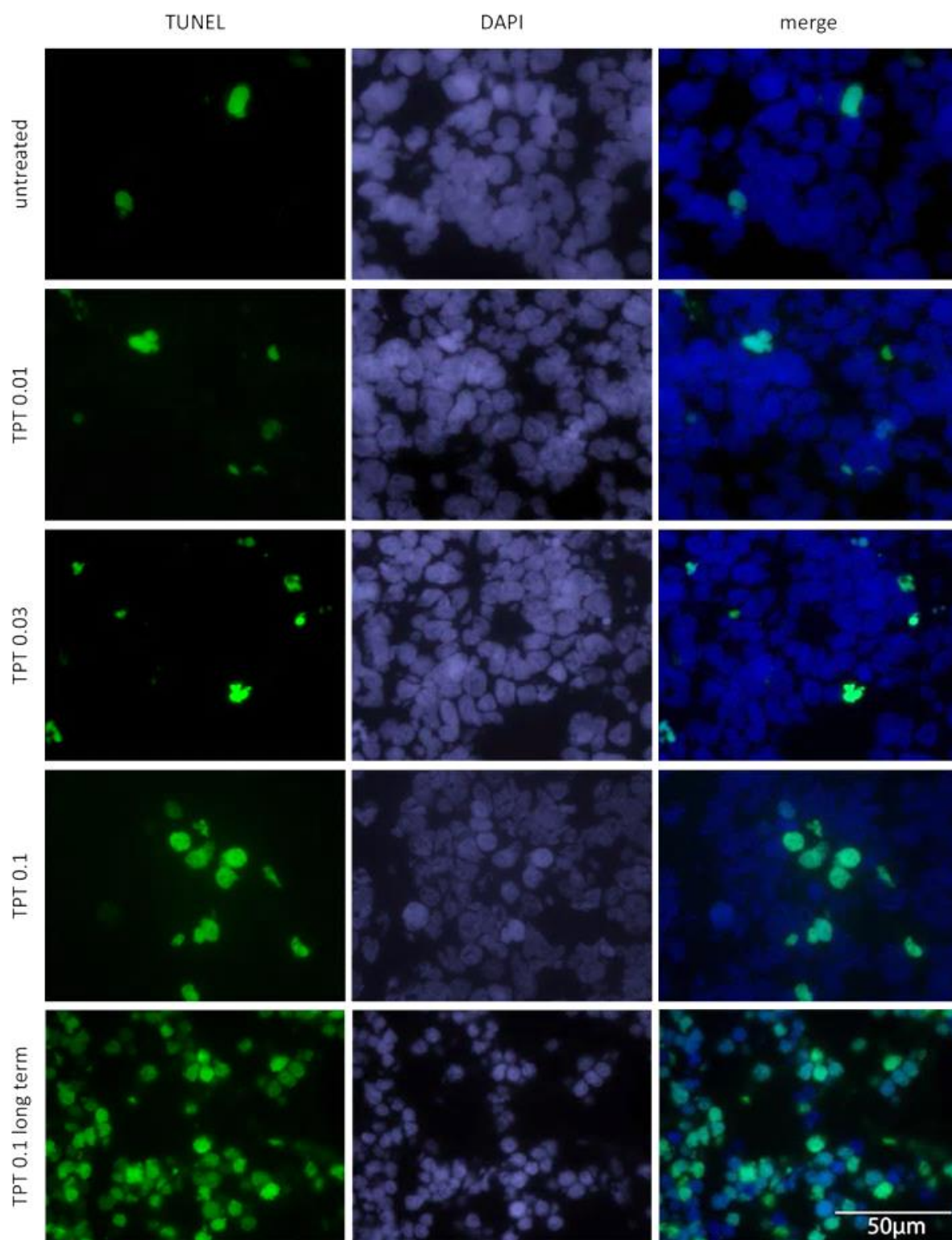
Fig. 13 | Apoptosis in tumors, shown by TUNEL stainings. Apoptotic cells are shown in the TUNEL-labeled column, counterstained nuclei are shown in blue in the DAPI column. Untreated refers to untreated control tumors, TPT 0.01/0.03/0.1 refers to daily doses in mg Topotecan per kg of body weight.

While there was no significant increase of apoptotic cells observed in 0.01 mg/kg/d TPT treated tumors compared to untreated control samples, higher doses (0.03/0.1 mg/kg/d) of TPT induced significantly higher apoptosis rates (p<0.01) in tumors (Fig. 14).
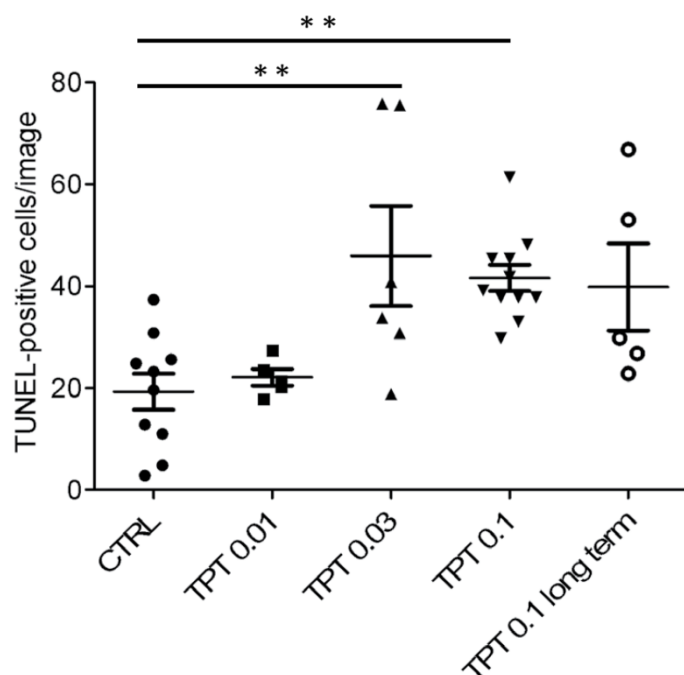
Fig. 14 I Analysis of apoptosis in tumors by counting TUNEL positive cells. Cells were counted manually under 100x lens in a fluorescent microscope by three independent researchers. Areas of comparable cell density were chosen and number of positive cells per image were recorded. CTRL refers to untreated tumors, TPT 0.01/0.03/0.1 refers to daily doses in mg Topotecan per kg of body weight. ** p value < 0.01.

In context with the previously performed SA-β-Gal staining (Fig. 11) and evaluation (Fig. 12) it became obvious though, that even if apoptosis was increased in 0.1 mg/kg/d TPT treated tumors, the predominant pathway which was active in those cells was the senescence program.

4.4 Proliferation pattern is altered in TPT treated tumors

Even though the tumor size declined when treated with TPT (depending on the dose used) it was not clear whether mechanisms, in addition to senescence, would contribute to this decrease. A proportion of tumor cells could still be proliferative active. Therefore, the proliferation patterns were analyzed via Ki67 staining. In untreated as well as TPT treated tumors there was a specific staining visible in all samples (see Fig. 15). Ki67 displays different staining patterns, depending on the phase of the cell cycle the cell is currently passing, so it is of importance to distinguish the type of staining. In untreated tumors, for example, there were several cells that show mitosis (top panel, Fig. 15) while the amount of those cells was lower in 0.1 mg/kg/d TPT treated tumor cells (fourth panel, Fig. 15). In contrast, in 0.1 mg/kg/d TPT treated tumors most of the Ki67 positive cells had the specific staining confined to nucleoli and not distributed all over the nuclei (fourth panel, Fig. 15).

For quantitatively evaluating the Ki67 staining, a specific in-house developed, Matlab-based software was in use. There are softwares commercially available which detect nuclear stainings and measure the amount of fluorescent signal based on microscope images. However, we had some specific requirements to optimize the analysis concerning segmentation and other parameters (e.g. Ki67 staining patterns). Therefore the in-house tailor-made Software "Advanced Nucleus Analyzer Utility" (ANAU) was used. After acquiring images on an automated microscope, they were analyzed concerning mean and median intensity, background intensity, Ki67 staining pattern and other parameters (for details see Material and Methods). The crucial feature of this program is the allocation of cells to Ki67 staining classes. This allowed the estimation of proliferative activity in each sample. Class 1 was defined as negative cells without big spots, low mean intensity and low standard deviation, so those cells would be regarded as negative for Ki67 and cells being in G0 phase of the cell cycle. Class 2 contains cells with 1-4 big spots and not more than two small, weakly stained spots, which would refer to S and early G2 phase. The Ki67 staining pattern for cells in class 3 is defined as sharing 1-4 big spots and several (>2) small spots, which would describe nuclei in G1 phase. Class 4 consists of cells that display several (>2) small spots but no big spots which is the case for cells in the onset of G1. Finally, cells that undergo mitosis would show strong overall positivity and are allocated in class 5. Class 0

only served as an additional group for potential cells that could not be related to any of the classes with the described patterns.
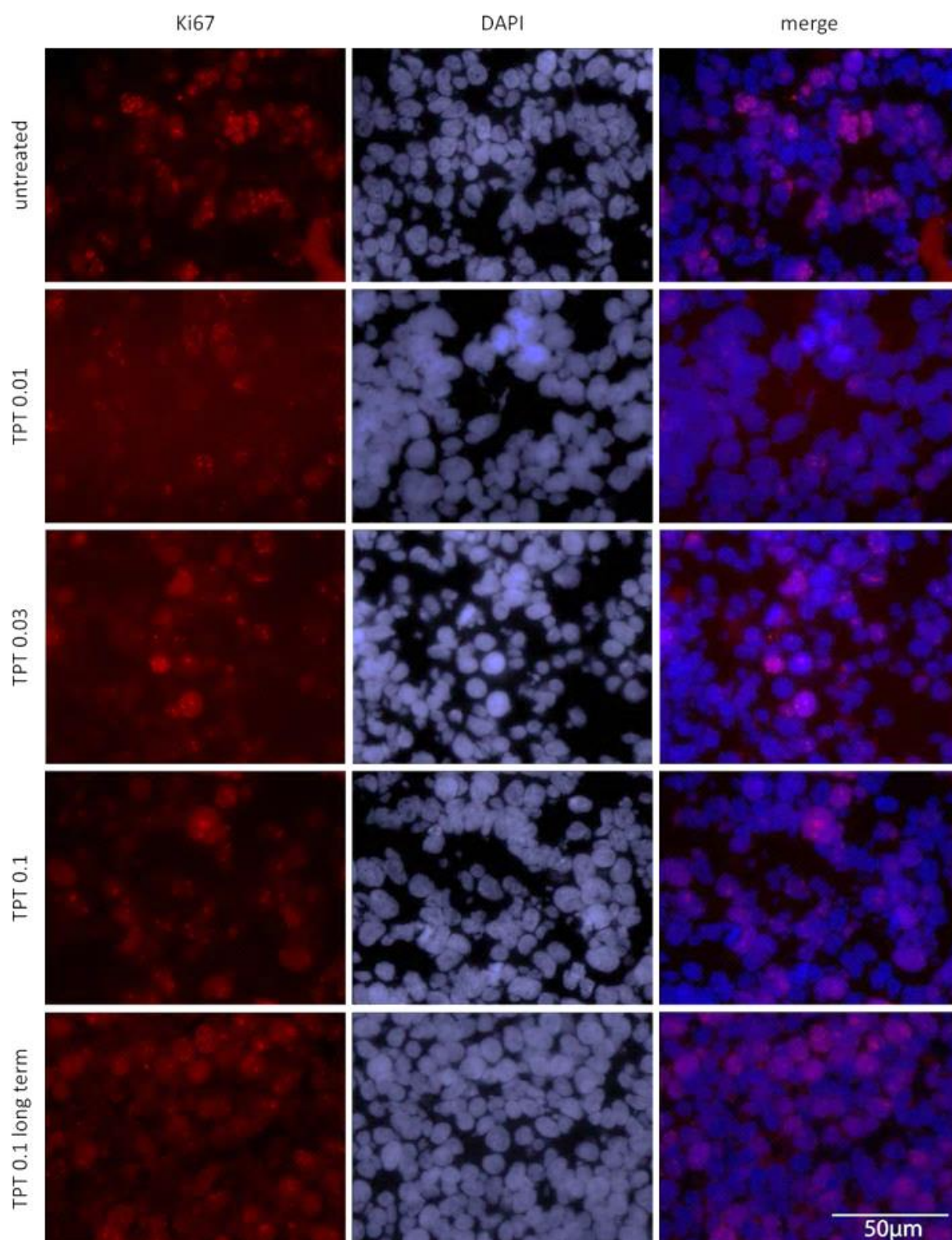
Fig. 15 | Proliferation in tumors, shown by Ki67 stainings. Proliferating cells are shown in the Ki67-labeled column, counterstained nuclei are shown in blue in the DAPI column. Untreated refers to untreated control tumors, TPT 0.01/0.03/0.1 refers to daily doses in mg Topotecan per kg of body weight.

A
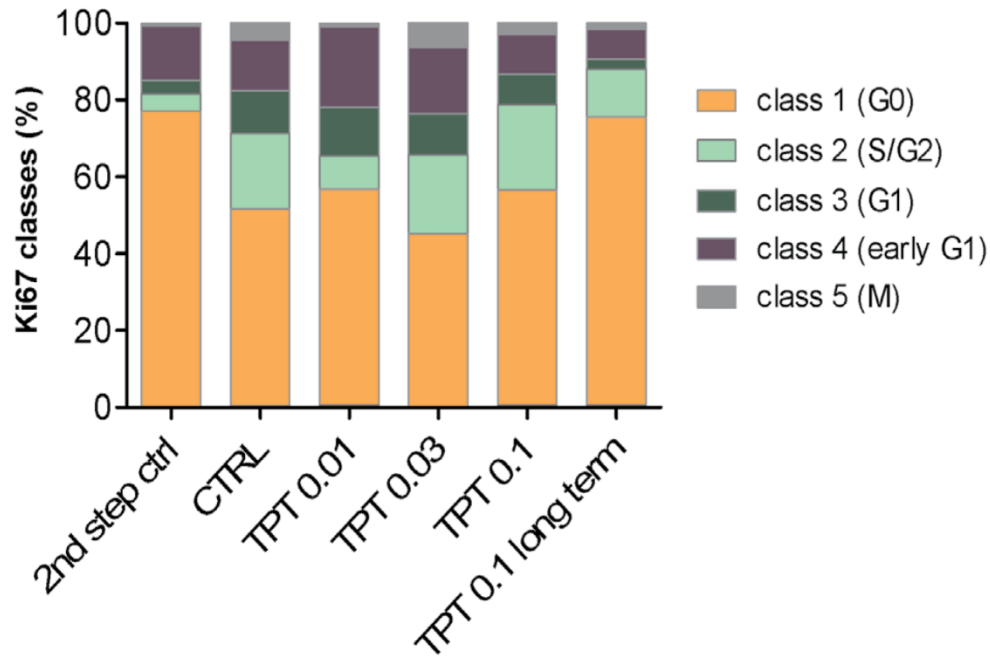
B

	2nd step ctrl	CTRL	TPT 0.1
class 0	0.32 ± 0.20	0.39 ± 0.48	0.54 ± 0.28
class 1	76.68 ± 23.08	51.32 ± 14.32	56.12 ± 5.58
class 2	4.61 ± 3.75	19.47 ± 4.20	22.11 ± 6.67
class 3	3.51 ± 5.16	11.26 ± 9.08	7.92 ± 4.25
class 4	14.12 ± 12.75	13.07 ± 5.74	10.46 ± 6.10
class 5	0.75 ± 1.50	4.49 ± 5.88	2.85 ± 4.46
	TPT 0.03	**TPT 0.01**	**TPT 0.1 long term**
class 0	0.06 ± 0.12	0.64 ± 0.49	0.56 ± 0.31
class 1	45.17 ± 23.03	56.26 ± 13.44	75.07 ± 11.17 *
class 2	20.51 ± 11.20	8.51 ± 1.79	12.46 ± 5.34
class 3	10.60 ± 6.06	12.63 ± 6.05	2.50 ± 1.55
class 4	17.36 ± 3.76	21.11 ± 6.58	7.79 ± 3.81
class 5	6.31 ± 6.64	0.84 ± 0.80	1.62 ± 1.30

Fig. 16 I Analysis of proliferation in tumors by analyzing Ki67 positive cells. Images were acquired with automated microscopy and cells analyzed on a Matlab-based in-house developed software (A). Software analysis was performed for 5 tumors from each treatment group. The given results are mean values from all 5 samples and show the distribution from cells over all classes of Ki67 staining patterns in percent, including standard deviation (B). 2nd step ctrl refers to a tumor slide without Ki67 antibody which serves as a background control, CTRL refers to untreated tumors, TPT 0.01/0.03/0.1 refers to daily doses in mg Topotecan per kg of body weight. * $p < 0.05$, significant compared to CTRL sample.

In untreated controls, the amount of negative cells (class 1) was lower than in all TPT treated tumors, except for the group that had received 0.03 mg/kg/d TPT (Fig. 16). In contrast, the amount of mitotic cells was higher in untreated samples compared to TPT treated groups, except for the 0.03 mg/kg/d TPT dose group. Taking a closer look at class 4 (several small spots, but no big spots and no mitosis), it can be doubted that the software reliably allocated all cells properly because of the high percentage of class 4 cells in the 2nd step control (14.12 ± 12.75%). Concerning negative cells, the most striking difference happened to be in the long term treatment and observation group (TPT 0.1 long term), where 75.07 ± 11.17 % of cells were Ki67 negative, which means that the number of cells in Go phase was significantly lower compared to untreated control samples (Fig. 16 B).

If comparing only untreated and 0.1 mg/kg/d TPT treated tumors, there is a tendency towards lower proliferation rates in all positive classes (class 2-5) in 0.1 mg/kg/d TPT treated samples and the long term TPT treatment group (Fig. 16 A). In comparison with untreated samples, both 0.1 mg/kg/d TPT groups show less positive cells in S and early G2 phase, in mitosis, as well as G2 phase. This would indicate a decrease in proliferation levels in a low-dose range of TPT treatment, but very low doses did not seem to efficiently inhibit proliferation. The most instable class across 5 individual samples seems to be class 5 (mitosis) in all groups, demanding for improvements in the software´s class annotation features.

I*n vitro* Ki67 stainings on two different TPT treated NB cell lines show confined staining patterns (Fig. 17 A). In the two tested NB cell lines the evaluation showed high proliferation rates in untreated samples (ctrl) whereas TPT treatment evoked a decrease in proliferation (Fig. 17 B).

Taken together, our data show a down-regulation of proliferation upon low-dose TPT treatment which is triggered over time (with longer treatment) and is expressed by the higher number of cells in Go phase compared to untreated control samples.
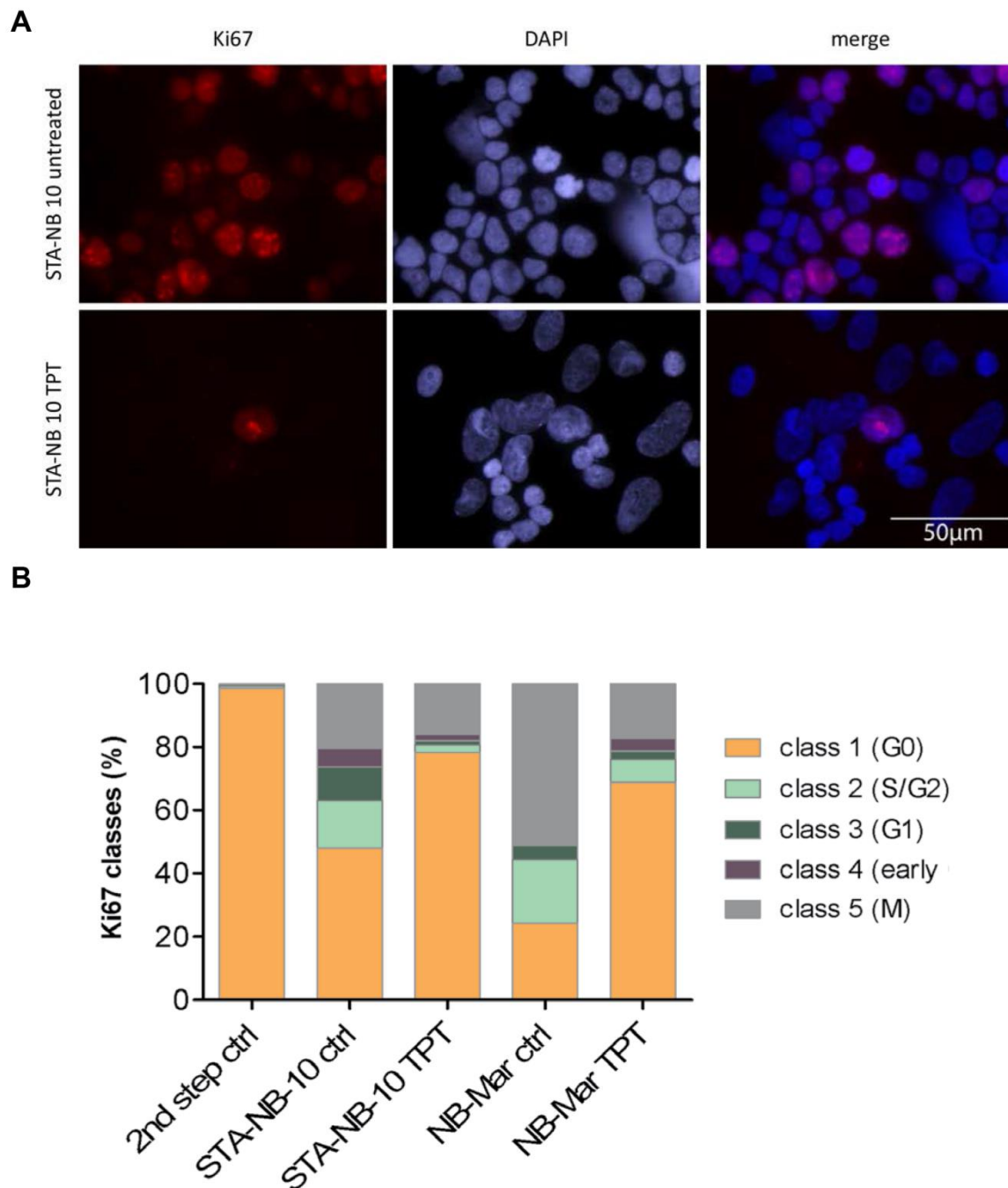
Fig. 17 ǀ Proliferation in TPT treated NB cell lines, shown by Ki67 stainings and analysis. Proliferating cells are shown in the Ki67-labeled column, counterstained nuclei are shown in blue in the DAPI colum (A). Quantitative evaluation of in vitro analysis (B).

4.5 Angiogenesis is reduced by TPT treatment

The induction of senescence offers potential advantages concerning the inhibition of further tumor growth and thereby serves as a barrier to tumorigenesis, but it has also been suspected to play a role in the promotion of tumors via the secretion of several growth factors, cytokines and hormones (Cahu, Bustany, & Sola, 2012; Kuilman & Peeper, 2009). Therefore we asked whether angiogenesis, a tumor promoting function, would be evoked by the low-dose treatment with TPT alongside with the induction of senescence.

To study the level of vascularization, tumor samples were stained for CD31 which is an endothelial marker and can be found on the surface of blood vessels. It was important to assure that only CD31 specific signals, but no auto fluorescence was measured. Thus, images were acquired by the automatic microscope in the TRITC as well as FITC channel. Blood vessels found within tumor tissue are built up by mouse endothelial cells which are typically visible as long, flat cells (Fig. 18, DAPI panel). Blood vessels were found in all samples but in untreated and 0.03 mg/kg/d TPT treated samples there were more blood vessels of greater length, compared to other dose groups (Fig. 18 and Fig. 19). As mentioned before, not only the tumors themselves but also the surrounding tissue was different and there were more subcutaneous bleedings noted in untreated and very-low-dose TPT treated animals.

For evaluation of the staining, 30 images were selected randomly from each sample and in each channel and CD31 specific signal was measured. The cumulative lengths of blood vessels were calculated (Fig. 19). All TPT treated tumors show lower mean cumulative lengths compared to untreated control tumors, except for the 0.03 mg/kg/d TPT treatment group (Fig. 19). However, no statistically significant difference could be observed but there is a tendency that TPT treated tumors showed lower levels of vascularization compared to untreated sample (Fig. 19).
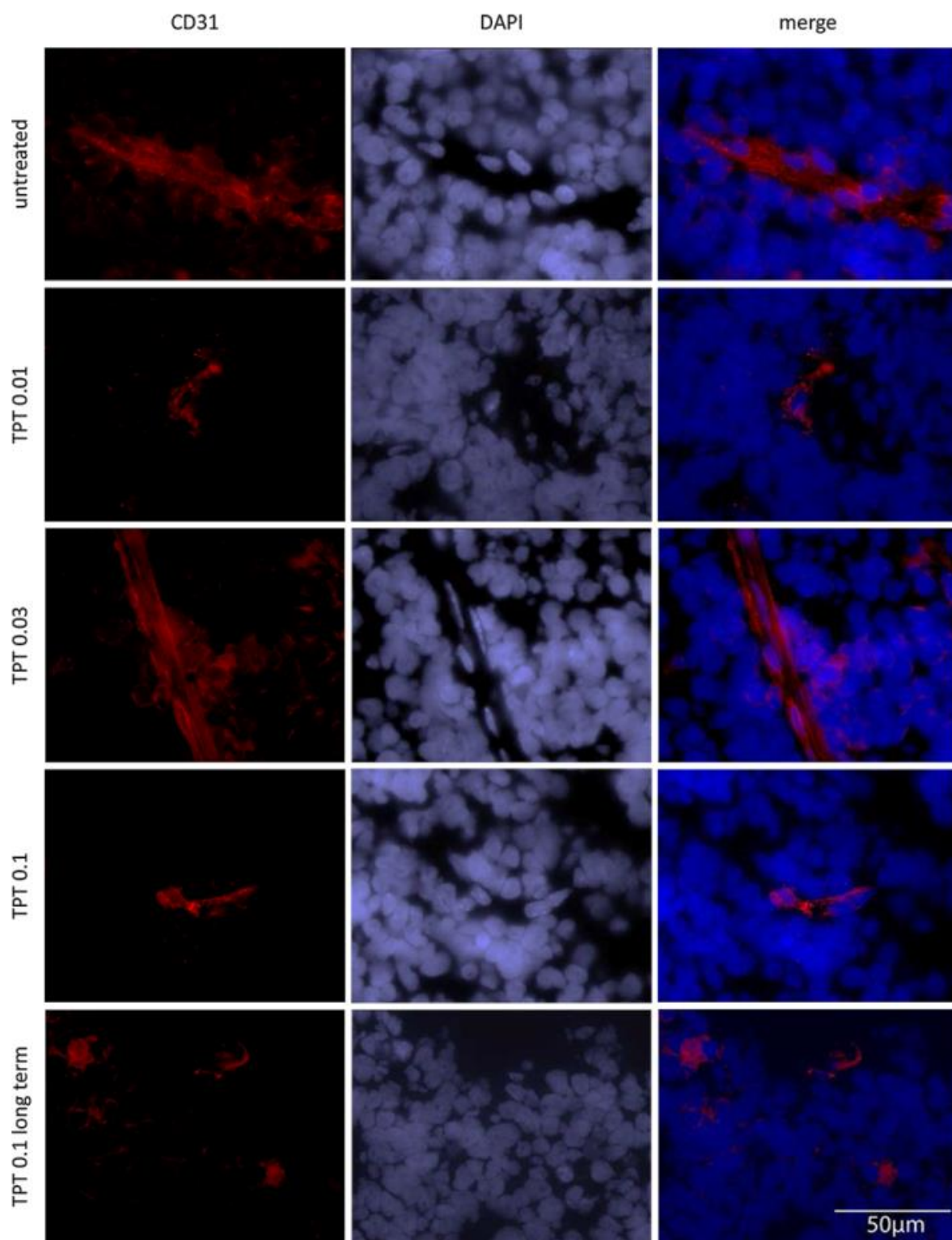
Fig. 18 l Vascularization in tumors, shown by CD31 stainings. Blood vessels stained for CD31 in red (left column), counterstained nuclei are shown in blue in the DAPI (middle) column. Untreated refers to untreated control tumors, TPT 0.01/0.03/0.1 refers to daily doses in mg Topotecan per kg of body weight. Blood vessels along the edges of samples were not taken into account.
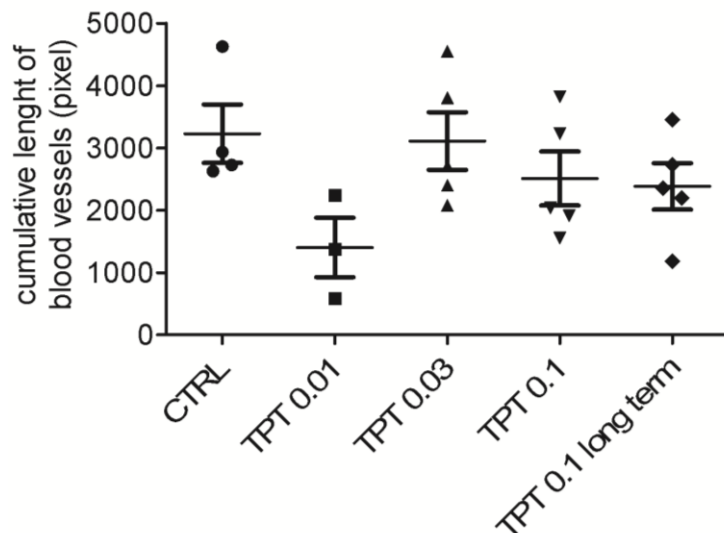
Fig. 19 l Analysis of vascularization in tumors by analyzing level of CD31 positivity. Images were acquired with automated microscopy and lengths of specific signals were measured in pixel on 30 randomly selected images and cumulative mean lengths calculated for each group. CTRL refers to untreated tumors, TPT 0.01/0.03/0.1 refers to daily doses in mg Topotecan per kg of body weight.

Along with the CD31 staining evaluation, it was also interesting to relate the results of expression arrays that had been performed with 3 untreated and 3 TPT treated (0.1 mg/kg/d) samples with angiogenesis genes. It was most striking to find vascular endothelial growth factor a (VEGFA) to be the strongest down-regulated gene in the panel of differentially expressed genes in 0.1 mg/kg/d TPT treated tumor samples (Fig. 20). The down-regulation of the VEGFA gene and the lower level of vascularization clearly show that TPT treatment does not promote further tumor growth via angiogenesis in this model.
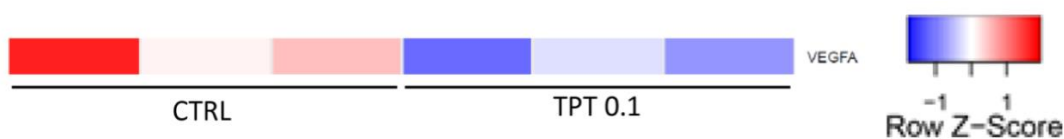
Fig. 20 l Heatmap of VEGFA in expression array. RNA was isolated from 3 untreated and 3 TPT (0.1 mg/kg/d) treated samples and expression arrays performed. Heatmap is shown for all samples for the VEGFA gene. Fold-changes are indicated by the row z-score color key.

4.6 Analysis of DNA damage and double strand breaks

Topotecan acts via a DNA damage (DD) inducing mechanism by inhibiting topoisomerase I enzyme and evoking DNA double strand breaks (DSBs). It is known that senescence is triggered by stress signals such as DD mechanisms and therefore it was expected to also see an increase in DD and DSBs in TPT treated tumors. To this end, γH2AX stainings were performed on tumor tissue sections. H2AX is a variant of the H2A core histone harboring a C-terminal extension which is used for DNA repair and if this terminus gets γ-phosphorylated this is a signal for DSBs.

Untreated control tumors showed elevated γH2AX positivity compared to 0.01 mg/kg/d TPT treated samples but less specific signal compared to 0.1 mg/kg/d TPT treated samples (Fig. 21). There was strong activity detectable in 0.1 mg/kg/d TPT treated tumor samples, but this varied strongly within the same treatment group. γH2AX is usually described as a staining with defined spots indicating DSBs (Ivashkevich et al., 2011). However, on NB tumor tissue sections this pattern could not be observed but a rather blurred nuclear staining was seen. Due to this staining pattern, also the software analysis was not reliably reproducible and evaluations of the γH2AX spotcount showed tremendous differences within same treatment groups. Therefore there is no quantitative analysis included here as the evaluations that were performed on the in-house developed software yielded inconclusive results due to difficulties with the automatic assessment of the staining pattern.

In order to assess DSB generation by low-dose TPT *in vitro*, untreated, short-term or long-term treated STA-NB-10 cells were stained for γH2AX. In untreated samples, already a significant proportion of cells display focal, nuclear γH2AX staining. When treated for 4 days with 10nM TPT, the amount of such positive cells was higher and when treated for 5 weeks, there was a correlation of high γH2AX positivity in large, flattened, senescent cells (Fig. 22).

In summary, the induction of DSBs via TPT treatment could be observed *in vitro* but the staining on untreated and TPT treated NB tumor tissue showed not such a clear pattern and was not appropriate for further quantitative analysis.
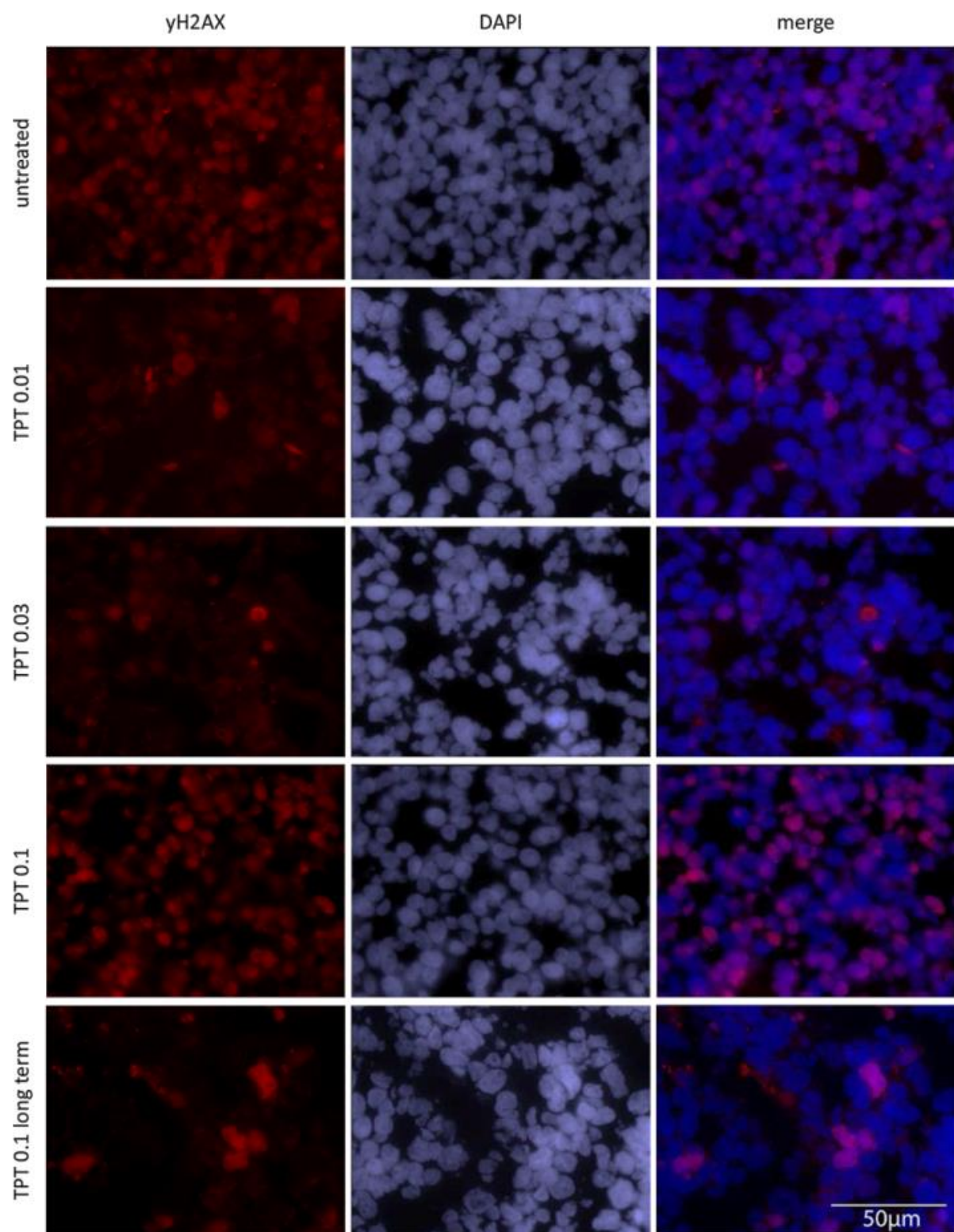
Fig. 21 I DNA damage and double strand breaks, shown by γH2AX stainings. DNA damage is indicated by γH2AX positive signal, shown in the first column, counterstained nuclei are shown in blue in the DAPI column. Untreated refers to untreated control tumors, TPT 0.01/0.03/0.1 refers to daily doses in mg Topotecan per kg of body weight.
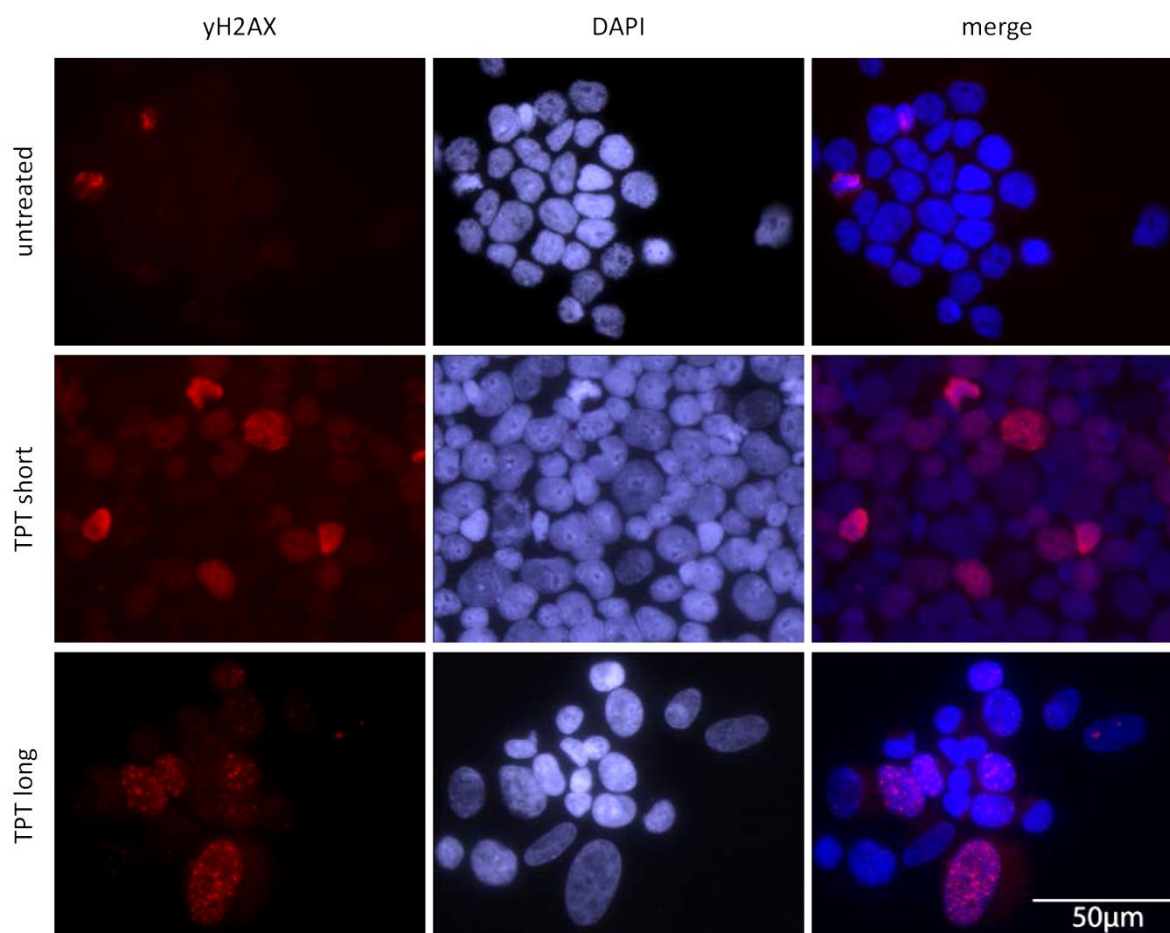
Fig. 22 l DNA damage and double strand breaks, shown by γH2AX stainings on cytospin preparations on STA-NB-10 cells. DNA damage is indicated by γH2AX positive signal, shown in the first column, counterstained nuclei are shown in blue in the DAPI column.

4.7 TPT treated and untreated tumors show differential expression profiles

To analyze the effects of low-dose TPT treatment in xenograft NB-tumors in terms of global changes in gene expression, RNA was isolated from untreated as well as TPT treated samples (for details see Material and Methods). 3 samples from the control group and 3 samples from the 0.1 mg/kg/d TPT treated group were chosen to perform PrimeView expression arrays (Affymetrix).

First, it was crucial to see whether untreated and TPT treated tumors even showed differential expression and if they would group together when an unsupervised clustering was performed (Fig. 23). This revealed that untreated samples clustered together and that the expression pattern was different from the drug treated group which also clustered together (Fig. 23).
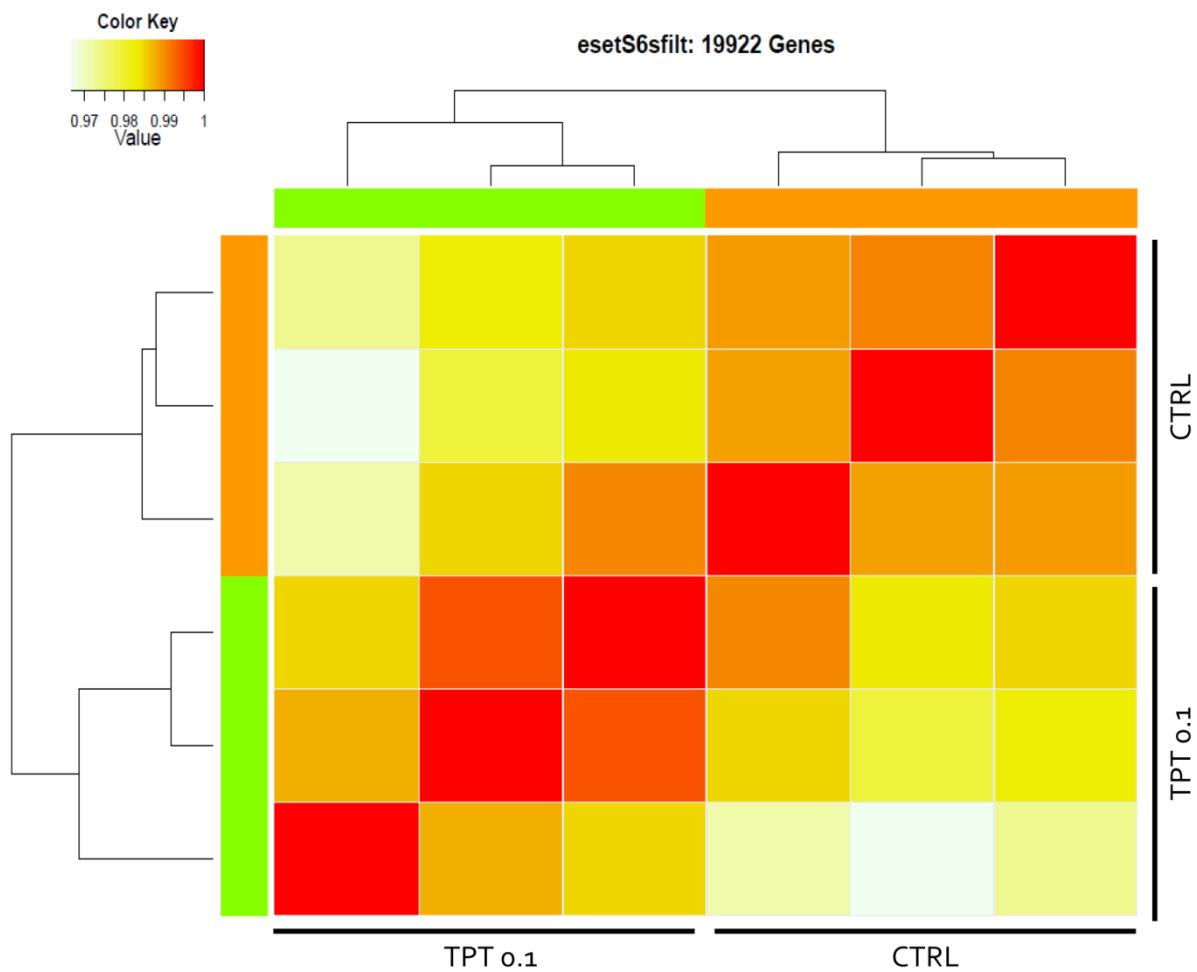
Fig. 23 | Unsupervised Clustering of untreated and TPT treated tumors in expression arrays. RNA was isolated from 3 untreated and 3 TPT (0.1 mg/kg/d) treated samples and expression arrays performed. Unsupervised clustering showed that all three untreated (CTRL) as well as all three TPT treated (TPT 0.1) samples clustered together concerning their gene expression (19922 genes). Orange bars indicate similarity of untreated samples, green bars indicate similarity of TPT treated samples.

Next, log2 expression values of both groups were compared. Cut-off levels were defined as having a fold change of ≥ 1.0 (when up-regulated, compared to the untreated control), or ≤ -1.0 (when down-regulated) of the log2 ratios of TPT and control samples. A ranking of TPT treated samples was produced for the top 30 up-regulated and top 30 down-regulated genes, always in comparison to untreated samples (Fig. 24). As mentioned before, the strongest down-regulated gene in TPT samples was VEGFA, followed by metabolic enzymes involved in lipid metabolism as well as receptors, transcription factors and kinases (Fig. 24). Topoisomerase I was found among the 30 top up-regulated genes which may be

due to a feedback mechanism because cells that were already damaged intend to reinforce their enzyme activity and therefore express higher levels of topoisomerase.

Overall, 1422 RNAs were differentially expressed (with an adjusted p-value ≤ 0.05). When only transcripts were considered significantly changed with a cutoff value below -1 or higher than +1 log2 ratio, then 20 transcripts were down-regulated and 336 transcripts were up-regulated in TPT treated samples. Among up-regulated transcripts, TPT treated samples genes were found that had been expected to be expressed higher, such as CDKN1A which is a marker of senescence. Also the increase in fibronectin and CD44 expression was affirmative for their indicative role in neuroblastoma cell senescence. Another up-regulated gene was IL-6 which encodes interleukin 6, responsible for evoking acute immune response and is in charge of several other tasks related to immunomodulation. IL-6 can attract macrophages which might help in degrading senescent cells.

To see if drug-induced, senescent tumor cells would change their gene expression in the same way *in vitro* as *in vivo*, expression arrays were performed with the same STA-NB 10 cell line with untreated and low-dose TPT treated cells.

These differential expression patterns show that tumor promoting genes are not up-regulated after low-dose TPT treatment and they serve as a useful database for the elaboration of potential markers for drug-induced senescent NB cells.
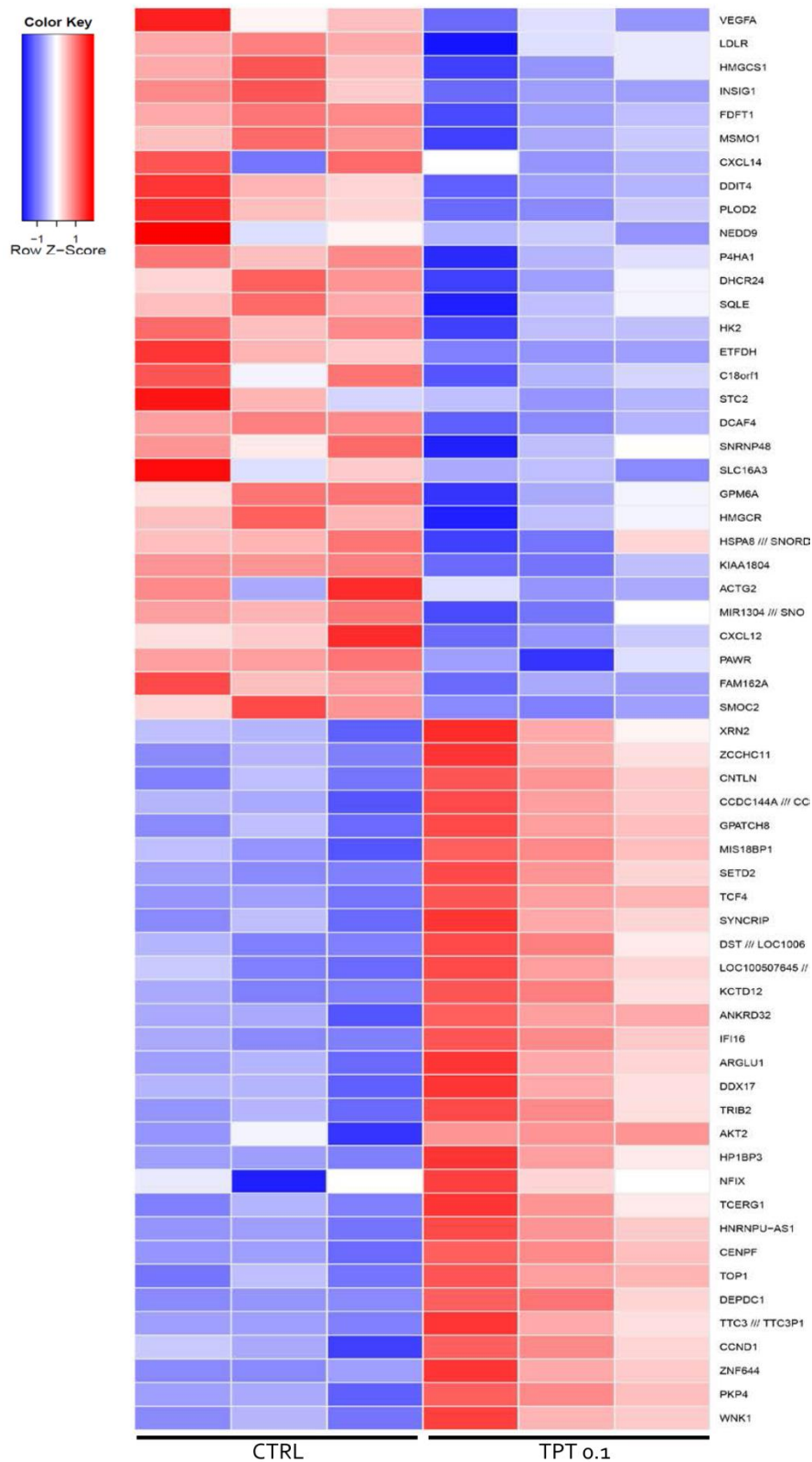
Fig. 24 | Top up- and down-regulated genes in TPT treated tumors compared to untreated tumors in expression arrays. RNA was isolated from 3 untreated and 3 TPT (0.1 mg/kg/d) treated samples and expression arrays were performed. Top 30 up-regulated and top 30 down-regulated genes in TPT treated samples (0.1 mg/kg/d) compared to untreated tumors are shown in this heatmap. Fold-changes can be interpreted using the color key on the right side.

4.8 Potential candidate marker for drug-induced senescent neuroblastoma cells

Expression arrays showed a significantly up-regulated expression pattern for TPT treated in comparison to control tumors in 336 transcripts. This list of up-regulated genes in TPT treated samples served as a database for further investigation on potential novel senescence markers. If candidate markers could be validated on tumor samples as well as on *in vitro* TPT treated NB cells, they later on could serve as a prognostic tool in patients or be of use as additional markers for senescent tumor cells.

One gene of interest is *ATRX* whose gene product is a chromatin remodeler and has been shown to undergo cell cycle-dependent phosphorylation which correlates with reorganization of chromatin (Bérubé *et al.* 2000). It contains ATPase and helicase functions and is suggested to play a role during mitosis, especially in the segregation of chromosomes. Another interesting link to senescence is the reported connection of *ATRX* to a mechanism of alternative telomere lengthening (Heaphy *et al.* 2011, Lovejoy *et al.* 2012, Abedalthagafi *et al.* 2013, Clynes *et al.* 2013, Watson *et al.* 2013). ATRX mutations also play a role in a subset of NB cases and there seems to be a correlation between the absence of MNA and *ATRX* mutations (Cheung *et al.* 2013).

There are different ATRX staining patterns in untreated and TPT treated samples visible *in vitro* as well as *in vivo* (Fig. 25). Untreated NB tumor tissue samples show less ATRX positivity and less focal staining than low-dose TPT treated samples (Fig. 25 A). The same is true for cytospin preparations of STA-NB-10 cells where untreated control cells showed low positivity while in different samples of 10nM TPT treated cells there was a clear, focal ATRX staining visible in senescent cells (Fig. 25 B). *In vitro* senescent cells are more easily detectable because of their altered morphology, characterized by enlarged and flattened nuclei and a rather crooked, curved shape. Not only the overall intensity of ATRX staining but also the amount of defined spots is higher in TPT treated samples (Fig. 25 B).
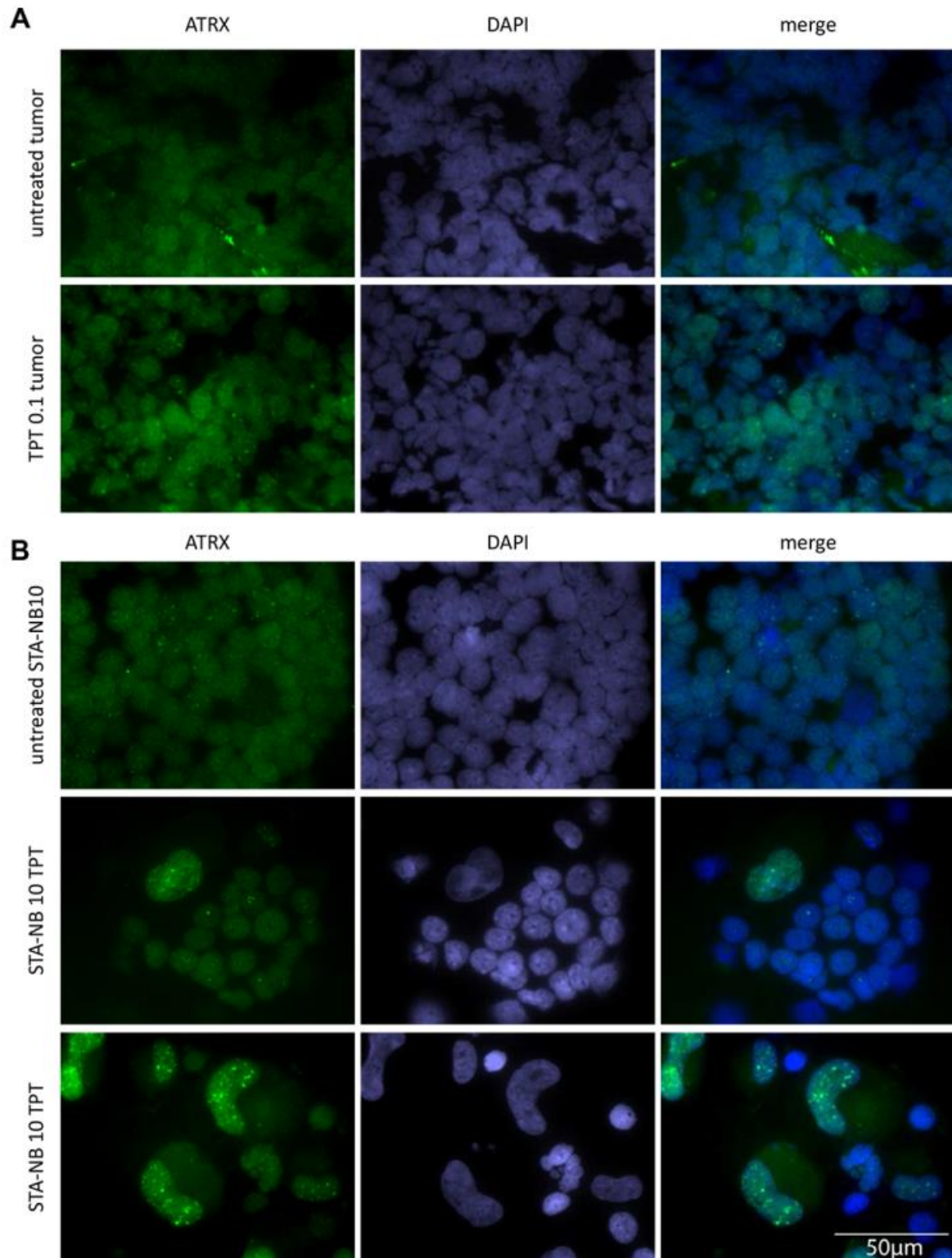
Fig. 25 | ATRX stainings in untreated and TPT treated xenograft NB-tumor samples and STA-NB-10 cell line. ATRX staining in green, shown in the first column, counterstained nuclei are shown in blue in the DAPI column. A shows untreated (upper row) and 0.1 mg/kg/d TPT treated tumor samples (bottom row). B shows untreated cytospin preparations of STA-NB-10 cell line (upper row) and STA-NB-10 cells that were treated with 10nM TPT over 2 weeks (two bottom rows).

Measured profiles of DAPI channel and ATRX (FITC channel) reveal a positive correlation between the DAPI and ATRX, showing that in weakly stained DAPI regions such as nucleoli ATRX is not present (Fig. 26).
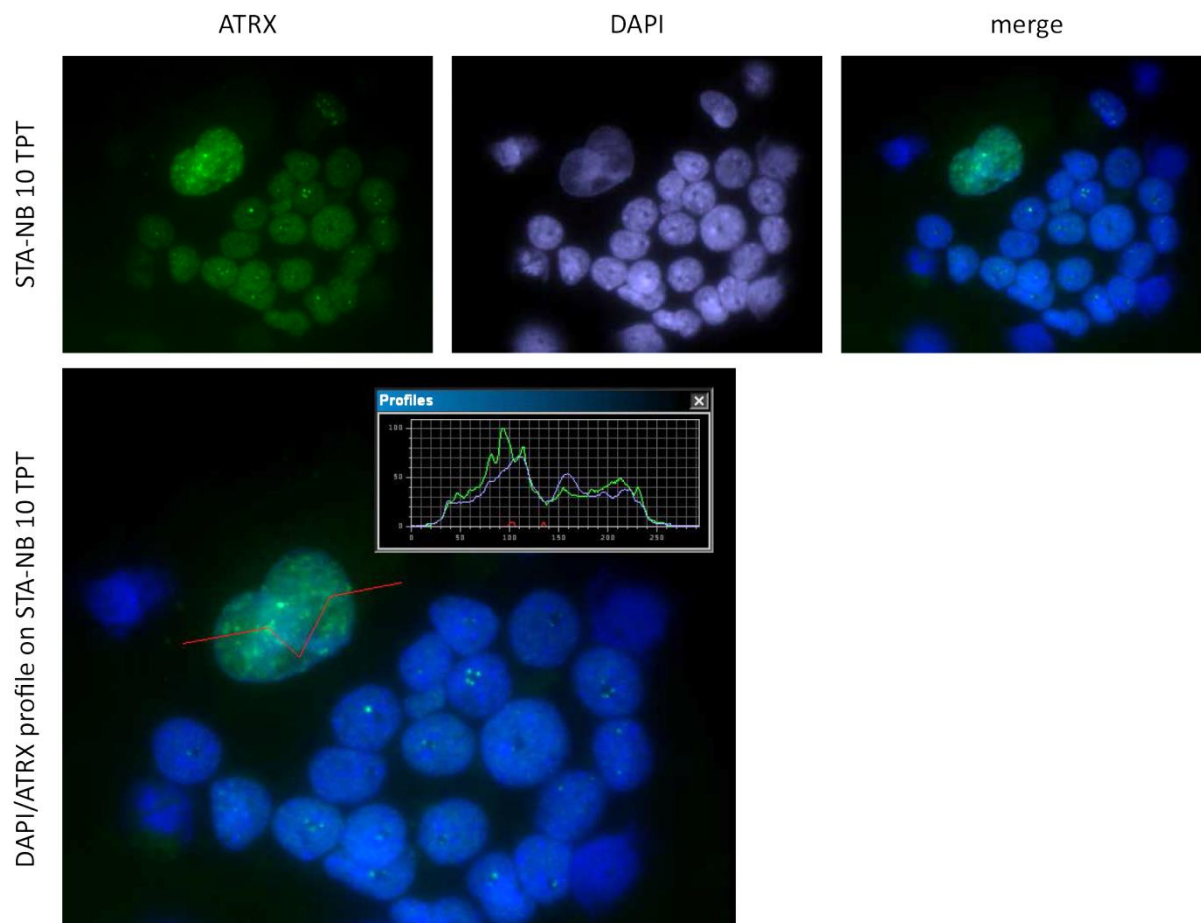
Fig. 26 I ATRX staining on TPT treated STA-NB-10 cells and profile measurements. ATRX staining in green, DAPI counterstain in blue. Profiles were measured (Histogram in lower panel) for both channels and show correlation. Red line indicates the measured path, direction was from left to right.

Thus, our data suggest that ATRX transcript and protein is up-regulated *in vitro* as well as *in vivo* upon low-dose TPT treatment. Furthermore, ATRX displays a focal staining pattern in TPT treated cells. Further samples will be stained and evaluated by microscopy and automated quantification.

5. Discussion

5.1 TIS as a feasible treatment approach in NB

One of the main questions of this study was if drug treatment would induce senescence in a xenotransplant NB-model at low doses. HU and TPT treated samples were analyzed concerning their ability to induce senescence. After SA-β-Gal staining revealed that HU – at least in this specific NB-xenotransplant model – could not evoke the activation of a tumor cell senescence program in those samples (data not shown), different dose groups of TPT were tested to treat animals (see Experimental Setup). According to SA-β-Gal activity in low-dose TPT treated NB cells and tumor tissue, senescence was also confirmed by the altered morphology of senescent cells *in vitro* and on the level of expression arrays by positivity for other markers such as p21 and fibronectin *in vivo* and *in vitro*. Tumor suppressor p16 is known to be accumulated in stress-induced senescence such as OIS and DD-mediated TIS (Herbig, Jobling, Chen, Chen, & Sedivy, 2004; Itahana et al., 2003; Kosar et al., 2011; Schmitt et al., 2002; Serrano et al., 1997; Stein, Drullinger, Soulard, & Dulic, 1999), and therefore can serve as surrogate senescence marker in TPT induced senescent cells. However, p16 stainings on cytospin preparations of TPT or CPT treated and untreated control STA-NB-10 cells showed no specific pattern of p16 presence in senescent cells (Fig. XX). Some morphologically distinctive senescent cells that also showed lipofuscin production were positive for p16 while others were completely negative. In contrast, BrdU treated NB cells show an up-regulation of p16 so the activity might be depending on the respective drug or mechanism of DD.

The IF staining of γH2AX on tissue sections presented a challenge because of missing or unspecific signals. Sections had to be stained freshly, right after preparation; otherwise it was not possible at all to stain cryopreserved tumor sections. Since the staining pattern seemed rather unspecific and not similar to the defined spots which were described in the literature, it was unreliable to trust the evaluation of the automated software analysis. *In vitro* stainings confirmed the accumulation of specific signal in most senescent NB cells after TPT treatment.

Senescent tumor cells were observed in the 0.1 mg/kg/d TPT treatment group, but not in the very-low-dose TPT treated groups where 0.03/0.01 mg/kg/d were applied. In the long term treatment (0.1 mg/kg/d TPT) and observation group it was interesting to see that there was no induction of senescence but a decrease in the portion of proliferating cells and most remarkably, huge areas of necrotic material. Tumors regressed in 3 out of 5 animals until they were not palpable anymore and at that point treatment was stopped in all animals. In the following weeks, tumors developed again in all 5 animals. This showed that the timespan of low-dose treatment may probably be prolonged for efficient tumor clearance. Even if the major portions of tumor cells had been senescent earlier, there might have been small non-senescent subpopulations that remained refractory to treatment, regrew and gave rise to a fast growing tumor after treatment stop. The question if complete tumor elimination is possible with prolonged low-dose TPT treatment will be answered in the up-coming study.

This approach finally aims to target residual tumor cells in MRD patients and the particular feature about it is the administration at low doses. TPT has been used in NB patients, mostly in combination with other cytotoxic agents in induction therapy, but at high doses (Kramer, Kushner, & Cheung, 2003; Kumar et al., 2013; Kushner, Kramer, Meyers, Wollner, & Cheung, 2000; Merritt et al., 2009; Park et al., 2011; Sottile, Gnemmi, Cantilena, D'Acunto, & Sala, 2012). Current therapies are often given at MTD (maximal tolerated dose) e.g. 5 times per week for 1 week (in a 3 week cycle). In contrast to that, metronomic therapy is administered in low doses but continuously, e.g. daily. These daily applications at lower doses likely target other pathways or types of cells, such as the tumor stroma or blood vessels and therefore could show more efficacy, especially when combined with anti-angiogenic agents (Lien, Georgsdottir, Sivanathan, Chan, & Emmenegger, 2013). A very recent study in NB xenotransplants has shown an anti-angiogenic effect of metronomic TPT treatment in combination with Pazapanib, however, the senescence pathway was not investigated in this model (Kumar et al., 2013).

Another goal is the identification of novel (*in vivo*) senescence markers and validation on tumor samples from treated NB patients. This can currently only be done on patients that have received high-dose cytotoxic treatment. We have identified several cases in which a NB patient had undergone a combinatory induction therapy with several cytotoxic agents,

among them drugs that induce DSBs. These patient samples were stained for DAPI and SA-β-Gal revealing a very strong activity of SA-β-Gal in the tumor. In contrast to the densely packed tissue in xenotransplant tumors, those tumor tissues were more loosely and cells showed the typical senescent cell morphology, containing enlarged, flattened nuclei with altered, crooked shapes. Because of this strong indication of senescence induction, also other (potential) markers, such as γH2AX and ATRX, will be IF-stained on those and additional samples.

5.2 Relating angiogenesis, proliferation and apoptosis in TPT treated tumors

In addition to the extent of senescence in TPT treated tumors, also other pathways including angiogenesis, proliferation and apoptosis were analyzed. Opposing to several reports on senescent cells – mostly fibroblasts – that their secretion pattern (SASP) would include pro-angiogenic factors, such as VEGF (Coppe et al., 2006; Rodier & Campisi, 2011), vascularization was not higher in TPT treated senescent tumor cells. CD31 stainings showed that the cumulative length of blood vessels in TPT treated tumors was less compared to untreated control tumors. In the 0.01 mg/kg/d TPT treatment group the values were surprisingly low, but that might have been due to suboptimal staining or irregularities in image acquisition by automated microscopy since there were two samples where no blood vessels were detected at all. Apart from that, the lowest values were found in the 0.1 mg/kg/d TPT short term treated and long term treated groups. This findings are in line with previously published data which show that metronomic TPT administration exerts anti-angiogenic functions in a model of ovarian cancer where the drug was applied metronomically (0.5/1.0/1.5 mg/kg/d) and in MTD ranges (7.5/15.0 mg/kg/week) (Merritt et al., 2009). This study also observed that apoptosis was induced upon metronomic TPT treatment, while angiogenesis and tumor growth were reduced.

In line with those findings, also in the study at hand apoptosis was induced and tumor growth, as well as vascularization declined upon low-dose, continuously given TPT. The differences in proliferation were not so distinct in tumors *in vivo* in short treatment time spans (2 weeks) but in the 0.1 mg/kg/d TPT long term treatment and observation group and in *in vitro* Ki67 stainings of TPT treated NB cells, clear changes in proliferation patterns were noted. The ratios of proliferation and apoptosis were reversed in TPT treated compared to

untreated tumors, especially in the long term treated group. Concerning apoptosis, this treatment group was the most distinct since there were areas in all tumors of the long term treatment group that showed around 70-100% apoptotic cells. However, if different parts of the tumor pieces were analyzed, TUNEL stainings showed a similar pattern as in short term treated 0.1 mg/kg/d TPT tumors. Nevertheless, the overall proportion of apoptotic cells was higher in the long term group compared to all other groups and proliferation was lower at the same time. Still, SA-β-Gal activity was not observed there. This could be explained by the potential removal of senescent cells by infiltrating macrophages.

Both, senescence and apoptosis can be induced by DD and mediated by p53 (Chang et al., 1999; Schmitt et al., 2002; Suzuki et al., 2001) but it is still not completely answered which factors decide the outcome when p53 is triggered in tumor cells, e.g. by DD via cytotoxic drugs. It was speculated that the decision follows a temporal manner and apoptosis would precede senescence, since apoptosis is the first, acute answer towards stress e.g. DD and at a later onset senescence would come into play as a sort of back-up mechanism (Kahlem et al., 2004). In contrast Knizhnik *et al.* report that the pathways of autophagy, apoptosis and senescence were intermingled in such a manner that autophagy can trigger senescence and both cell programs precede apoptosis, with the balance of all three being the decisive factor of cell fate (Knizhnik et al., 2013). Another influential fact might be due to p53 variants found in tumor cells. Although p53 is rarely mutated in NB patients, codon 72 shows polymorphisms (Cattelani et al., 2012). Apparently, there is a certain genotype (p53-72 Pro/Pro) that enhances senescence while it reduces apoptosis, regardless whether patients share MNA or not (ibid.).

5.3 Concordant and conflicting findings *in vitro* and *in vivo*

Most markers that were analyzed on tumor samples from the xenotransplant experiment were also analyzed on *in vitro* TPT treated STA-NB-10 cells. Ki67, for example, showed no huge differences *in vivo*, except for the long term treatment group (0.1 mg/kg/d TPT) in which percentages for all positive Ki67 classes were smaller than in the control group (Fig. 11). *In vitro*, however, Ki67 revealed very distinct differences in the staining patterns between untreated control cells and TPT treated (10nM, 14 days) STA-NB-10 cells (Fig. 12). Proliferative activity decreased strongly in TPT treated NB cells and automated evaluation

of Ki67 classes fitted to the expected decrease. In general, markers showed a more explicit staining pattern *in vitro* than *in vivo* and this was also true for SA-β-Gal, γH2AX and ATRX.

Differences could also be found in expression patterns of TPT treated cells *in vitro* and xenotransplanted tumor samples. This does not come as a surprise since the environment of *in vitro* cultured tumor cells and tumor cells in animals varies a lot. For example, there is no cell-cell interaction with other cell types in culture. Those samples are "purified", without additional apoptotic cells or differentiated cells. In mice, on the other hand, there is always the possibility of mouse-stroma cell interactions with tumor cells and even if the nude mice used in this study do not develop any T-cells, there are still cells of the innate immune system which could interfere, provoke an immune response or destroy tumor cells. Therefore NB cells most likely react differently to TPT treatment *in vivo* as compared to *in vitro* studies. The question of applicability of findings in mice for human patients is always a delicate one, so just some differences shall be pointed out: the immune system of those mice contained e.g. NK cells, macrophages and B cells, but no T cells which means that they lack adaptive immunity. Further on, the detoxification system in mice works more efficiently for most substances (Djuric, Corbett, Valeriote, Heilbrun, & Baker, 1995), so higher doses are needed and are not absolutely comparable, related to their bodyweight.

5.4 Additional potential markers and alternative cell fates

Although SA-β-Gal is ubiquitously in use as a senescence marker, it would be assuring to detect additional markers on TPT treated tumor cells. IF stainings were not only conducted *in vivo* but also *in vitro* on TPT treated STA-NB-10 cells. Another well described senescence marker is p16 but it did not serve as a suitable marker for senescence in STA-NB-10 cells. On stained cytospin preparations p16 did not show ubiquitous expression in e.g. TPT treated senescent cells, with some cells being positive and some negative for this marker.

Besides from drug-induced senescence pathway, it would be also interesting to evaluate other fates of tumor cells, e.g. differentiation. What if, for example, tumor cells have differentiated and became senescent afterwards? To investigate this option, there is currently work in progress to stain neurofilament markers such as NF-160 and NF-200 to evaluate the portion of differentiated cells in TPT treated tumors (Ponzoni, Casalaro, Lanciotti, Montaldo, & Cornaglia-Ferraris, 1992). Wainwright *et al.* suggest that upon RA treatment the type of cell cycle arrest decides if it either leads to differentiation or

senescence in human NB cells (Wainwright, Lasorella, & Iavarone, 2001). They propose that senescence would be induced by rapid inhibition of cyclin-dependent kinases (CDKs) through RA administration and neuronal differentiation would thereby be inhibited. Another NB study on differentiation and senescence showed that RA administration alone drove NB cells into differentiation but in combination with Tyrosine phosphatase inhibitors, a novel, p53-independent form of senescence pathway was activated (Clark, Daga, & Stoker, 2013).

Based on the finding of massive necrotic areas in the long term treatment and in the observation group (0.1 mg/kg/d TPT), the necrosis marker Caspase 8 would help to elucidate the contribution of this pathway to the destruction of tumor tissue (Wang et al., 2003). Concerning the role of immune responses of the innate immune system in our xenotransplant model, macrophages as well as natural killer (NK) cells should be evaluated and this is asked also in the context of the ultimate fate of cells in NB tumors: What happens to cells that "disappear" when the tumor declines? If there are necrotic areas, as in long term TPT (0.1 mg/kd/d) treated and monitored tumors, maybe there was also macrophage infiltration occurring at the same time. The presence of type 1 macrophages could be analyzed by IF stainings or FACS-analysis using CD11b, TNF-α and F4/80 as markers (Duclos, Haddad, & Baines, 1995). In order to study Natural Killer (NK) cell activity, a different syngeneic mouse model of NB would be needed, e.g. A/J mice bearing subcutaneous NXS2 NB (Yang et al., 2013) or *ALK* mutated transgenic mice (Heukamp et al., 2012), as it is not possible to directly compare human and murine NK-systems in this study.

We have previously observed that drug-treated NB cell lines that had a *MYCN* amplification display reduced *MYCN* copies compared to non-treated cells. This is most likely caused by expulsion of *MYCN* copies by micronucleus formation (Narath, 2007). Thus, the MYCN copy number and the down-regulation of the *MYCN* gene are of interest and remain to be addressed with FISH and Western Blot. While the role of epithelial to mesenchymal transition (EMT) has been investigated in NB as a potential marker for aggressiveness and metastasis, it has not been questioned in connection with senescence so far (Lee, Dedhar, Kalluri, & Thompson, 2006; Nozato, Kaneko, Nakagawara, & Komuro, 2013). It would be of interest if EMT genes such as twist, snail, vimentin or fibronectin show altered expression profiles and protein expression in TPT treated tumor samples.

Finally, we could identify ATRX as a new candidate factor to be involved in senescence. This is supported by the up-regulation of ATRX in TPT treated NB cell lines and by an increase in local ATRX staining in these cells (Fig. 20). The *ATRX* gene is mutated in the X-linked mental retardation syndrome associated with α-thalassaemia and interestingly has been reported to be involved in the remodeling of chromatin (Berube, 2011). The ATRX protein belongs to a family of proteins with helicase and ATPase functions (Carlson & Laurent, 1994; Eisen, Sweder, & Hanawalt, 1995; Picketts et al., 1996). This family consists of Switch 2, sucrose non-fermenting 2 (SWI2/SNF2) proteins that display remodeling activity of chromatin. ATRX shows distinct staining patterns, depending on the phase of cell-cycle and the related phosphorylation status since this influences the association of ATRX with chromatin and the status of the nuclear matrix (Berube, Smeenk, & Picketts, 2000). Another function of ATRX involves a telomerase-independent mechanism called alternative Lengthening of Telomeres (ALT) which is found in 10-15% of cancers. It has been shown that loss of ATRX is associated with ALT and resulted in genomic instability (Abedalthagafi et al., 2013; Lovejoy et al., 2012). ALT-immortalized cell lines had mutations in the *ATRX* gene and loss of protein, respectively. The loss of ATRX and concomitant ALT phenotype were found in pediatric cancers that showed high-grade solid tumors (Abedalthagafi et al., 2013; Cheung et al., 2012). The disruption of the *ATRX* gene often comes along with aberrations in the *DAXX* gene since those encode proteins that interact with each other in chromatin remodeling and both mutations are often found together in the onset of the ALT mechanism (Heaphy et al., 2011). Further studies have shown that also histone H3.3 mutations contribute to the ALT pathway and this suggests that the *ATRX/DAXX/H3.3* pathway normally would suppress ALT (Clynes & Gibbons, 2013). Both, ATRX and DAXX mutations were also found in pancreatic neuroendocrine tumors and could contribute to the development of cancer by epigenetic remodeling (Elsasser, Allis, & Lewis, 2011) since ATRX is involved in the regulation of DNA methylation (De La Fuente, Baumann, & Viveiros, 2011). ATRX defects do not only lead to perturbations of telomere function but the absence of the protein in *ATRX*-null mouse brains can also evoke replicative damage at telomeres and this is supported by loss of p53 and ATM activation in mice (Watson et al., 2013). It is not only appealing to further investigate this gene in connection with drug-induced senescence since ATRX is involved in chromatin remodeling and telomere dysfunction but it is also a prominent indicator of outcome in neuroblastoma. Cheung *et al* found that *ATRX* mutations

were associated with the absence of the ATRX protein and with long telomeres in NB patients (Cheung et al., 2012). In addition, the patients' age contributes to the probability of *ATRX* mutations since none such aberrations were found in the cohort of patients that were younger than 18 months.

5.5 Outlook for further studies

This study shows the induction of senescence via low-dose TPT treatment as feasible in xenotransplant NB tumors. Further, it shows that senescence induction is not associated with a tumor-promoting but rather a tumor-inhibiting function. However, it is still not known how this setting would apply in cancer patients and, if senescence can be induced, whether this would also lead to the cure of patients in terms of complete tumor regression. Another prospective NB-xenotransplant experiment will investigate the question of remission in the previously described mouse model. Tumors will be treated at low-dose (0.1 mg/kg/d TPT) until no tumors are palpable and for further 4 weeks. After that, treatment will be stopped and mice will be monitored over an extended period of time until relapse or 2 months after treatment stop, at the latest. In comparison, the same dose will be applied in a short term experiment like in the Experimental Setup for this study. There will also be a high-dose group (1 mg/kg/d TPT) that might reveal whether senescence is also induced at higher doses or if e.g. apoptosis is the predominant pathway.

Further drug screens to identify candidate agents able to induce senescence in NB could be carried out in a zebrafish model (Stewart et al., 2010) since this system has the advantages of being cost-effective, showing fast development and numerous offspring. *In vivo* imaging is very much facilitated in comparison to mice and drugs can be tested by adding agents into the water. A downside of this model is the restriction of time span since a long term treatment setting would not be feasible in such a short-lived organism. The workflow from aquarium to bedside would include the screening of several drug candidates, validating the most promising and adapting them to a NB mouse model.

Concerning the identification and validation of new markers that would allow the detection of senescent tumor cells *in vivo* more easily, array data of expression analysis are of great use. Based on array data it is planned to elaborate markers of TIS in drug treated tumor cells, confirm their presence on tumors of xenotransplanted mice and later on apply them on tumor samples from patients for validation.

6. Conclusion

Data in this study showed the induction of senescence in NB tumor cells *in vivo* in a preclinical xenotransplant mouse model via Topotecan treatment (Fig. 26). Importantly, this was achieved by administering low doses in a daily manner. Concomitantly, levels of vascularization were lower in TPT treated tumors compared to untreated controls and apoptosis levels rose in treated samples.

In vitro experiments supported this concept by showing that cell cycle arrest was achieved in low-dose TPT treated NB cells and proliferation also decreased. Findings were affirmed by SA-β-Gal positivity and elevated levels of the DNA damage marker γH2AX.

In both, *in vivo* and *in vitro* settings it was demonstrated that the amount of tumor cells declined and growth was impaired upon continuous low-dose TPT treatment while the portion of senescent tumor cells was elevated (Fig. 26). Since IF stainings and expression arrays showed the induction of senescence in this specific NB mouse model but did not reveal accompanying tumor growth promoting functions, e.g. increased angiogenesis, this approach could potentially serve as an additional therapeutic application for high-risk NB patients in an MRD setting in the long run.
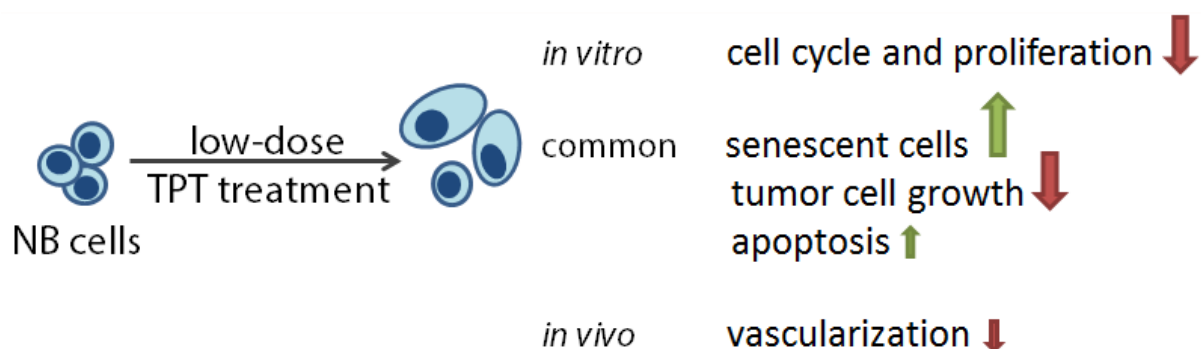

Fig. 26 I Conclusive scheme of drug induced senescence in neuroblastoma cells and NB-xenotransplant mice. Neuroblastoma were treated with low-dose Topotecan and indicated changes were observed in vitro and in vivo. Directions and colors of arrows indicate up-/down-regulation, sizes indicate the extent of respective features.

7. References

Abedalthagafi, M., Phillips, J. J., Kim, G. E., Mueller, S., Haas-Kogen, D. A., Marshall, R. E., . . . Perry, A. (2013). The alternative lengthening of telomere phenotype is significantly associated with loss of ATRX expression in high-grade pediatric and adult astrocytomas: a multi-institutional study of 214 astrocytomas. *Mod Pathol*. doi: 10.1038/modpathol.2013.90

Acosta, S., Lavarino, C., Paris, R., Garcia, I., de Torres, C., Rodriguez, E., . . . Mora, J. (2009). Comprehensive characterization of neuroblastoma cell line subtypes reveals bilineage potential similar to neural crest stem cells. *BMC Dev Biol, 9*, 12. doi: 10.1186/1471-213x-9-12

Ahmann, D. L., Hahn, R. G., & Bisel, H. F. (1972). Clinical evaluation of 5-(3,3-dimethyl-1-triazeno)imidazole-4-carboxam-ide (NSC-45388), melphalan (NSC-8806), and hydroxyurea (NSC-32065) in the treatment of disseminated malignant melanoma. *Cancer Chemother Rep, 56*(3), 369-372.

Ambros, I. M., Rumpler, S., Luegmayr, A., Hattinger, C. M., Strehl, S., Kovar, H., . . . Ambros, P. F. (1997). Neuroblastoma cells can actively eliminate supernumerary MYCN gene copies by micronucleus formation--sign of tumour cell revertance? *Eur J Cancer, 33*(12), 2043-2049.

Ambros, I. M., Zellner, A., Roald, B., Amann, G., Ladenstein, R., Printz, D., . . . Ambros, P. F. (1996). Role of ploidy, chromosome 1p, and Schwann cells in the maturation of neuroblastoma. *N Engl J Med, 334*(23), 1505-1511. doi: 10.1056/nejm199606063342304

Bartkova, J., Horejsi, Z., Koed, K., Kramer, A., Tort, F., Zieger, K., . . . Bartek, J. (2005). DNA damage response as a candidate anti-cancer barrier in early human tumorigenesis. *Nature, 434*(7035), 864-870. doi: 10.1038/nature03482

Bartkova, J., Rezaei, N., Liontos, M., Karakaidos, P., Kletsas, D., Issaeva, N., . . . Gorgoulis, V. G. (2006). Oncogene-induced senescence is part of the tumorigenesis barrier imposed by DNA damage checkpoints. *Nature, 444*(7119), 633-637. doi: 10.1038/nature05268

Berube, N. G. (2011). ATRX in chromatin assembly and genome architecture during development and disease. *Biochem Cell Biol, 89*(5), 435-444. doi: 10.1139/011-038

Berube, N. G., Smeenk, C. A., & Picketts, D. J. (2000). Cell cycle-dependent phosphorylation of the ATRX protein correlates with changes in nuclear matrix and chromatin association. *Hum Mol Genet, 9*(4), 539-547.

Bodnar, A. G., Ouellette, M., Frolkis, M., Holt, S. E., Chiu, C. P., Morin, G. B., . . . Wright, W. E. (1998). Extension of life-span by introduction of telomerase into normal human cells. *Science, 279*(5349), 349-352.

Braig, M., Lee, S., Loddenkemper, C., Rudolph, C., Peters, A. H., Schlegelberger, B., . . . Schmitt, C. A. (2005). Oncogene-induced senescence as an initial barrier in lymphoma development. *Nature, 436*(7051), 660-665. doi: 10.1038/nature03841

Braig, M., & Schmitt, C. A. (2006). Oncogene-induced senescence: putting the brakes on tumor development. *Cancer Res, 66*(6), 2881-2884. doi: 10.1158/0008-5472.can-05-4006

Brodeur, G. M. (2003). Neuroblastoma: biological insights into a clinical enigma. *Nat Rev Cancer, 3*(3), 203-216. doi: 10.1038/nrc1014

Brodeur, G. M., Seeger, R. C., Schwab, M., Varmus, H. E., & Bishop, J. M. (1984). Amplification of N-myc in untreated human neuroblastomas correlates with advanced disease stage. *Science, 224*(4653), 1121-1124.

Cahu, J., Bustany, S., & Sola, B. (2012). Senescence-associated secretory phenotype favors the emergence of cancer stem-like cells. *Cell Death Dis, 3*, e446. doi: 10.1038/cddis.2012.183

Campisi, J. (2005). Senescent cells, tumor suppression, and organismal aging: good citizens, bad neighbors. *Cell, 120*(4), 513-522. doi: 10.1016/j.cell.2005.02.003

Campisi, J., & d'Adda di Fagagna, F. (2007). Cellular senescence: when bad things happen to good cells. *Nat Rev Mol Cell Biol, 8*(9), 729-740. doi: 10.1038/nrm2233

Carlson, M., & Laurent, B. C. (1994). The SNF/SWI family of global transcriptional activators. *Curr Opin Cell Biol, 6*(3), 396-402.

Cattelani, S., Ferrari-Amorotti, G., Galavotti, S., Defferrari, R., Tanno, B., Cialfi, S., . . . Calabretta, B. (2012). The p53 codon 72 Pro/Pro genotype identifies poor-prognosis neuroblastoma patients: correlation with reduced apoptosis and enhanced senescence by the p53-72P isoform. *Neoplasia, 14*(7), 634-643.

Chabner, B. A., & Roberts, T. G., Jr. (2005). Timeline: Chemotherapy and the war on cancer. *Nat Rev Cancer, 5*(1), 65-72. doi: 10.1038/nrc1529

Chang, B. D., Xuan, Y., Broude, E. V., Zhu, H., Schott, B., Fang, J., & Roninson, I. B. (1999). Role of p53 and p21waf1/cip1 in senescence-like terminal proliferation arrest induced in human tumor cells by chemotherapeutic drugs. *Oncogene, 18*(34), 4808-4818. doi: 10.1038/sj.onc.1203078

Chen, Z., Trotman, L. C., Shaffer, D., Lin, H. K., Dotan, Z. A., Niki, M., . . . Pandolfi, P. P. (2005). Crucial role of p53-dependent cellular senescence in suppression of Pten-deficient tumorigenesis. *Nature, 436*(7051), 725-730. doi: 10.1038/nature03918

Cheung, N. K., Lazarus, H., Miraldi, F. D., Abramowsky, C. R., Kallick, S., Saarinen, U. M., . . . Berger, N. A. (1987). Ganglioside GD2 specific monoclonal antibody 3F8: a phase I study in patients with neuroblastoma and malignant melanoma. *J Clin Oncol, 5*(9), 1430-1440.

Cheung, N. K., Zhang, J., Lu, C., Parker, M., Bahrami, A., Tickoo, S. K., . . . Dyer, M. A. (2012). Association of age at diagnosis and genetic mutations in patients with neuroblastoma. *JAMA, 307*(10), 1062-1071. doi: 10.1001/jama.2012.228

Clark, O., Daga, S., & Stoker, A. W. (2013). Tyrosine phosphatase inhibitors combined with retinoic acid can enhance differentiation of neuroblastoma cells and trigger ERK- and AKT-dependent, p53-independent senescence. *Cancer Lett, 328*(1), 44-54. doi: 10.1016/j.canlet.2012.09.014

Clynes, D., & Gibbons, R. J. (2013). ATRX and the replication of structured DNA. *Curr Opin Genet Dev, 23*(3), 289-294. doi: 10.1016/j.gde.2013.01.005

Cohn, S. L., Pearson, A. D., London, W. B., Monclair, T., Ambros, P. F., Brodeur, G. M., . . . Matthay, K. K. (2009). The International Neuroblastoma Risk Group (INRG) classification system: an INRG Task Force report. *J Clin Oncol, 27*(2), 289-297. doi: 10.1200/jco.2008.16.6785

Collado, M., Blasco, M. A., & Serrano, M. (2007). Cellular senescence in cancer and aging. *Cell, 130*(2), 223-233. doi: 10.1016/j.cell.2007.07.003

Collado, M., & Serrano, M. (2006). The power and the promise of oncogene-induced senescence markers. *Nat Rev Cancer, 6*(6), 472-476. doi: 10.1038/nrc1884

Coppe, J. P., Kauser, K., Campisi, J., & Beausejour, C. M. (2006). Secretion of vascular endothelial growth factor by primary human fibroblasts at senescence. *J Biol Chem, 281*(40), 29568-29574. doi: 10.1074/jbc.M603307200

Coppe, J. P., Patil, C. K., Rodier, F., Sun, Y., Munoz, D. P., Goldstein, J., . . . Campisi, J. (2008). Senescence-associated secretory phenotypes reveal cell-nonautonomous functions of oncogenic RAS and the p53 tumor suppressor. *PLoS Biol, 6*(12), 2853-2868. doi: 10.1371/journal.pbio.0060301

d'Adda di Fagagna, F. (2008). Living on a break: cellular senescence as a DNA-damage response. *Nat Rev Cancer, 8*(7), 512-522. doi: 10.1038/nrc2440

De La Fuente, R., Baumann, C., & Viveiros, M. M. (2011). Role of ATRX in chromatin structure and function: implications for chromosome instability and human disease. *Reproduction, 142*(2), 221-234. doi: 10.1530/rep-10-0380

Deyell, R. J., & Attiyeh, E. F. (2011). Advances in the understanding of constitutional and somatic genomic alterations in neuroblastoma. *Cancer Genet, 204*(3), 113-121. doi: 10.1016/j.cancergen.2011.03.001

Di Micco, R., Cicalese, A., Fumagalli, M., Dobreva, M., Verrecchia, A., Pelicci, P. G., & di Fagagna, F. (2008). DNA damage response activation in mouse embryonic fibroblasts undergoing replicative senescence and following spontaneous immortalization. *Cell Cycle, 7*(22), 3601-3606.

Di Micco, R., Fumagalli, M., Cicalese, A., Piccinin, S., Gasparini, P., Luise, C., . . . d'Adda di Fagagna, F. (2006). Oncogene-induced senescence is a DNA damage response triggered by DNA hyper-replication. *Nature, 444*(7119), 638-642. doi: 10.1038/nature05327

Di Micco, R., Sulli, G., Dobreva, M., Liontos, M., Botrugno, O. A., Gargiulo, G., . . . d'Adda di Fagagna, F. (2011). Interplay between oncogene-induced DNA damage response and heterochromatin in senescence and cancer. *Nat Cell Biol, 13*(3), 292-302. doi: 10.1038/ncb2170

Dimri, G. P., Lee, X., Basile, G., Acosta, M., Scott, G., Roskelley, C., . . . et al. (1995). A biomarker that identifies senescent human cells in culture and in aging skin in vivo. *Proc Natl Acad Sci U S A, 92*(20), 9363-9367.

Diskin, S. J., Hou, C., Glessner, J. T., Attiyeh, E. F., Laudenslager, M., Bosse, K., . . . Maris, J. M. (2009). Copy number variation at 1q21.1 associated with neuroblastoma. *Nature, 459*(7249), 987-991. doi: 10.1038/nature08035

Djuric, Z., Corbett, T. H., Valeriote, F. A., Heilbrun, L. K., & Baker, L. H. (1995). Detoxification ability and toxicity of quinones in mouse and human tumor cell lines used for anticancer drug screening. *Cancer Chemother Pharmacol, 36*(1), 20-26.

Duclos, A. J., Haddad, E. K., & Baines, M. G. (1995). Presence of activated macrophages in a murine model of early embryo loss. *Am J Reprod Immunol, 33*(5), 354-366.

Eisen, J. A., Sweder, K. S., & Hanawalt, P. C. (1995). Evolution of the SNF2 family of proteins: subfamilies with distinct sequences and functions. *Nucleic Acids Res, 23*(14), 2715-2723.

Elsasser, S. J., Allis, C. D., & Lewis, P. W. (2011). Cancer. New epigenetic drivers of cancers. *Science, 331*(6021), 1145-1146. doi: 10.1126/science.1203280

Ewald, J. A., Desotelle, J. A., Wilding, G., & Jarrard, D. F. (2010). Therapy-induced senescence in cancer. *J Natl Cancer Inst, 102*(20), 1536-1546. doi: 10.1093/jnci/djq364

Freund, A., Patil, C. K., & Campisi, J. (2011). p38MAPK is a novel DNA damage response-independent regulator of the senescence-associated secretory phenotype. *EMBO J, 30*(8), 1536-1548. doi: 10.1038/emboj.2011.69

Gentleman, R. C., Carey, V. J., Bates, D. M., Bolstad, B., Dettling, M., Dudoit, S., . . . Zhang, J. (2004). Bioconductor: open software development for computational biology and bioinformatics. *Genome Biol, 5*(10), R80. doi: 10.1186/gb-2004-5-10-r80

Harley, C. B., Futcher, A. B., & Greider, C. W. (1990). Telomeres shorten during ageing of human fibroblasts. *Nature, 345*(6274), 458-460. doi: 10.1038/345458a0

Hayflick, L. (1965). THE LIMITED IN VITRO LIFETIME OF HUMAN DIPLOID CELL STRAINS. *Exp Cell Res, 37*, 614-636.

Hayflick, L., & Moorhead, P. S. (1961). The serial cultivation of human diploid cell strains. *Exp Cell Res, 25*, 585-621.

Heaphy, C. M., de Wilde, R. F., Jiao, Y., Klein, A. P., Edil, B. H., Shi, C., . . . Meeker, A. K. (2011). Altered telomeres in tumors with ATRX and DAXX mutations. *Science, 333*(6041), 425. doi: 10.1126/science.1207313

Herbig, U., Jobling, W. A., Chen, B. P., Chen, D. J., & Sedivy, J. M. (2004). Telomere shortening triggers senescence of human cells through a pathway involving ATM, p53, and p21(CIP1), but not p16(INK4a). *Mol Cell, 14*(4), 501-513.

Heukamp, L. C., Thor, T., Schramm, A., De Preter, K., Kumps, C., De Wilde, B., . . . Schulte, J. H. (2012). Targeted expression of mutated ALK induces neuroblastoma in transgenic mice. *Sci Transl Med, 4*(141), 141ra191. doi: 10.1126/scitranslmed.3003967

Irizarry, R. A., Hobbs, B., Collin, F., Beazer-Barclay, Y. D., Antonellis, K. J., Scherf, U., & Speed, T. P. (2003). Exploration, normalization, and summaries of high density oligonucleotide array probe level data. *Biostatistics, 4*(2), 249-264. doi: 10.1093/biostatistics/4.2.249

Itahana, K., Zou, Y., Itahana, Y., Martinez, J. L., Beausejour, C., Jacobs, J. J., . . . Dimri, G. P. (2003). Control of the replicative life span of human fibroblasts by p16 and the polycomb protein Bmi-1. *Mol Cell Biol, 23*(1), 389-401.

Ivanov, A., Pawlikowski, J., Manoharan, I., van Tuyn, J., Nelson, D. M., Rai, T. S., . . . Adams, P. D. (2013). Lysosome-mediated processing of chromatin in senescence. *J Cell Biol, 202*(1), 129-143. doi: 10.1083/jcb.201212110

Ivashkevich, A. N., Martin, O. A., Smith, A. J., Redon, C. E., Bonner, W. M., Martin, R. F., & Lobachevsky, P. N. (2011). gammaH2AX foci as a measure of DNA damage: a computational approach to automatic analysis. *Mutat Res, 711*(1-2), 49-60. doi: 10.1016/j.mrfmmm.2010.12.015

Kahlem, P., Dorken, B., & Schmitt, C. A. (2004). Cellular senescence in cancer treatment: friend or foe? *J Clin Invest, 113*(2), 169-174. doi: 10.1172/jci20784

Knizhnik, A. V., Roos, W. P., Nikolova, T., Quiros, S., Tomaszowski, K. H., Christmann, M., & Kaina, B. (2013). Survival and death strategies in glioma cells: autophagy, senescence and apoptosis triggered by a single type of temozolomide-induced DNA damage. *PLoS One, 8*(1), e55665. doi: 10.1371/journal.pone.0055665

Kosar, M., Bartkova, J., Hubackova, S., Hodny, Z., Lukas, J., & Bartek, J. (2011). Senescence-associated heterochromatin foci are dispensable for cellular senescence, occur in a cell type- and insult-dependent manner and follow expression of p16(ink4a). *Cell Cycle, 10*(3), 457-468.

Kramer, K., Kushner, B. H., & Cheung, N. K. (2003). Oral topotecan for refractory and relapsed neuroblastoma: a retrospective analysis. *J Pediatr Hematol Oncol, 25*(8), 601-605.

Kuilman, T., Michaloglou, C., Mooi, W. J., & Peeper, D. S. (2010). The essence of senescence. *Genes Dev, 24*(22), 2463-2479. doi: 10.1101/gad.1971610

Kuilman, T., & Peeper, D. S. (2009). Senescence-messaging secretome: SMS-ing cellular stress. *Nat Rev Cancer, 9*(2), 81-94. doi: 10.1038/nrc2560

Kumar, S., Mokhtari, R. B., Oliveira, I. D., Islam, S., Toledo, S. R., Yeger, H., & Baruchel, S. (2013). Tumor dynamics in response to antiangiogenic therapy with oral metronomic topotecan and pazopanib in neuroblastoma xenografts. *Transl Oncol, 6*(4), 493-503.

Kushner, B. H., Kramer, K., Meyers, P. A., Wollner, N., & Cheung, N. K. (2000). Pilot study of topotecan and high-dose cyclophosphamide for resistant pediatric solid tumors. *Med Pediatr Oncol, 35*(5), 468-474.

Ladenstein, R., Ambros, I. M., Potschger, U., Amann, G., Urban, C., Fink, F. M., . . . Ambros, P. F. (2001). Prognostic significance of DNA di-tetraploidy in neuroblastoma. *Med Pediatr Oncol, 36*(1), 83-92. doi: 10.1002/1096-911x(20010101)36:1<83::aid-mpo1020>3.0.co;2-9

Ladenstein, R., Valteau-Couanet, D., Brock, P., Yaniv, I., Castel, V., Laureys, G., . . . Pearson, A. (2010). Randomized Trial of prophylactic granulocyte colony-stimulating factor during rapid COJEC induction in pediatric patients with high-risk neuroblastoma: the European HR-NBL1/SIOPEN study. *J Clin Oncol, 28*(21), 3516-3524. doi: 10.1200/jco.2009.27.3524

Lee, J. M., Dedhar, S., Kalluri, R., & Thompson, E. W. (2006). The epithelial-mesenchymal transition: new insights in signaling, development, and disease. *J Cell Biol, 172*(7), 973-981. doi: 10.1083/jcb.200601018

Lien, K., Georgsdottir, S., Sivanathan, L., Chan, K., & Emmenegger, U. (2013). Low-dose metronomic chemotherapy: A systematic literature analysis. *Eur J Cancer*. doi: 10.1016/j.ejca.2013.06.038

Lock, R. B., & Ross, W. E. (1987). DNA topoisomerases in cancer therapy. *Anticancer Drug Des, 2*(2), 151-164.

Look, A. T., Hayes, F. A., Nitschke, R., McWilliams, N. B., & Green, A. A. (1984). Cellular DNA content as a predictor of response to chemotherapy in infants with unresectable neuroblastoma. *N Engl J Med, 311*(4), 231-235. doi: 10.1056/nejm198407263110405

Lovejoy, C. A., Li, W., Reisenweber, S., Thongthip, S., Bruno, J., de Lange, T., . . . Meeker, A. K. (2012). Loss of ATRX, genome instability, and an altered DNA damage response are hallmarks of the alternative lengthening of telomeres pathway. *PLoS Genet, 8*(7), e1002772. doi: 10.1371/journal.pgen.1002772

Maris, J. M. (2010). Recent advances in neuroblastoma. *N Engl J Med, 362*(23), 2202-2211. doi: 10.1056/NEJMra0804577

Mason, D. X., Jackson, T. J., & Lin, A. W. (2004). Molecular signature of oncogenic ras-induced senescence. *Oncogene, 23*(57), 9238-9246. doi: 10.1038/sj.onc.1208172

Matthay, K. K., Villablanca, J. G., Seeger, R. C., Stram, D. O., Harris, R. E., Ramsay, N. K., . . . Reynolds, C. P. (1999). Treatment of high-risk neuroblastoma with intensive chemotherapy, radiotherapy, autologous bone marrow transplantation, and 13-cis-retinoic acid. Children's Cancer Group. *N Engl J Med, 341*(16), 1165-1173. doi: 10.1056/nejm199910143411601

Merritt, W. M., Danes, C. G., Shahzad, M. M., Lin, Y. G., Kamat, A. A., Han, L. Y., . . . Sood, A. K. (2009). Anti-angiogenic properties of metronomic topotecan in ovarian carcinoma. *Cancer Biol Ther, 8*(16), 1596-1603.

Millis, A. J., McCue, H. M., Kumar, S., & Baglioni, C. (1992). Metalloproteinase and TIMP-1 gene expression during replicative senescence. *Exp Gerontol, 27*(4), 425-428.

Molenaar, J. J., Koster, J., Zwijnenburg, D. A., van Sluis, P., Valentijn, L. J., van der Ploeg, I., . . . Versteeg, R. (2012). Sequencing of neuroblastoma identifies chromothripsis and defects in neuritogenesis genes. *Nature, 483*(7391), 589-593. doi: 10.1038/nature10910

Monclair, T., Brodeur, G. M., Ambros, P. F., Brisse, H. J., Cecchetto, G., Holmes, K., . . . Pearson, A. D. (2009). The International Neuroblastoma Risk Group (INRG) staging system: an INRG Task Force report. *J Clin Oncol, 27*(2), 298-303. doi: 10.1200/jco.2008.16.6876

Narath, R., Ambros, I. M., Kowalska, A., Bozsaky, E., Boukamp, P., & Ambros, P. F. (2007). Induction of senescence in MYCN amplified neuroblastoma cell lines by hydroxyurea. *Genes Chromosomes Cancer, 46*(2), 130-142. doi: 10.1002/gcc.20393

Narita, M., Nunez, S., Heard, E., Lin, A. W., Hearn, S. A., Spector, D. L., . . . Lowe, S. W. (2003). Rb-mediated heterochromatin formation and silencing of E2F target genes during cellular senescence. *Cell, 113*(6), 703-716.

Nozato, M., Kaneko, S., Nakagawara, A., & Komuro, H. (2013). Epithelial-mesenchymal transition-related gene expression as a new prognostic marker for neuroblastoma. *Int J Oncol, 42*(1), 134-140. doi: 10.3892/ijo.2012.1684

Park, J. R., Scott, J. R., Stewart, C. F., London, W. B., Naranjo, A., Santana, V. M., . . . Matthay, K. K. (2011). Pilot induction regimen incorporating pharmacokinetically guided topotecan for treatment of newly diagnosed high-risk neuroblastoma: a Children's Oncology Group study. *J Clin Oncol, 29*(33), 4351-4357. doi: 10.1200/jco.2010.34.3293

Picketts, D. J., Higgs, D. R., Bachoo, S., Blake, D. J., Quarrell, O. W., & Gibbons, R. J. (1996). ATRX encodes a novel member of the SNF2 family of proteins: mutations point to a common mechanism underlying the ATR-X syndrome. *Hum Mol Genet, 5*(12), 1899-1907.

Ponzoni, M., Casalaro, A., Lanciotti, M., Montaldo, P. G., & Cornaglia-Ferraris, P. (1992). The combination of gamma-interferon and tumor necrosis factor causes a rapid and extensive differentiation of human neuroblastoma cells. *Cancer Res, 52*(4), 931-939.

Rodier, F., & Campisi, J. (2011). Four faces of cellular senescence. *J Cell Biol, 192*(4), 547-556. doi: 10.1083/jcb.201009094

Roninson, I. B. (2003). Tumor cell senescence in cancer treatment. *Cancer Res, 63*(11), 2705-2715.

Rowinsky, E. K., Grochow, L. B., Hendricks, C. B., Ettinger, D. S., Forastiere, A. A., Hurowitz, L. A., . . . et al. (1992). Phase I and pharmacologic study of topotecan: a novel topoisomerase I inhibitor. *J Clin Oncol, 10*(4), 647-656.

Sager, R. (1991). Senescence as a mode of tumor suppression. *Environ Health Perspect, 93*, 59-62.

Sarkisian, C. J., Keister, B. A., Stairs, D. B., Boxer, R. B., Moody, S. E., & Chodosh, L. A. (2007). Dose-dependent oncogene-induced senescence in vivo and its evasion during mammary tumorigenesis. *Nat Cell Biol, 9*(5), 493-505. doi: 10.1038/ncb1567

Schellenberg, A., Lin, Q., Schuler, H., Koch, C. M., Joussen, S., Denecke, B., . . . Wagner, W. (2011). Replicative senescence of mesenchymal stem cells causes DNA-methylation changes which correlate with repressive histone marks. *Aging (Albany NY), 3*(9), 873-888.

Schleiermacher, G., Michon, J., Ribeiro, A., Pierron, G., Mosseri, V., Rubie, H., . . . Couturier, J. (2011). Segmental chromosomal alterations lead to a higher risk of relapse in infants with MYCN-non-amplified localised unresectable/disseminated neuroblastoma (a SIOPEN collaborative study). *Br J Cancer, 105*(12), 1940-1948. doi: 10.1038/bjc.2011.472

Schmitt, C. A., Fridman, J. S., Yang, M., Lee, S., Baranov, E., Hoffman, R. M., & Lowe, S. W. (2002). A senescence program controlled by p53 and p16INK4a contributes to the outcome of cancer therapy. *Cell, 109*(3), 335-346.

Schwarze, S. R., Fu, V. X., Desotelle, J. A., Kenowski, M. L., & Jarrard, D. F. (2005). The identification of senescence-specific genes during the induction of senescence in prostate cancer cells. *Neoplasia, 7*(9), 816-823.

Seluanov, A., Gorbunova, V., Falcovitz, A., Sigal, A., Milyavsky, M., Zurer, I., . . . Rotter, V. (2001). Change of the death pathway in senescent human fibroblasts in response to DNA damage is caused by an inability to stabilize p53. *Mol Cell Biol, 21*(5), 1552-1564. doi: 10.1128/mcb.21.5.1552-1564.2001

Serrano, M., Lin, A. W., McCurrach, M. E., Beach, D., & Lowe, S. W. (1997). Oncogenic ras provokes premature cell senescence associated with accumulation of p53 and p16INK4a. *Cell, 88*(5), 593-602.

Shay, J. W., & Roninson, I. B. (2004). Hallmarks of senescence in carcinogenesis and cancer therapy. *Oncogene, 23*(16), 2919-2933. doi: 10.1038/sj.onc.1207518

Shay, J. W., & Wright, W. E. (2005). Senescence and immortalization: role of telomeres and telomerase. *Carcinogenesis, 26*(5), 867-874. doi: 10.1093/carcin/bgh296

Sherwood, S. W., Rush, D., Ellsworth, J. L., & Schimke, R. T. (1988). Defining cellular senescence in IMR-90 cells: a flow cytometric analysis. [Research Support, U.S. Gov't, P.H.S.]. *Proceedings of the National Academy of Sciences of the United States of America, 85*(23), 9086-9090.

Smith, M. A., Seibel, N. L., Altekruse, S. F., Ries, L. A., Melbert, D. L., O'Leary, M., . . . Reaman, G. H. (2010). Outcomes for children and adolescents with cancer: challenges for the twenty-first century. *J Clin Oncol, 28*(15), 2625-2634. doi: 10.1200/jco.2009.27.0421

Smyth, G. K. (2004). Linear models and empirical bayes methods for assessing differential expression in microarray experiments. *Stat Appl Genet Mol Biol, 3*, Article3. doi: 10.2202/1544-6115.1027

Sohn, J. J., Schetter, A. J., Yfantis, H. G., Ridnour, L. A., Horikawa, I., Khan, M. A., . . . Harris, C. C. (2012). Macrophages, nitric oxide and microRNAs are associated with DNA damage response pathway and senescence in inflammatory bowel disease. *PLoS One, 7*(9), e44156. doi: 10.1371/journal.pone.0044156

Sottile, F., Gnemmi, I., Cantilena, S., D'Acunto, W. C., & Sala, A. (2012). A chemical screen identifies the chemotherapeutic drug topotecan as a specific inhibitor of the B-MYB/MYCN axis in neuroblastoma. *Oncotarget, 3*(5), 535-545.

Spallarossa, P., Altieri, P., Aloi, C., Garibaldi, S., Barisione, C., Ghigliotti, G., . . . Brunelli, C. (2009). Doxorubicin induces senescence or apoptosis in rat neonatal cardiomyocytes by regulating the expression levels of the telomere binding factors 1 and 2. *Am J Physiol Heart Circ Physiol, 297*(6), H2169-2181. doi: 10.1152/ajpheart.00068.2009

Stein, G. H., Drullinger, L. F., Soulard, A., & Dulic, V. (1999). Differential roles for cyclin-dependent kinase inhibitors p21 and p16 in the mechanisms of senescence and differentiation in human fibroblasts. *Mol Cell Biol, 19*(3), 2109-2117.

Stewart, R. A., Lee, J. S., Lachnit, M., Look, A. T., Kanki, J. P., & Henion, P. D. (2010). Studying peripheral sympathetic nervous system development and neuroblastoma in zebrafish. *Methods Cell Biol, 100*, 127-152. doi: 10.1016/b978-0-12-384892-5.00005-0

Sulli, G., Di Micco, R., & d'Adda di Fagagna, F. (2012). Crosstalk between chromatin state and DNA damage response in cellular senescence and cancer. *Nat Rev Cancer, 12*(10), 709-720. doi: 10.1038/nrc3344

Suzuki, K., Mori, I., Nakayama, Y., Miyakoda, M., Kodama, S., & Watanabe, M. (2001). Radiation-induced senescence-like growth arrest requires TP53 function but not telomere shortening. *Radiat Res, 155*(1 Pt 2), 248-253.

te Poele, R. H., Okorokov, A. L., Jardine, L., Cummings, J., & Joel, S. P. (2002). DNA damage is able to induce senescence in tumor cells in vitro and in vivo. *Cancer Res, 62*(6), 1876-1883.

Verheijen, R., Kuijpers, H. J., van Driel, R., Beck, J. L., van Dierendonck, J. H., Brakenhoff, G. J., & Ramaekers, F. C. (1989). Ki-67 detects a nuclear matrix-associated proliferation-related antigen. II. Localization in mitotic cells and association with chromosomes. *J Cell Sci, 92 (Pt 4)*, 531-540.

Von Hoff, D. D., McGill, J. R., Forseth, B. J., Davidson, K. K., Bradley, T. P., Van Devanter, D. R., & Wahl, G. M. (1992). Elimination of extrachromosomally amplified MYC genes from human tumor cells reduces their tumorigenicity. *Proc Natl Acad Sci U S A, 89*(17), 8165-8169.

Wainwright, L. J., Lasorella, A., & Iavarone, A. (2001). Distinct mechanisms of cell cycle arrest control the decision between differentiation and senescence in human neuroblastoma cells. *Proc Natl Acad Sci U S A, 98*(16), 9396-9400. doi: 10.1073/pnas.161288698

Wang, X., Ryter, S. W., Dai, C., Tang, Z. L., Watkins, S. C., Yin, X. M., . . . Choi, A. M. (2003). Necrotic cell death in response to oxidant stress involves the activation of the apoptogenic caspase-8/bid pathway. *J Biol Chem, 278*(31), 29184-29191. doi: 10.1074/jbc.M301624200

Watson, L. A., Solomon, L. A., Li, J. R., Jiang, Y., Edwards, M., Shin-ya, K., . . . Berube, N. G. (2013). Atrx deficiency induces telomere dysfunction, endocrine defects, and reduced life span. *J Clin Invest, 123*(5), 2049-2063. doi: 10.1172/jci65634

Wei, S., & Sedivy, J. M. (1999). Expression of catalytically active telomerase does not prevent premature senescence caused by overexpression of oncogenic Ha-Ras in normal human fibroblasts. *Cancer Res, 59*(7), 1539-1543.

Wu, C. H., van Riggelen, J., Yetil, A., Fan, A. C., Bachireddy, P., & Felsher, D. W. (2007). Cellular senescence is an important mechanism of tumor regression upon c-Myc inactivation. *Proc Natl Acad Sci U S A, 104*(32), 13028-13033. doi: 10.1073/pnas.0701953104

Yang, R. K., Kalogriopoulos, N. A., Rakhmilevich, A. L., Ranheim, E. A., Seo, S., Kim, K., . . . Sondel, P. M. (2013). Intratumoral treatment of smaller mouse neuroblastoma tumors with a recombinant protein consisting of IL-2 linked to the hu14.18 antibody increases intratumoral CD8+ T and NK cells and improves survival. *Cancer Immunol Immunother, 62*(8), 1303-1313. doi: 10.1007/s00262-013-1430-x

Yu, A. L., Gilman, A. L., Ozkaynak, M. F., London, W. B., Kreissman, S. G., Chen, H. X., . . . Sondel, P. M. (2010). Anti-GD2 antibody with GM-CSF, interleukin-2, and isotretinoin for neuroblastoma. *N Engl J Med, 363*(14), 1324-1334. doi: 10.1056/NEJMoa0911123

Zhu, J., Woods, D., McMahon, M., & Bishop, J. M. (1998). Senescence of human fibroblasts induced by oncogenic Raf. *Genes Dev, 12*(19), 2997-3007.

8. List of Abbreviations

BrdU	5-bromo-2'-deoxyuridine
BSA	bovine serum albumin
CD	cluster of differentiation
CPT	camptothecin
Cy3	Cyanine 3
d	day/daily
DAPI	4',6-diamidino-2-phenylindole
DMSO	Dimethylsulfoxid
DNA	deoxyribonucleic acid
DSB	double strand breaks
d.p.i.	days post inoculation
dUTP	Desoxyuridintriphosphat
FACS	Fluorescence Activated Cell Sorting
Fig	figure
FITC	fluoresceinisothiocyanat
HU	hydroxyurea
IF	immunofluorescence
IL	interleukin
i.p.	intraperitoneally
kg	kilogramm
mg	milligramm
MHC	major histocompatibility complex
MICA	MHC class I chain-related molecules A
MICB	MHC class I chain-related molecules B
min.	minutes
MNA	*MYCN* amplification
MYCN	V-myc myelocytomatosis viral related oncogene, neuroblastoma derived (avian)

NB	neuroblastoma
n.s.	not significant
NK-cells	natural killer cells
ON	over night
PBS	phosphate buffered saline
RNA	ribonucleic acid
rpm	revolutions per minute
RPMI medium	Roswell Park Memorial Institute medium
RT	room temperature
sec.	seconds
SSC	saline-sodium citrate buffer
TdT	terminal desoxynucleotidyl transferase
TPT	topotecan
TRITC	Tetramethylrhodamine isothiocyanate
TUNEL	TdT-mediated dUTP-biotin nick end labeling
u	unit

9. Abstract

Neuroblastoma (NB) is a solid tumor of the sympathetic nervous system. Since the overall survival rate of high-risk NB patients, frequently having an amplification of the *MYCN* oncogene, is still very poor there is a need for the establishment of additional therapeutic approaches. In this study, we approach this need by exploring the tumor-inhibitory potential of drug-induced senescent NB tumor cells *in vivo.* Topotecan (TPT), a camptothecin (CPT) derivative, is a topoisomerase I inhibitor and is given to cancer patients as high-dose cytotoxic therapy. Preliminary *in vitro* findings revealed that continuous low - dose treatment with CPT and TPT leads to a reduction in *MYCN* copy number, protein expression and induces tumor cell senescence in low passage NB cell lines. This is associated with a less aggressive expression and secretory pattern and reduced tumor cell growth of co-cultured non-senescent NB cells. Thus, we evaluated low dosis TPT effects (≤0.1 mg/kg/d *in vivo*) compared to high doses (1 mg/kg/d) in a NB-xenotransplantation mouse model. Therefore, *MYCN*-amplified STA-NB10 cells were subcutaneously injected into nude mice. After tumors had reached a size of 0.53 (±0.2) cm^3, treatment was carried out i.p. with four different doses of TPT (1 mg/kg/d, 0.1 mg/kg/d, 0.03 mg/kg/d, 0.01 mg/kg/d) over a period of 2 weeks, respectively. Tumors regressed completely at 1 mg/kg/d TPT and tumor growth was declining in a dose-dependent manner. Further, we analysed senescence-associated β-galactosidase activity on CTRL and TPT treated tumors which showed no or very low positivity in untreated controls (n=7) and intermediate to high positivity in 0.1 mg/kg/d TPT treated samples (n=10). Moreover, the induction of senescence could be confirmed in expression arrays where markers associated with senescence of NB cell lines *in vitro,* such as p21, fibronectin and CD44, were up-regulated. TUNEL staining showed a higher percentage of apoptotic cells in TPT treated tumors compared to untreated ones. Lower levels of CD31 positive blood vessels were observed in TPT treated tumors. Concomitantly expression arrays showed a strong down regulation of VEGFA in 0.1 mg/kg/d TPT treated samples compared to CTRL tumors. These findings suggest that, in contrast to reports on tumor-promoting properties of senescent normal cells, continuous low-dose TPT treatment in NB induce tumor cell senescence and is associated with tumor-inhibitory effects *in vitro* and *in vivo*. Further we show that also low-dose (0.1 mg/kg/d) TPT treatment inhibits tumor growth and exerts pro-apoptotic and anti-angiogenic functions.

10. Zusammenfassung

Das Neuroblastom (NB) ist ein solider Tumor des vegetativen Nervensystems. Da die langfristige Überlebensrate von Hoch-Risiko-PatientInnen, welche oft eine Amplifizierung des MYCN Onkogens besitzen, noch sehr gering ist, ist die Etablierung von weiteren Therapiemöglichkeiten notwendig. In dieser Arbeit wird das Tumor-hemmende Potenzial von seneszenten NB Tumorzellen *in vivo* untersucht, welche durch Medikamente seneszenz-induziert wurden. Topotecan (TPT), ein Camptothecin (CPT)-Derivat, wird aufgrund seiner Wirkung als Topoisomerase I Inhibitor an KrebspatientInnen in cytotoxischer Hochdosistherapie verabreicht. Dieser Studie vorangegangene Daten zeigten *in vitro*, dass niedrig dosierte Behandlung mit CPT und TPT zu einer Reduktion der Kopienzahl, als auch des Proteins von MYCN führt und Tumorzellseneszenz in NB-Zelllinien induziert. Dies ging mit weniger aggressiven Expressions- und Sekretionsprofilen einher, weiters wurde das Tumorzellwachstum von co-kultivierten, nicht seneszenten NB-Zellen verringert. Somit wurden diese Niedrigdosiseffekte (≤0.1 mg/kg/d *in vivo*, verglichen mit Hochdosis 1 mg/kg/d) vonTPT in einem NB-Xenotransplant-Mousmodell evaluiert. Dazu wurden 40 Nacktmäusen jeweils 10^7 Zellen der MYCN-amplifizierte Zelllinie (STA-NB 10) subcutan injiziert. Nachdem die Tumore eine Größe von 0.53 (±0.2) cm^3 erreicht hatten, wurde die intraperitoneale Behandlung in vier verschiedenen Dosisgruppen (1 mg/kg/d, 0.1 mg/kg/d, 0.03 mg/kg/d, 0.01 mg/kg/d) TPT für zwei Wochen durchgeführt. Tumore bildeten sich bei 1 mg/kg/d TPT vollständig zurück, allgemein nahm das Tumorwachstum in einer Dosisabhängigkeit ab. Weiters wurde Senescence-associated β-galactosidase Aktivität analysiert, wobei unbehandelte Kontrolltumore (n=7) keine oder sehr geringe Aktivität aufwiesen, während 0.1 mg/kg/d TPT behandelte Tumore (n=10) mittlere bis hohe Aktivität zeigten. Die Induktion von Seneszenz konnte zudem auch in Expressionsexperimenten bestätigt werden, in welchen *in vitro* NB-Seneszenz-Marker wie p21, Fibronectin und CD44 hinauf reguliert wurden. TUNEL Färbungen zeigten einen höheren Prozentsatz an apoptotischen Zellen in TPT behandelten Tumoren, verglichen mit unbehandelten Proben. In TPT behandelten Tumoren wurden zudem weniger CD31 positive Blutgefäße detektiert. Dementsprechend korrelierte auch die Expression in 1 mg/kg/d TPT behandelten Tumoren, wo VEGFA das am stärksten runter-regulierte Transkript stellte. Diese Daten legen Nahe, dass – entgegen Studien über Tumor-verstärkende Wirkungen von seneszenten

Normalzellen – kontinuierliche TPT Behandlung mit niedriger Dosis Tumorzellseneszenz im NB hervorrufen kann und dies sowohl *in vitro* als auch *in vivo* mit Tumor-inhibierenden Effekten einhergeht. Weiters wurde auch gezeigt, dass auch niedrig dosierte TPT Behandlung (0.1 mg/kg/d) Tumorwachstum hemmt und pro-apoptotische, als auch anti-angiogenetische Eigenschaften hervorruft.

11. Curriculum vitae

Personal Data

Name: **Magdalena SCHWARZ**

Address: Children's Cancer Research Institute (CCRI)

                                            Zimmermannplatz 10

                                            1090 Vienna, Austria

Phone: +43-1-40470-4054

E-mail: magdalena.schwarz@ccri.at

Nationality: Austrian

Professional experience and Internships

Sept. 2012 – present   **Master work at the CCRI, Vienna, Austria**

                            Investigation on Senescence, apoptosis and angiogenesis upon Topotecan treatment in a xenotransplantation neuroblastoma mouse model

                            Group: Peter F. Ambros, PhD

May 2012   **Internship at the CCRI, Vienna, Austria**

                            Investigation on EWS-FLI1 expression in Ewing´s sarcoma cell lines

                            Group: Heinrich Kovar, PhD

April 2012   **Internship at the Dept. for Molecular Evolution and Development, University of Vienna, Austria**

                            Investigation on evolutionary aspects of muscle development in *Aurelia aurita*

                            Group: Ulrich Technau, PhD

July 2011 – Aug. 2011   **"Genspace" Project, New York City, USA**

Collaboration in short-term projects on gene expression,

Teaching support in summer courses for High school students

Supervision: Oliver Medvedik, PhD

March 2010 – May 2010	**Internship at the Department of Plant Biochemistry and Molecular Biology of the Centro de Investigaciones Científicas, Sevilla, Spain**

Investigation on the purification of membrane-embedded proteins

Group: Aurelio Serrano, PhD

July 2009 – August 2009	**Tropical Research Station, La Gamba, Costa Rica**

Field work in the tropical rain forest, analysis of soil samples

2008	**Internship at the IMP Vienna, Austria**

Investigation on neuronal development and axon guidance in *drosophila melanogaster*

Group: Barry Dickson, PhD

Education

Oct. 2011 – present	Master programme Molecular Biology (with a focus on Molecular Medicine) at the University of Vienna, Austria
Oct. 2011 – present	Bachelor programme International Development Studies at the University of Vienna, Austria
June 2011	BSc in Molecular Biology from the University of Technology, Graz, Austria
Feb. 2010 – July 2010	Studies in Molecular Biology at the Universidad de Sevilla, Spain (Erasmus fellowship)
Oct. 2008 – June 2011	Bachelor programme Molecular Biology at the University of Technology, Graz, Austria
Sept. 2004 – June 2008	BG/BRG/BORG Hartberg 8230, Edelseegasse 13
	High school diploma (Matura 2008)

Research interests and technical skills

Main research interests:	Mechanisms of disease in general, especially cancer biology;
	Investigation of potential therapy targets and development of novel therapeutic applications, including tumor cell senescence; "neglected" diseases of the developing world
Techniques:	Common molecular biology techniques (e.g. DNA/RNA isolation, purification, PCR), histology (tissue sampling, cryosections, tissue staining, microscopy), immunochemistry (Western Blot, IF on cells and tissue), cell culture work (mammalian), basic microbiology tools, experience with animal models (*Drosophila melanogaster, Aurelia aurita*, CD1 nude mice), xenograft experiments in mice

Scientific Presentations

July 20th-23rd 2013	"Cell Senescence in Cancer and Ageing"
	Conference, Cambridge, UK
	Oral presentation: "Tumor cell senescence and apoptosis induced by continuous low-dose topotecan is associated with tumor-inhibitory effects in neuroblastoma xenotransplant tumors"
June 7th-8th 2013	**"Pediatric Cancer Research at the Interface"**
	Symposium, Vienna, Austria
	Poster presentation: "Continuous low-dose topotecan treatment selectively induces pre-mature senescence in *MYCN*-amplified neuroblastoma cells *in vitro* and *in vivo*"

Additional Skills

Languages:	German (native tongue)
	English (IELTS score: 8.5)
	Spanish (reference system: C1)
Computing:	MS Office, Adobe Acrobat, Photoshop, InDesign, Diva (LSRII), TissueQuest

Writing:
Nov. 2011: Article "Getting to know your DNA" published online in a popular scientific magazine (United Academics Magazine)

Sept. 2011-May 2012: Editor of a magazine (Korso), Graz, Austria

12. Lebenslauf

Persönliche Daten

Name:	**Magdalena SCHWARZ**
Adresse:	St. Anna Kinderkrebsforschung (CCR)
	Zimmermannplatz 10
	1090 Wien, Österreich
Mobiltelefon:	+43-1-40470-4054
E-mail:	magdalena.schwarz@ccri.at
Nationalität:	Österreicherin

Professionelle Erfahrung und wissenschaftliche Praktika

seit Sept. 2012	**Masterarbeit an der St. Anna Kinderkrebsforschung (CCRI), Wien, Österreich**
	Erforschung von "Seneszenz, Differenzierung und Apoptose nach Hydroxyurea oder Topotecan Behandlung in einem Xenotransplant Neuroblastom Mausmodell"
	Gruppe: Peter F. Ambros, PhD
Mai 2012	**Praktikum an der St. Anna Kinderkrebsforschung (CCRI), Wien, Österreich**
	Erforschung von EWS-FLI1 Expression in Ewing Sarkom Zelllinien
	Gruppe: Heinrich Kovar, PhD
April 2012	**Praktikum am Department für Molekulare Evolution und Entwicklung, Universität Wien, Österreich**
	Erforschung von evolutionären Aspekten der Muskelentwicklung in *Aurelia aurita*
	Gruppe: Ulrich Technau, PhD

Juli 2011 – Aug. 2011	**"Genspace" Projektlabor, New York City, USA**
	Mitarbeit in Kurzzeitprojekten, z.B. Genexpression, Unterstützung beim Unterrichten von Sommerkursen für High-School-schüler
	Betreuung: Oliver Medvedik, PhD
März 2010 – Mai 2010	**Praktikum am Department für Pflanzenbiochemie und Molekularbiologie, Zentrum für wissenschaftliche Forschung Sevilla, Spanien**
	Erforschung der Purifikation von membrangebundenen Proteinen
	Gruppe: Aurelio Serrano, PhD
Juli 2009 – August 2009	**Mitarbeit an der Tropenstation in La Gamba,**
	Costa Rica
	Wiederaufforstung, Mitarbeit in der Baumschule, Analyse von Bodenproben
2008	**Praktikum am Institut für molekulare Pathologie (IMP) Vienna, Austria**
	Erforschung von neuronaler Entwicklung und Axonwachstum in *drosophila melanogaster*
	Gruppe: Barry Dickson, PhD

Ausbildung

seit Okt. 2011	Masterstudium Molekularbiologie (Schwerpunkt Molekulare Medizin) an der Universität Wien
seit Okt. 2011	Bachelorstudium Internationale Entwicklung an der Universität Wien
Juni 2011	BSc in Molekularbiologie an der TU Graz
Feb. 2010 – Juli 2010	Erasmus-Aufenthalt in Molekularbiologie an der Universidad de Sevilla, Spanien
Okt. 2008 – Juni 2011	Bachelorstudium Molekularbiologie an der TU Graz
Sept. 2004 – Juni 2008	BG/BRG/BORG Hartberg 8230, Edelseegasse 13
	Matura 2008 mit Auszeichnung
	(naturwissenschaftlicher Schwerpunkt)

Forschungsinteressen und Fähigkeiten

Hauptforschungsinteresse:	Mechanismen um die Entstehung von Krankheiten, im speziellen Krebsbiologie; Erforschung von potentiellen Therapiemöglichkeiten und Entwicklung von neuen therapeutischen Anwendungen, besonders Tumorzellseneszenz; Interesse an "neglected diseases" von Entwicklungsländern
Techniken:	Standardtechniken der Molekularbiologie (z.B. DNA/RNA Isolation, Purifikation, PCR), Histologie (Gewebe- und Probenaufbereitung, Färbungen, Mikroskopie), Immunchemische Verfahren (Western Blot, IF auf Zellen und Gewebe), Zellkultur (Säugetierzellen), grundlegende mikrobiologische Fertigkeiten, Tiermodelle (*Drosophila melanogaster, Aurelia aurita*, CD1 Nacktmäuse), Xenograft-studien in Mäusen

Wissenschaftliche Präsentationen

20.-23. Juli 2013	"Cell Senescence in Cancer and Ageing"
	Konferenz, Cambridge, UK
	Vortrag: "Tumor cell senescence and apoptosis induced by continuous low-dose topotecan is associated with tumor-inhibitory effects in neuroblastoma xenotransplant tumors"
7.-8. Juni 2013	"Pediatric Cancer Research at the Interface"
	Symposium, Wien, Österreich
	Posterpräsentation: "Continuous low-dose topotecan treatment selectively induces pre-mature senescence in *MYCN*-amplified neuroblastoma cells *in vitro* and *in vivo*"

Zusätzliche Fähigkeiten

Sprachen:	Deutsch (Mutterspruche)
	Englisch (IELTS punkte: 8.5)
	Spanisch (Referenzsystem: C1)
Computer:	MS Office, Adobe Acrobat, Photoshop, InDesign, Diva (LSRII), TissueQuest

Schreiben:

Nov. 2011: Artikel "Getting to know your DNA" online in dem populärwissenschaftlichen Magazin „United Academics Magazine" publiziert

Sept. 2011-Mai 2012: Redaktionelle Mitarbeit bei dem Monatsmagazin "Korso", Graz